PROBABILISTIC STRUCTURAL DESIGN: EFFECTS OF MULTI-STAGE TESTING AND MULTIPLE FAILURE MODES

By

CHAN-YOUNG PARK

A DISSERTATION PRESENTED TO THE GRADUATE SCHOOL
OF THE UNIVERSITY OF FLORIDA IN PARTIAL FULFILLMENT
OF THE REQUIREMENTS FOR THE DEGREE OF
DOCTOR OF PHILOSOPHY

UNIVERSITY OF FLORIDA

2013

This dissertation is dedicated to my family who has always supported me.

ACKNOWLEDGMENTS

First and foremost, I would like to express my deep and sincere gratitude to my advisors Dr. Nam-Ho Kim and Dr. Raphael T. Haftka for giving me a great opportunity to do research and providing invaluable guidance throughout this research. Their vision, sincerity, and motivation have deeply inspired me. I especially appreciate their patience for teaching me the methodology to carry out the research and to present the research results. I have wholeheartedly enjoyed the challenge of researching a controversial issue that could greatly impact engineering design instead of just performing another educational study. I could not have wished for better advisors.

I am also grateful to the committee members Dr. Sankar and Dr. Gurley who have contributed to this dissertation by giving valuable feedback and different perspectives for organizing ideas.

I would like to thank the members of the Multidisciplinary Design and Optimization group at the University of Florida for their support, and invaluable comments. Technical discussions with them gave me opportunities for consolidating and solidifying my knowledge.

Financial support by the National Science Foundation grant CMMI-0856431 and the Air Force Research Laboratory grant under the contract 84796 is gratefully acknowledged.

Finally, special recognition goes out to my parents Dae-Sik Park and Hye-Sug Kim for their support, and patience during my pursuit of the Doctorate in Mechanical Engineering as well as in my life, and especially to my dear wife Aeraena Yang, who provided emotional support and constant encouragement during the entire process shall be with me forever, and to our two little children, Soogyeom Park and Soorin Park.

TABLE OF CONTENTS

page

LIST OF TABLES

LIST OF FIGURES

LIST OF ABBREVIATIONS

AFRL	Air Force Research Laboratory
CDF	Cumulative Density Function
COV	Coefficient of Variation
FAA	Federal Aviation Administration
FEM	Finite Element Method
GUI	Graphical User Interface
MCS	Monte Carlo Simulation
PDF	Probability Density Function
PF	Probability of Failure
PTD	Possible True Distribution
RBDO	Reliability Based Design Optimization

Abstract of Dissertation Presented to the Graduate School
of the University of Florida in Partial Fulfillment of the
Requirements for the Degree of Doctor of Philosophy

PROBABILISTIC STRUCTURAL DESIGN: EFFECTS OF MULTI-STAGE TESTING AND MULTIPLE FAILURE MODES

By

Chan-Young Park

December 2013

Chair: Nam-Ho Kim
Co-Chair: Raphael T. Haftka
Major: Mechanical Engineering

Traditional probabilistic design methods are in the lack of capability in representing practical design processes. In practice, design of complex engineering system is based on a hierarchical process in which system design is decomposed into multiple stages, called the building-block process.

In this research, as a first step in the building-block process, the effects of the numbers of coupon and element tests on design weight are studied under various uncertainties. Based on a simulation model, structural elements for failure prediction under combined loads are designed with two test stages of coupon and element tests. It is found that the weight penalty associated with no element test is significant, and it is greatly reduced by more element tests , but the effect of the number of coupon tests is much smaller unless the failure theory is very accurate.

Error in reliability of a structure with multiple failure modes originates in errors in failure predictions for failure modes. In most cases, however, a single test is performed due to limited resources. Here, we developed an approach to reduce errors in multiple predictions of failure load with a single test.

When a probabilistic approach is applied to design of a structure with multiple failure modes, dependence between failures modes is often ignored in order to simplify system reliability calculation. A study of the effect of ignoring dependence between failure modes on system reliability is carried out. Interestingly, for high system reliability, the error decreases regardless strong dependence.

CHAPTER 1
INTRODUCTION

Probabilistic design with multi-stage testing

Current probabilistic design frameworks assume that the information of all uncertainties, either aleatory or epistemic [1], is available at the design stage and fixed throughout the product lifecycle. However, for complex engineering system design, uncertainties are progressively quantified and updated. That is because system design is progressively updated based on evolving design of various components at increasing complexity [59,60], and components are progressively validated with multi-stage testing [61]. This study is to provide approaches to apply probabilistic design frameworks to system design based on multi-stage testing.

This multi-stage test approach, also referred to the building-block approach shown in Fig. 2-1, has been integrated with the structural design process of aircraft [2,3]. The first stage of the building block approach is the coupon test that characterizes the behavior and statistics of material properties. Element and subcomponent testings are followed to characterize failure modes that are not addressed in coupon specimens. Note that elements are simple and standard structural components, such as curved panels and stiffened panels. Subcomponents typically refer to larger specimens than elements and non-standardized configurations [2,3,12]. When elements are tested individually, the test can only approximate the boundary conditions applied by adjacent elements. Therefore, component (e.g. wing) testing is the part of certification or qualification process that ensures elements are also tested under the correct loading and boundary conditions [62,63].

The purpose of building-block testing is to prevent failing the certification test by reducing uncertainty in failure prediction of complex structures with simple component tests in early stages of design [3]. In this dissertation, a probabilistic approach is presented for structural element design by predicting conservative element strength satisfying a certain safety level based on two test stages, coupon and element tests.

Aircraft designers use conservative measures, such as A- or B-basis allowables, to compensate for uncertainty in material strength prediction as in MIL-HDBK [2]. For example, the B-basis introduces conservativeness in two ways. To compensate for variability, the B-basis uses the lower 10% value of the material strength distribution. However, calculating the lower 10% relies on the number of coupons, which brings in epistemic uncertainty. Thus, the B-basis requires an additional 95% confidence level to compensate for the epistemic uncertainty. That is, the B-basis provides a value that belongs to the lower 10% with 95% probability. The B-basis is calculated based on a sample mean and standard deviation with a factor for one-sided tolerance limit with an assumed population distribution. MIL-HDBK [2] and Owen *et al.* [64] presented tables of factors with various population distributions.

Another conservative measure is taken at the element level. To compensate for the error in a failure theory, it is common practice to repeat element tests three times and then select the lowest test result as a conservative estimate of the failure envelope; this process can be interpreted as applying a knockdown factor on the average test result.

These conservative statistical approaches have worked successfully to achieve the safety of structural designs. However, they were applied at an individual test stage

without considering their overall efficiency to achieve the safety level at the final stage. Also, it has not been quantified how much these tests reduce the weight penalty compared to the design without tests.

When we use failure theory to predict the strength of an element, we propagate uncertainty in coupons and combine it with uncertainty in the failure theory. There are two major sources of epistemic uncertainties (uncertainty associated with lack of information) in the process. The first is error in the failure theory to predict failure, and the second source is sampling error in material properties measured due to a finite number of coupons. Then, we build and test the structural element in order to reduce the combined uncertainty. By quantifying the remaining uncertainty after tests, we calculate conservative element strength based on the uncertainty and the required safety level [2,3,64].

However, structural tests have variability due to various uncertainties, such as uncertainty in applied loads, boundary conditions, measurements, etc. Repetition of tests reduces the uncertainty in test data [5]. The effects of coupon tests and element tests on reducing uncertainty is collectively reflected as the amount of reduced uncertainty by the tests, which is compensated by design weight to achieve a safety requirement as the design weight is inversely proportional to the amount of reduced uncertainty. Since the effects of coupon tests and element tests are different, quantifying the influences of each set of tests on reducing design weight is an important issue for designing with multi-stage testing.

In the perspective of resource allocation, coupon tests are relatively cheap compared to element tests, and therefore, we usually perform more coupon tests

(several dozens) than element tests (a handful). It is useful to investigate the effect of the number of tests on making a conservative element strength prediction and to analyze the tradeoff between the number of coupons and elements for reducing the conservativeness.

There are also several studies investigating the effect of tests on safety and reducing uncertainty in computational models. Jiao and Moan [20] investigated the effect of proof tests on structural safety using Bayesian inference. They showed that proof tests reduce uncertainty in the strength of a structure, and thus provide a substantial reduction in the probability of failure (PF). An *et al.* [4] investigated the effect of structural element tests on reducing uncertainty in element strength using Bayesian inference. Acar *et al.* [5] modeled a simplified building-block process with safety factors and knockdown factors. Bayesian inference is used to model the effect of structural element tests. They show the effect of the number of tests on the design weight for the same PF, and vice versa. Jiang and Mahadevan [78] studied the effect of tests in validating a computational model by obtaining an expected risk in terms of the decision cost. Urbina and Mahadevan [21] assessed the effects of system level tests for assessing reliability of complex systems. They built computational models of a system and predicted the performance of the system. Tests are then incorporated into the models to estimate the confidence in the performance of the systems. Park *et al*. [22] estimated uncertainty in computational models and developed a methodology to evaluate likelihood using both test data and a computational model. McFarland and Bichon [23] estimated PF by incorporating test data for a bistable MEMS device.

This dissertation models the process of predicting conservative strength of an element design to ensure a certain level of safety with coupon and element tests and simulates the process to quantify the effects of coupon and element tests.

Estimating reliability of a structure with multiple failure modes for probabilistic structural design

Another issue of this dissertation is probabilistic design of structures with multiple failure modes. Structural design with multiple failure modes benefits by applying probabilistic design approach. Qu *et al.* [36] studied that design of cryogenic tanks made by composite materials that has two competing failure modes: matrix cracking by the residual thermal strains and mechanical failure due to excessive stress in the fiber. This study concluded that the high PFs of deterministic designs motivate probabilistic design. Acar *et al.* [82] investigated the tradeoff between airplane design safety and design weight for a wing and a horizontal tail. The study showed that balancing safety margins between the components with probabilistic design gives a lighter and even safer design than applying the same safety margins for all components.

In probabilistic design, taking account of the effect of structural tests on reducing error in evaluating reliability of structures is an important issue as mentioned in the previous section. Designers rely on computational models to predict failures of design and to evaluate reliability according to uncertainties. However, computational models have epistemic uncertainty due to the lack of knowledge of physics [69]. Structural tests are followed to reduce the epistemic uncertainty in computational models by calibrating the models. By reducing the uncertainty in computational models, error in evaluating reliability is also reduced as a consequence of tests. To clearly quantify the effect of

tests on reducing the error in reliability calculation, the contribution of epistemic uncertainty has to be separated from that of the other uncertainties.

Separated treatment of epistemic uncertainty has been introduced by literatures. Noh *et al*. [37] quantified the contribution of epistemic uncertainty caused by the finite number of samples in input parameters as uncertainty in output. Matsumura *et al*. [75] and Villanueva *et al*. [76] considered the effect of epistemic uncertainty in a computer model on estimating PF of an integrated thermal protection system of a space vehicle and obtained a distribution of the PF to model the effect of epistemic uncertainty on the PF.

In this dissertation, since a method for multiple failure modes is needed to be developed, the epistemic uncertainties in potential failure modes are modeled using a joint PDF and the effect on reducing the uncertainty by tests is modeled by obtaining a distribution of PF. The effect of tests on reducing the uncertainty is translated into the PF distribution.

When we have two failure modes, we have two epistemic uncertainties. However, a single test is usually available due to restricted budget for testing [7,18] and only one failure mode is observed from the test. It may appear that only one of two errors can be reduced by the test, a strategy to reduce error in both failure predictions with a single test is developed.

A thin composite panel with a hole with buckling and strength failure modes is used as an application example of this study. Composite materials have been widely used for aircraft structures due to superior stiffness per unit weight and better corrosion and fatigue resistance than aluminum alloys [71]. The recently developed Boeing 787

and Airbus 350 aircraft use composite materials for approximately 50% of structural weight [8]. However, these good properties come at the cost of additional stiffness and strength parameters that need to be estimated, and which are often correlated [14]. Therefore, correlations between composite material properties are taken into account. Since buckling failure of the curved composite panel is very sensitive to imperfections [72,73,74], uncertainties in geometric imperfections are taken into account for calculating PF. Nonlinear analysis is used to predict buckling load and strain using Abaqus. [79].

Another interesting issue of applying probabilistic design approach is to consider statistical correlation between failure modes when calculating PF. We propose a method to calculate PF by using decomposed distributions of structural responses without losing statistical correlation between failure modes. It has an obvious advantage that building the decomposed distributions requires estimating only a handful of parameters for the decomposed distributions.

The Effect of Ignoring Dependence between Failure Modes for Calculating System Reliability

Evaluating system reliability has been recognized as an important step in design. Although many reliability analysis methods have been developed, calculating system reliability including dependence between failure modes is still challenging [80].

Reliability analysis methods can largely be categorized by sampling-based methods (e.g., Monte Carlo Simulation (MCS), importance sampling and surrogate-based methods) and analytical methods (e.g., first-order reliability method (FORM) and second-order reliability method (SORM)).

MCS is a universal method, but it can be computationally expensive to achieve a reasonable accuracy, even when using importance sampling techniques to reduce the variance of MCS [41-43]. To evaluate reliability, surrogate-based methods have been developed to reduce computational cost [44]. Sampling-based methods using surrogates can model dependence between failure modes, but the computational cost of constructing surrogate models increases rapidly with dimensions, often called the curse of dimensionality [45].

Since analytical methods are computationally efficient, they are computationally favorable to calculate reliability [43,46]. However, they have difficulties in accounting for dependence between failure modes. Consequently, approximate approaches, such as the lower-upper bound method [47-49] and PNET method [56], have been developed.

However, it is not well known that dependence between failure events can be weak when PF is low [38]. In other words, the effect of dependence between failure events can be ignored at a high reliability level.

Often structures are required to be highly reliable [39]. For example, the U.S. Army's introduction of a structural fatigue reliability criterion for rotorcraft has been interpreted as a requirement for component lifetime reliability of 0.999999 [40]. With such a high level of reliability, failures are extremely rare events. For such rare events, dependence between failure modes often becomes weak.

Ignoring dependence between input uncertainties can result in large errors in calculating system reliability [42]. Consequently modeling and identifying dependence between input model uncertainty is an important issue [37,50]. However, surprisingly,

ignoring dependence between failure modes, which is recognizable as dependence between output uncertainties, may not result in large errors in system reliability.

In this dissertation, the error in calculating system reliability on the strength of dependence between two failure modes and the ratio between the two marginal failure modes is investigated. For varying strength of dependence and the ratio between two marginal failure modes, the error due to ignoring dependence is calculated in terms of system reliability. The errors in system PF and in system reliability are presented. The reason of the behavior of the error will be explained. To study the effects of different dependence models, copulas are introduced and applied to define various dependences. A RBDO problem of two trusses is solved with two ways of calculating system reliability, with and without considering dependence. The effects of ignoring dependence on the optimal solution and the corresponding design weight of the RBDO problem are shown.

Objectives

The main objectives of this dissertation are as follows:

1. Developing a method to estimate a conservative element strength for required safety level and quantifying the effect of the multi-stage testing on reducing design conservativeness and the corresponding design weight while ensuring a certain safety level in terms of the number of coupon tests and element tests.
2. Developing a strategy to include the effect of tests and to efficiently reduce the error on calculating system reliability of a curved composite panel with correlated buckling and strength failure modes with a single structural test.
3. Investigating the effect of ignoring dependence between failure modes on evaluating system reliability in terms of the dependence strength, the dependence model and the ratio between individual PFs with various examples using copulas.

Outline

Chapter 2 introduces a strategy of predicting conservative element strength to achieve a certain safety level. The effects of coupon and element tests on reducing uncertainty in predicting the element strength and the corresponding conservativeness and design weight are demonstrated. Chapter 2 allows us to identify uncertainty sources in predicting element strength and to model the identified uncertainties. Then the way of using the quantified uncertainty to predict the conservative element strength is presented. From creating a model simulating the prediction process, the effects of tests on the conservativeness in the element strength prediction and the corresponding expected design weight are quantified. The effects of tests on different situations are also simulated and studied using the model.

Chapter 3 introduces the effect of an element test on the PF distribution with correlated multiple failure modes. Two typical static failure modes, correlated buckling and strength failure modes and their errors in numerical model to predict the failures are modeled. The effect of errors to estimate PF of a structure is quantified. Also the contribution of a single element test to reduce the errors in the numerical model is calculated and translated into a distribution of PF. A decomposition method to consider correlation between failure modes is presented and is used to calculate system PF. As demonstration examples, one simply supported beam and a curved composite panel with a hole are used.

Chapter 4 shows the effect of ignoring dependence between failure modes on evaluating system reliability. In this chapter, structures having a specific dependence model between two failure modes and system reliability are assumed and the errors due to ignoring dependence are measured as a function of the dependence model and the

system reliability. Dependence is typically modeled with a joint PDF and a dependence measure, such as the linear correlation coefficient or Kendall's tau. For investigating the effects of various dependence models, as well as the widely known bivariate normal distribution, copulas are employed to model various possible joint PDFs parametrically.

Finally in Chapter 5 we provide concluding remarks and future work suggestions.

CHAPTER 2
HOW COUPON AND ELEMENT TESTS REDUCE CONSERVATIVENESS IN ELEMENT FAILURE PREDICTION

Motivation and Scope

Uncertainty has always been a major concern in structural design. For example, predicting the strength of a structural element has two major sources of epistemic uncertainty (uncertainty associated with the lack of information). The first comes from errors in failure prediction based on calculated stresses and a failure theory. The second source is errors in measuring variability of material properties. Coupon tests are performed to measure material variability, but the estimated variability also has error due to the limited number of coupons.

In this dissertation, we assume that with an infinite number of coupons and elements, the epistemic uncertainty associated with samples and failure theory can be eliminated. With a finite number of tests, the epistemic uncertainty is compensated for by using a conservative mean value at the 95% confidence level, in the context of the B-basis. The aleatory uncertainty can then be compensated for either by 90% of the population or by specifying probabilities of failure. We focus on the effect of the number of tests on the conservative estimate of element strength and the resulting weight penalty compared to the case with an infinite number of tests. To have the conservative estimate, we predict the mean element strength and its uncertainty by combining two uncertainties from coupon tests and a failure theory, using a convolution integral. Then, Bayesian inference is incorporated with element tests in order to reduce the epistemic uncertainty. With the proposed two-stage uncertainty model, it is possible to identify the effect of two types of tests on reducing uncertainty and corresponding conservativeness and weight penalty.

The chapter is composed of six sections. First section is to introduce the building-block test process used in this dissertation, which is composed of coupon and element test stages, and sources of uncertainty. Second section is to provide uncertainty modeling of the building-block test process to estimate the element strength and its uncertainty. Third section is to introduce different measures that are used to evaluate the efficiency of different tests. This third section has three subsections: coupon tests, element design and element tests. Fourth section introduces different measures that are used to evaluate the efficiency of different tests. Fifth section is to presents numerical results. Finally, summary of this chapter is presented.

Uncertainty Sources in Design with Building-Block Approach

For aircraft structures, the building-block test process (Fig. 2-1) is used to find design errors and to reduce uncertainties in design and manufacturing. At each level, analytical/numerical models are calibrated to account for discrepancies between model prediction and test results. Since the errors are unknown at the modeling stage, they may be modeled as uncertainty (epistemic), and test results may be used to reduce the uncertainty. Starting from simple coupon tests at the bottom level, structural complexity gradually increases further up the building-block pyramid. The number of tests gradually reduces from bottom to top; for example, 50 coupons, 3 elements, and 1 component. In higher-level tests, it is difficult to understand deviations from analytical predictions, tests are more expensive and any design modification can be expensive. The building-block test process is designed to detect modeling errors at a lowest level.

Although building-block tests are designed to reduce uncertainty, it is difficult to quantify how much tests in each level can contribute to uncertainty reduction, which is the main objective of this dissertation. Once the contribution of tests to uncertainty

reduction is understood, a design engineer can decide how to allocate resources to different levels in order to achieve the target reliability at minimum cost.

Although the actual building-block test process has many levels, this dissertation only considers coupon and element tests to demonstrate the effect of these tests on uncertainty reduction. Table 2-1 shows the objectives of these two tests and the sources of uncertainty.

In this dissertation, the failure stress of a structural element is simulated with randomly generated test results. True distributions are used only for generating test samples and assessing the estimated failure stress.

Modeling Uncertainty in the Building-Block Test Process

In order to model the two-level building-block test process, it is assumed that the strength of coupons and elements follows a normal distribution due to material variability. This assumption can easily be removed when actual test results are available and the type of distribution can be identified using various statistical methods, such as the one in MIL-HDBK [2]. In the following subsections, uncertainties at each stage are modeled.

Coupon Test: Modeling Uncertainty in Estimating Statistical Properties

Due to inherent variability, the material strength shows a statistical distribution. Coupon tests are conducted to estimate the distribution and to determine regulatory (e.g., FAA) strength allowables (e.g., A-basis or B-basis) that compensate for the uncertainty. It is assumed that the true material strength, $\hat{\tau}_{c,true}$, follows a normal distribution, as

$$\hat{\tau}_{c,true} \sim N\left(\mu_{c,true}, \sigma_{c,true}\right) \tag{2-1}$$

where $\mu_{c,true}$ and $\sigma_{c,true}$ are, respectively, the mean and standard deviation of $\hat{\tau}_{c,true}$. The circumflex symbol represents a random variable. The subscript "*c*" is used to denote coupons. In this dissertation, Eq. (2-1) is only used for the purpose of simulating coupon tests; the true distribution is unknown to the designer.

Since the true distribution parameters are estimated with a finite number of coupons, the estimated parameters have sampling uncertainty (or error). Thus, it is natural to consider these parameters as distributions rather than deterministic values. In this dissertation, this estimated distribution is called the possible true distribution (PTD) of the parameter. For example, if $\mu_{c,true}$ is estimated from 50 coupons, with a sample mean of 1.02 and sample standard deviation of 0.1, then the PTD of the mean is a distribution following $N(1.02, 0.1)$.

In this setting, the estimated material strength essentially becomes a distribution of distributions. The PTD of material strength can be obtained using a double-loop Monte Carlo simulation (MCS), as shown in Fig. 2-2. In the figure, the outer loop generates N samples of the two distribution parameters, from which N pairs of normal distributions, $N(\mu_i, \sigma_i)$, can be defined. In the inner loop, M samples of material strengths are generated from each $N(\mu_i, \sigma_i)$. Then, all $N \times M$ samples are used to obtain the PTD of material strength, which includes both material variability and sampling errors.

In order to model the above MCS process analytically, the PTD of material strength, $\hat{\tau}_{c,Ptrue}$, is firstly defined as a conditional distribution as

$$\hat{\tau}_{c,Ptrue} \left| \left(\hat{\mu}_{c,Ptrue} = \mu_{c,Ptrue}, \hat{\sigma}_{c,Ptrue} = \sigma_{c,Ptrue} \right) \sim N\left(\mu_{c,Ptrue}, \sigma_{c,Ptrue} \right) \right. \tag{2-2}$$

where the left-hand side is a conditional random variable given $\mu_{c,Ptrue}$ and $\sigma_{c,Ptrue}$. Since $\hat{\mu}_{c,Ptrue}$ and $\hat{\sigma}_{c,Ptrue}$ are random, Eq. (2-2) corresponds to an incident of possible true distributions. In Fig. 2-2, randomly generated μ_i and σ_i correspond to $\mu_{c,Ptrue}$ and $\sigma_{c,Ptrue}$, respectively.

Note that $\hat{\mu}_{c,Ptrue}$ and $\hat{\sigma}_{c,Ptrue}$ depend on the number of coupons. With n_c coupons, $\hat{\mu}_{c,Ptrue}$ is nothing but the distribution of the sample mean and can be estimated as

$$\hat{\mu}_{c,Ptrue} \sim N\left(\mu_{c,test}, \frac{\sigma_{c,test}}{\sqrt{n_c}}\right) \tag{2-3}$$

where $\mu_{c,test}$ and $\sigma_{c,test}$ are, respectively, the mean and standard deviation of coupons. With an infinite number of coupons, $\hat{\mu}_{c,Ptrue}$ will become a deterministic value; i.e., no sampling error.

It is also well-known that the standard deviation $\hat{\sigma}_{c,Ptrue}$ follows a chi-distribution of order $n_c - 1$. In a way similar to the mean, $\hat{\sigma}_{c,Ptrue}$ can be estimated as

$$\hat{\sigma}_{c,Ptrue} = \frac{\sigma_{c,test}}{\sqrt{n_c - 1}} \chi\left(n_c - 1\right) \tag{2-4}$$

where $\chi\left(n_c - 1\right)$ is the chi-distribution of the order $n_c - 1$.

Let $f_{\mu c,Ptrue}\left(\mu_{c,Ptrue}\right)$ and $f_{\sigma c,Ptrue}\left(\sigma_{c,Ptrue}\right)$ be the PDFs of $\hat{\mu}_{c,Ptrue}$ and $\hat{\sigma}_{c,Ptrue}$, respectively. Then, the PDF of $\hat{\tau}_{c,Ptrue}$ is derived as

$$\begin{aligned} & f_{c,Ptrue}\left(\tau_{c,Ptrue}\right) \\ & = \int_0^\infty \int_{-\infty}^\infty \varphi\left(\tau_{c,Ptrue} \mid \mu_{c,Ptrue}, \sigma_{c,Ptrue}\right) f_{\mu c,Ptrue}\left(\mu_{c,Ptrue}\right) f_{\sigma c,Ptrue}\left(\sigma_{c,Ptrue}\right) d\mu_{c,Ptrue} d\sigma_{c,Ptrue} \end{aligned} \tag{2-5}$$

where the notation $\varphi(x \mid a,b)$ denotes the value of a normal PDF with mean *a* and standard deviation *b* at *x*.

Figure 2-3 compares the PDF of $\hat{\tau}_{c,true} \sim N(1.1, 0.077)$ with that of $\hat{\tau}_{c,Ptrue}$ with different numbers of coupons. In the case of 30 coupons, the samples have $\mu_{c,test} = 1.053$ and $\sigma_{c,test} = 0.096$. Using Eqs. (2-3) and (2-4), the standard deviations of $\hat{\mu}_{c,Ptrue}$ and $\hat{\sigma}_{c,Ptrue}$ are estimated to be 0.018 and 0.013, respectively, which reflect the randomness of the samples. Note that in the case of 30 coupons, the mean was slightly underestimated, but a large standard deviation compensates for it. In the case of 80 coupons, the samples have $\mu_{c,test} = 1.113$ and $\sigma_{c,test} = 0.083$. The standard deviations of $\hat{\mu}_{c,Ptrue}$ and $\hat{\sigma}_{c,Ptrue}$ are 0.009 and 0.007, respectively. As expected, $\hat{\tau}_{c,Ptrue}$ with 80 coupons yields a narrower estimate than that of 30 coupons.

Element Design: Combining Uncertainties

To design a structural element, the material strength from coupon tests must be generalized to multi-axial stress states using a failure theory. Since the failure theory is not perfect, additional error (i.e., epistemic uncertainty) is introduced, which needs to be combined with the sampling error in the coupon test. Since the uncertainty in element strength can be represented using the distributions of the mean and standard deviation, the uncertainties of these two random variables are modeled separately [26].

A failure theory provides a relation between uni-axial strength and multi-axial strength. In this dissertation, this relation is represented using a prediction factor $k_{3d,true}$ as

$$\tau_{e,true} = k_{3d,true}\tau_{c,true} \tag{2-6}$$

where $\tau_{c,true}$ is a true uni-axial material strength, and $\tau_{e,true}$ is a true multi-axial equivalent strength. Subscript "*e*" is used to denote that the variable is for an element. For example, when the von Mises criterion is used, $k_{3d,true}=1$. The relation between the two mean values can be obtained from Eq. (2-6) as

$$\mu_{e,true}=k_{3d,true}\mu_{c,true} \tag{2-7}$$

Again, $k_{3d,true}$ is unknown to designers; only its estimate $k_{3d,calc}$ is given from the failure theory. Therefore, the epistemic uncertainty in the failure theory can be represented using the PTD of the prediction factor as

$$\hat{k}_{3d,Ptrue}=\left(1-\hat{e}_{k,Ptrue}\right)k_{3d,calc} \tag{2-8}$$

where error $\hat{e}_{k,Ptrue}$ is assumed to follow a uniform distribution with bounds of $\pm b_e$, which reflect the designer's confidence in the failure theory. Then, the designer's estimated relationship corresponding to Eq. (2-7) can be written as

$$\hat{\mu}_{e,Ptrue}=\hat{k}_{3d,Ptrue}\hat{\mu}_{c,Ptrue} \tag{2-9}$$

Figure 2-4 shows the process of obtaining $\hat{\mu}_{e,Ptrue}$ through MCS. First, *N* samples from $\hat{\mu}_{c,Ptrue}$ and *M* samples from $\hat{k}_{3d,Ptrue}$ are generated. Then, $\hat{\mu}_{e,Ptrue}$ is estimated from *N*×*M* samples that are obtained by taking every possible combination of the two sets of samples.

In this dissertation, a convolution integral is used to calculate the PDF of $\hat{\mu}_{e,Ptrue}$. The convolution integral provides an accurate PDF using numerical integration, whereas MCS brings in additional uncertainty. A comparison between MCS and the

convolution integral is given in the example section. In the case of a normally distributed mean and uniformly distributed error, the PDF of $\hat{\mu}_{e,Ptrue}$ can be written as

$$f_{\mu e,Ptrue}\left(\mu_{e,Ptrue}\right)=\int_{\frac{\mu_{e,Ptrue}}{(1-b_e)}}^{\frac{\mu_{e,Ptrue}}{(1+b_e)}}\frac{1}{2b_e\mu_{c,Ptrue}}\varphi\left(\mu_{c,Ptrue}\mid\mu_{c,test},\frac{\sigma_{c,test}}{\sqrt{n_c}}\right)d\mu_{c,Ptrue} \tag{2-10}$$

where b_e is error bound of the $\hat{e}_{k,Ptrue}$ and $k_{3d,calc}=1$ is assumed. See Appendix A for detailed derivations. The integral domain is divided to 200 segments, and the integral is evaluated using Gaussian quadrature with 3 points for each of the 200 segments.

Figure 2-5 shows the PDF of typical $\hat{\mu}_{e,Ptrue}$ for n_c = 10 and 50. As the number of coupons increases, the PDF approaches a uniform distribution, which corresponds to the uncertainty in the failure theory. When the number of coupons is small, the distribution has a long tail because of sampling errors in the coupon tests. This $\hat{\mu}_{e,Ptrue}$ serves as the prior distribution representing the designer's knowledge before element tests.

Unlike the mean, there is only a weak relationship between the standard deviation of coupon strength and that of element strength. Usually test conditions are well controlled to minimize uncertainty; the standard deviation of the test is substantially smaller than that of material properties. The distribution of $\hat{\sigma}_{e,Ptrue}$ is defined as a uniform distribution with lower and upper bounds as

$$f_{\sigma e,Ptrue}\left(\sigma_{e,Ptrue}\right)=\frac{1}{\left(\sigma_e^{upper}-\sigma_e^{lower}\right)}I\left(\sigma_{e,Ptrue}\in\left[\sigma_e^{upper},\sigma_e^{lower}\right]\right) \tag{2-11}$$

where $I(\bullet)$ is the indicator function σ_e^{upper} and σ_e^{lower} are upper and lower bounds of the standard deviation of element strength, respectively. These bounds are estimated to cover a true standard deviation of the element test.

Element Test: Bayesian Inference to Reduce Errors

The PTDs in Eqs. (2-10) and (2-11) are the combined uncertainties from (a) material variability, (b) sampling errors in coupon tests and (c) error in the failure theory. Although material variability will always exist, the other two epistemic uncertainties can be reduced using element tests. In this section, the effect of element tests on reducing uncertainty is modeled using Bayesian inference.

For the purpose of Bayesian inference, Eqs. (2-10) and (2-11) are used as marginal prior distributions. Since no correlation information is available, these distributions are assumed to be independent. Therefore, the prior joint PDF is given as

$$f^{init}\left(\mu_{e,Ptrue},\sigma_{e,Ptrue}\right)=f_{\mu e,Ptrue}\left(\mu_{e,Ptrue}\right)\cdot f_{\sigma e,Ptrue}\left(\sigma_{e,Ptrue}\right) \tag{2-12}$$

In Bayesian inference, the updated joint PDF with n_e number of element tests is expressed as

$$f^{upd}\left(\mu_{e,Ptrue},\sigma_{e,Ptrue}\right)=\frac{1}{A}\prod_{i=1}^{n_e}\ell^{i}_{test}\left(\mu_{e,Ptrue},\sigma_{e,Ptrue}\right)f^{init}\left(\mu_{e,Ptrue},\sigma_{e,Ptrue}\right) \tag{2-13}$$

where A is a normalizing constant and $\ell^{i}_{test}\left(\mu_{e,Ptrue},\sigma_{e,Ptrue}\right)$ is the i[th] likelihood function for given $\mu_{e,Ptrue},\sigma_{e,Ptrue}$. From the assumption that the true element strength $\hat{\tau}_{e,true}$ follows a normal distribution and by ignoring errors associated with the test, the likelihood function can be defined as a probability of obtaining test result $\tau^{i}_{e,test}$ for given $\mu_{e,Ptrue}$ and $\sigma_{e,Ptrue}$ as

$$\ell^{i}_{test}\left(\mu_{e,Ptrue},\sigma_{e,Ptrue}\right)=\varphi\left(\tau^{i}_{e,test}\mid\mu_{e,Ptrue},\sigma_{e,Ptrue}\right) \tag{2-14}$$

Note that the likelihood function is not a probability distribution, but a conditional probability. The numerical scheme to evaluate the updated joint PDF is explained in Appendix B.

Using the updated joint PDF, the marginal PDFs of $\mu_{e,Ptrue}$ and $\sigma_{e,Ptrue}$ can be obtained as

$$f^{upd}_{\mu e,Ptrue}\left(\mu_{e,Ptrue}\right)=\int_{-\infty}^{\infty} f^{upd}\left(\mu_{e,Ptrue},\sigma_{e,Ptrue}\right)d\sigma_{e,Ptrue} \tag{2-15}$$

$$f^{upd}_{\sigma e,Ptrue}\left(\sigma_{e,Ptrue}\right)=\int_{-\infty}^{\infty} f^{upd}\left(\mu_{e,Ptrue},\sigma_{e,Ptrue}\right)d\mu_{e,Ptrue} \tag{2-16}$$

The above distributions represent the uncertainty in estimating the mean and standard deviation of the element strength. The standard deviations of distributions in Eqs. (2-15) and (2-16) are measures of remaining uncertainty after the element tests.

Conservative Prediction based on the Updated Possible True Distribution

In common practice, element strength prediction is updated with the lowest element test result of three tests and used as a design allowable. The process can be interpreted as applying a knockdown factor on the test average. In this paper, a conservative estimate of the mean element strength is used as a design allowable.

If a conservative estimate is wanted, the low 5th percentile of $f^{upd}_{\mu e,Ptrue}$ can be used for the 95% confidence level. The mean values of distributions in Eqs. (2-15) and (2-16) are, respectively, the estimate of the mean and standard deviation of element strength. The 5th percentile of the marginal PDF for the mean of element strength is expected to be less than the true mean of element strength with a 95% confidence level. The 5th percentile, $\tau_{0.05}$, is calculated using Eq. (2-15) as

$$\int_{-\infty}^{\tau_{0.05}} f^{upd}_{\mu e,Ptrue}\left(x\right)dx=0.05 \tag{2-17}$$

Figure 2-6 illustrates the effect of one element test on calculating the 5th percentile. In this illustration, we chose the coupon tests to have the true mean, and the element test to have the true mean of the element strength. Since the true mean of coupon test and the true mean of element test are assumed to 1 and 0.95, the element strength prediction based on failure theory is unconservative by 5%. However, by taking, the 5th percentile, the error in element strength prediction is compensated. Figure 2-6 shows the substantial reduction in uncertainty afforded even by a single element test. As a consequence, the 5th percentile is actually higher after the test, allowing a reduction in the weight. Note that the distribution is a marginal distribution of a posterior distribution so that it has a sharp peak.

The results shown in Figure 2-6 are merely an illustration for a particular set of coupon and element test result. To see a general observation, we repeated evaluating the 5th percentile for N random sets of coupon and element test results (N=100,000 here) and the distributions of the 5th percentiles shown in Fig. 2-7 were obtained. Due to the variability in test, the 5th percentile also has variability that is shown as the distributions in Fig. 2-7.

In Figure 2-7, the area of the gray shade is the probability of having an 5th percentile that is larger than the true mean element strength. Since design allowables, which are larger than the true mean, lead to unsafe design, the probability is referred as the probability of unsafe design (PUD) herein. PUD is calculated with the N random sets of test results as follows:

$$\mathrm{PUD} = \frac{1}{N}\sum_{i=1}^{N} I\left(\tau_{0.05}^{i} > \mu_{e,true}\right) \tag{2-18}$$

When we design the truss with the 5th percentile, we expect that the design will have PUD of 5%. However, it is not guaranteed since prior distribution affects the 5th percentile and the prior distribution is based on an element strength estimate using a failure theory. For example, a prior based on an un-conservative failure theory gives more weight for un-conservative errors than conservative errors. However, the tendency can be reduced by updating the prior with element tests. The effects of the prior on PUD are illustrated through examples.

Assessing the Merits of the Numbers of Element and Coupon Tests

The objective of this section is to assess the effect of coupon and element tests on reducing uncertainty, estimating design allowables and the corresponding weight penalty. For that purpose, a single set of test results is generated to calculate the 5th percentile and to compute the corresponding weight penalty due to conservativeness. These results are compared with the weight obtained with an infinite number of coupon and element tests. Since the results with a single set of tests are likely to be biased due to sampling error, the above process is repeated (100,000 times) to estimate the average weight penalty.

With an infinite number of tests, prediction should be the same with the true element mean, $\mu_{e,true}$, regardless of variability. If a truss member is designed with an axial load, the weight penalty due to the conservativeness in the 5th percentile is calculated as

$$w_i = \left(\frac{A^i_{0.05}}{A_\infty} - 1 \right) \times 100 = \left(\frac{F / \tau^i_{0.05}}{F / \mu_{e,true}} - 1 \right) \times 100 = \left(\frac{\mu_{e,true}}{\tau^i_{0.05}} - 1 \right) \times 100 \ (\%) \qquad (2\text{-}19)$$

where index *i* represents the *i*th set of tests results.

When w_i is 3% for (10/5), it means that a design with 10 coupon tests and 5 element tests is 3% heavier than a design with an infinite number of tests. Negative weight penalty indicates that the design is unsafe that the design allowable is larger than the true mean.

Figure 2-8 illustrates the weight penalty distribution, mean weight penalty, 95% weight penalty and PUD. The 0% weight penalty (the black filled circle) represents design weight with an infinite number of tests.

The mean of the weight penalty (the hollow circle) represents expected conservativeness in the design. The 95% weight penalty (the grey filled circle) is representing weight penalty for very conservative designs due to variability in tests. That can be interpreted as that the probability of having more conservative design weight than the 95% weight penalty is 5%. Those measures are calculated from N sets of test results (N = 100,000 here) as follows:

$$\mu_{0.05} = \frac{1}{N}\sum_{i=1}^{N} w_i \tag{2-20}$$

$$P_{0.95} = \frac{1}{N}\sum_{i=1}^{N} I\left(w_i \le w_{0.95}\right) \tag{2-21}$$

where i is the index of N test sets and the subscript 0.95 of $P_{0.95}$ represents that conservativeness in predicting element strength is 95% that $P_{0.95}$ is 0.95.

With N repetitions, N 5th percentiles are collected, and they are varied due to variability in test. Eq. (2-20) is to calculate the mean of weight penalty. Eq. (2-21) is to calculate the 95% percentile of weight penalty of the N sets of test results. For example, with 100,000 samples, 95th percentile $w_{0.95}$ is 95,000th 5th percentile of sorted samples in ascending order.

Since a design with a 5th percentile larger than the true mean element strength is defined as an unsafe design, PUD in Fig. 2-8 is exactly the same with PUD in Fig. 2-7 when N sets of test results for two distributions are the same.

This procedure needs to be performed for different realizations of the epistemic uncertainty. Here, for illustration, we repeat for four cases, 1% and 5% unconservative errors and 1% and 5% conservative errors. These appear to be sufficient to illustrate the effect of different values of the epistemic uncertainty.

Illustrative Examples for Estimating a Knockdown Factor based on Uncertainty Quantification

In this section, the effect of the number of tests is investigated in two steps. First, the conservative mean of the element strength is predicted using a single set of tests, after which the average prediction is estimated with multiple sets of tests.

The Effect of the Number of Tests with a Single set of Tests

In this section, estimation of mean element strength is illustrated with a single set of coupon and element tests. The test results were randomly generated from the true distributions defined in Table 2-2. The difference between the element mean and the coupon mean represents error in the failure theory, as assumed in Eq. (2-7). Since $k_{3d,calc} = 1.0$ is assumed in this dissertation and $k_{3d,true} = \mu_{e,true} / \mu_{c,true}$ is 0.95, the failure theory overestimates the element strength; that is, the error in the failure theory is unconservative. Randomly generated test results are given in Table 2-3. The coupon test column presents sample mean and sample standard deviation that will be used to generate coupon samples, and the element test column orderly presents element test results. For example, for 10 coupons and 3 elements (10/3), the mean and standard deviation of coupons were 0.972 and 0.091, respectively, and the first three data, 0.945,

0.955 and 0.987, are used as for three element test results. For four element test results, the first four data, 0.945, 0.955, 0.987 and 0.953 are used. The true distribution is only used for the purpose of simulating tests.

To estimate the mean of element strength, the prior is constructed based on the coupon test results and error bounds as shown in Eqs. (2-10) and (2-11). Table 2-4 gives the assumed error bounds b_e for the mean and $\left[\sigma_e^{lower}, \sigma_e^{upper}\right]$ for standard deviation. Recall that the error bounds represent the current estimate of the maximum error in the failure theory. Detailed procedure of numerical calculation is given in Appendix A.

Table 2-5 summarizes the 5th percentile value ($\tau_{0.05}$) and the weight penalty after Bayesian update. It is observed that the effect of element tests is more significant than that of coupon tests. As the number of element tests increases between n_e = 1 and 5, weight penalty decreases from 4-6% to 1.4-2.3%, and a 5th percentile strength converges to 0.95 monotonically. However the effect of the number of coupon tests is ambiguous and no clear trend is observed. This is because the error in the failure theory (Table 2-4) is much larger than the sampling error in coupons. For the cases of 50 and 90 coupons, n_e = 1 estimates more conservativeness than n_e = 0 because the particular element test results happen to be very conservative, as shown in Table 2-3 (0.896 and 0.917 from a normal distribution with the mean of 0.95 and the standard deviation of 0.0285).

The Effect of the Number of Tests averaged over Multiple Sets of Tests

The results from the previous subsection depend on the particular samples of coupons and elements. In order to measure the expected effect of tests, the same process is

repeated 100,000 times with randomly generated samples, from which 100,000 weight penalties are generated. The effect of the number of tests on the weight penalty is analyzed with three measurements, the mean and 95th percentile of the weight penalty and the probability of unsafe design (PUD). Two scenarios associated with epistemic uncertainty in the failure theory are considered.

The first scenario addresses the effect of relatively large epistemic uncertainty in the failure theory ($b_e = \pm 10\%$) compared to that in coupon samples. With 7% COV in material strength, the uncertainty in the mean coupon strength is small, even with ten coupons. The second scenario examines the effect of relatively small epistemic uncertainty in the failure theory ($b_e = \pm 2\%$). Each scenario is further divided into two cases: unconservative and conservative failure theory. The true mean of the element tests and its error bounds are set to reflect each scenario as shown in Table 2-6; the other settings are the same as the previous single set example.

The effect of the numbers of tests is related to the level of uncertainty in the coupon test and the failure theory. Increasing the number of coupon tests can reduce the uncertainty in the coupon test and the uncertainty in the failure theory can be reduced by increasing the number of element test. Since the uncertainty in predicting the 5th percentile is the combined uncertainty of these uncertainties, the contribution of each test is related to the relative degree of uncertainty. For example, if the uncertainty in the failure theory is larger than that of the coupon test, increasing the number of element tests is more efficient to reduce the combined uncertainty than increasing the number of coupon tests.

When the failure theory has relatively large epistemic uncertainty, the distributions of weight penalties as functions of the number of tests are shown in Fig. 2-9 for both conservative and unconservative failure theories. n_c=50 and n_e=3 are assumed as the nominal numbers of tests. The effects of the number of element and coupon tests are shown around the nominal numbers. It is shown that n_e is far more influential than n_c for shifting the distribution to a less conservative region and narrowing it.

With no element tests, the distribution is narrow, since it represents only the sampling uncertainty in 50 coupon tests. As the number of element tests increases, the distribution is first widened for a single element test, because a single test is quite variable, and then gradually narrowed. The updated distribution is also shifted closer to 0% weight penalty. For the unconservative case, Figure 2-9A, the shift is small because the conservativeness in the design with the unconservative failure theory is small. It is unusual that no element test distribution has 0% unsafe design even with un-conservative failure theory. This is because the prior distribution gives very conservative design allowable. As shown in Fig. 2-5, the prior distribution is similar to the uniform distribution, and the updated distribution is similar to a bell shaped normal distribution. If the prior and the updated distributions have the same standard deviation, the prior distribution has much conservative 5th percentile than that of the updated distribution, and the design allowable from the prior is much more conservative than that from the updated distribution. For example, 5th percentile of the uniform distribution with standard deviation of 1 is 0.1th percentile of the standard normal distribution. However, for the conservative case, Figure 2-9C, the shift is large since the conservative failure theory provides a very conservative design

Tables 2-7 and 2-8 summarize the distributions with three statistics–mean weight penalty, 95th percentile and PUD–in terms of the number of tests.

We first consider the case of minimal testing with only 10 coupon tests and no element tests. For the case of unconservative failure theory, shown in Table 2-7, minimal testing will cost us a 5.2% weight penalty on average, and a 2% chance that we will end up with unconservative design. For the case of conservative failure theory, in Table 2-8, the weight penalty shoots up to 16.3% and we do not run the chance of unconservative design. The weight penalties with the 95^{th} percentiles (corresponding to tests that happen to be on the conservative side) are about 10% higher.

With a single element test, the weight penalty drops significantly to 3.1% for the unconservative failure theory, in Table 2-7, and to 4.3% for the conservative case in Table 2-8. However, with only a single element test, we have a much higher chance of unconservative design: PUD of 10% and 5%, respectively. This is because the characteristics of failure theory is reflected on the prior and PUD. For un-conservative failure theory with 5% error, in Table 2-7, PUDs with a single element test are less than 10%, and they converge to 5% as the number of element tests increases. For conservative failure theory with 5% error, PUDs with a single element test are 5%, which are more conservative than PUDs with un-conservative failure theory presented in Table 2-7 as expected. However, the PUD is increased to 7% at 3 elements and then decreased to 6% for 5 elements. This unexpected behavior is related to the prior distribution with non-Gaussian shape, which is shown in Fig. 2-5, but PUDs always converge to 5% as the number of element tests increases. For no element tests, PUD is very close to zero. This is because of the difference in the shape of distribution. The 5th

percentile of prior, which resembles uniform distribution, is much more conservative than that of posterior distribution updated once with a single element test, which resembles Gaussian distribution, due to the shape of distribution. For example, the 5th percentile of a uniform distribution with standard deviation of 1 is 0.1^{th} percentile of a standard normal distribution. The weight penalties continue to drop substantially and the PUDs converge to 5% with more element tests. On the other hand, the effect of adding coupon tests is much smaller, and increasing coupon tests from 50 to 90 hardly make any difference.

The fact that, for this example, element tests are more important than coupon tests can be understood by observing the magnitude of two epistemic uncertainties. The variability in the coupon strength is 7% (see Table 2-2), so even with 10 coupon tests, the standard deviation of the mean coupon strength is only 2.2%, which is epistemic uncertainty in sampling. On the other hand, with ±10% error bounds, the standard deviation of the epistemic uncertainty in the failure theory is 5.8%. This is why element tests were more significant in reducing uncertainty. If, on the other hand, the failure theory was much more accurate, then element tests are expected to be less significant. For example, with ±2% error bounds, the magnitude of the epistemic uncertainty in failure theory is merely 1.2%. With such an accurate failure theory, it turns out that the number of coupon tests becomes more influential than the number of element tests

It turned out that increasing the number of element tests is more important than increasing the number of coupon tests when we have the large epistemic uncertainty (±10%) in the failure theory. However, when the epistemic uncertainty is small (±2%), the number of coupon tests becomes more influential than the number of element tests.

In parallel to Fig. 2-9, Fig. 2-10 shows a comparison between the effect of n_c and n_e on the weight penalty when the error in the failure theory is small. It is clearly seen that the effect of the number of coupon tests is more influential than the number of element tests for decreasing the chance of having very conservative designs and reducing the variation of design.

Compared to Tables 2-7 and 2-8, the increased accuracy of the failure theory reduces substantially the penalty associated with no element test. For 10 coupon tests, the weight penalty for no element test is reduced from 5.2% to 3.2% for unconservative error (Tables 2-7 and 2-9) and from 16.3% to 5.3% for conservative error (Tables 2-8 and 2-10). Also, because the epistemic uncertainties associated with the failure theory are not comparable to that in the mean of coupon tests, the contributions of the number of coupon and element tests become comparable. Increasing element tests from 1 to 5 for 10 coupon tests reduces the weight penalty from 3% to 2% (Table 2-9) and from 4.9% to 2.9% (Table 2-10). In comparison, for one element test, increasing the number of coupon tests from 10 to 90 reduces the weight penalty from 3% and 4.9% to 1.2% and 3.3%, respectively

For un-conservative failure theory with 1% error, shown in Table 2-9, PUDs increasingly converges to 5% through 1 to 5 element tests. For conservative failure theory with 1% error, Table 2-10, the behavior of PUD is also expected that PUDs increase as the number of element tests increases that the conservative prediction characteristics of failure theory is weaken as the number of element tests increases but the characteristics still remains with 5 element tests.

The above examples illustrate the effect of the number of tests to predict a design allowable using Bayesian inference. In the current design practice, the lowest element test result is used as a design allowable. A comparison between the two approaches is shown in the following section.

A Comparison between Current Statistical Method and the Proposed Bayesian Method

In the building-block process, the number of element tests is usually limited to three, due to the large number of structural elements to test [4,5]. In the current practice, analytical prediction of element strength based on failure theories is modified by applying the lowest ratio between the test results and the predicted failure stress. This process can be interpreted as applying an implicit knockdown factor to the average test failure stress to obtain a design allowable of element strength [4]. If the tests are repeated with different elements, the predicted failure stress will be changed as well as the implicit knockdown factor

In this dissertation, we propose a way to estimate a design allowable by adding certain conservativeness on estimated mean element strength using Bayesian inference. Bayesian inference has a strong point to combine information from different sources [81]. In the proposed method, we combine confidence interval information from analytical prediction (prior) with data from element tests while the current practice relies on data from element tests.

To compare the two approaches, the mean weight penalties are matched, by which we can compare the achieved safety for the same weight penalty in terms of PUD. For the current method, the lowest element strength of three is taken as the

conservative element strength so that the probability of being larger than the true mean is 12.5%.

$$0.125 = \Pr\left(\tau_{lowest} \geq \mu_{e,true}\right) \tag{2-22}$$

For the proposed method, since the conservative element strength is the 5th percentile of the mean element strength $\tau_{0.05}$, the probability can be calculated as

$$P_{Bayes} = \Pr\left(k\tau_{0.05} \leq \mu_{e,true}\right) \tag{2-23}$$

Note that the constant *k* is used to match their mean weight penalties. As we do in the previous examples, the weights of penalty for both methods are calculated using MCS with 100,000 samples.

$$\text{For current method} \qquad w_{i,curr} = \left(\frac{\mu_{e,true}}{\tau_{lowest}} - 1\right) \times 100\ (\%) \tag{2-24}$$

$$\text{For the proposed method} \quad w_i = \left(\frac{\mu_{e,true}}{k\tau_{0.05}^{i}} - 1\right) \times 100\ (\%) \tag{2-25}$$

where *i* represent index of a sample and the subscript curr represents current method.

Table 2-11 presents mean and 95th percentile of weight penalty for the proposed and current method. Both methods use three element tests, Ne=3. Since the proposed method combines the information from analytical prediction with data from coupon, the effect of the number of coupon tests is shown.

Figure 2-11. shows the distributions of weight penalty for the proposed and current method, and Table 2-11 characterizes the distribution with PUD representing safety and 95 percentile of weight penalty factor representing extreme cases for both methods. The proposed method shows better results in both measures. For PUD, the proposed method has at least 5% less PUD than current method; that is, the proposed method is

safer than current method by at least by 5%. For 95th percentile of weight penalty, the proposed method is less at least 0.7% and at most 3%. For cases of 5% errors in prediction, the number of coupon test is very limited.

The Accuracy of a Convolution Integral for Calculating a Conditional Distribution

It has been shown that double-loop MCS can be used to calculate the distribution in Eqs. (2-5) and (2-10) as shown in Figs. 2-2 and 2-4. However, MCS has a computational challenge in the tail region (low-probability region) as well as sampling error. For example, a 10^{-4} level of probability can be hardly estimated with 10,000 samples. Different from MCS, a convolution integral can calculate a nearly exact distribution without having sampling errors. In this section, the accuracy of the convolution integral is compared with that of MCS.

In order to illustrate the advantage of the convolution integral, the probability of the product of two random variables, $\hat{Z} = \hat{X} \times \hat{Y}$, are used. It is assumed that the two independent random variables are defined as $\hat{X} \sim N(1.1, 0.0096)$ and $\hat{Y} \sim U(0.9, 1.1)$. For MCS, one million samples are used to evaluate the probability of *Z* values at 0.955 and 0.975. Since MCS has sampling error, this process is repeated 1,000 times; the mean and coefficient of variation are listed in Table 2-12. For the convolution integral, the entire range is divided by 50 segments, and three-point Gauss quadrature in each segment is used in integrating Eq. (2-10) with b_e=0.1, $\mu_{c,test=}1.1$, and $\sigma_{c,test} / \sqrt{n_c} = 0.0096$. The results only differ by 0.2% when 400 segments are used. Different from MCS, there is no need for repetition because convolution integration does not have sampling error.

When the probability is of the order of 10^{-4}, MCS has about a 3.9% coefficient of variation (COV), while the convolution integral shows a very little calculation error.

When the probability is to the order of 10^{-7}, the MCS with 1 million samples is not meaningful, as reflected in the COV value of 210%. However, the convolution integral is still accurate, and the value can be obtained by a one-time calculation. Note that the estimated error in the mean PF with 1000 repetitions can be calculated as $4.93\times10^{-7}/1000^{0.5} = 1.56\times10^{-8}$.

Effect of the Number of Coupon Tests on Weight Following FAA Regulations

While from the standpoint of uncertainty reduction element tests may be more useful than coupon tests, there is substantial weight penalty for having a small number of coupon tests. This is due to the FAA regulations specifying the required conservativeness in failure stress. The regulations, (FAR 25.613) specify conservative material properties, called A-basis or B-basis that must be used as design allowables.

In this section we illustrate the effect of the number of coupon tests on design weight, calculating the required sectional area of a simple tension bar using the B-basis. The B-basis value is a statistically based material property which satisfying a 95% lower confidence bound on the tenth percentile of a specified population of measurements. Obviously, when the number of coupon tests is small, the 95% confidence bounds are wider. Indeed, the regulations specify that the B-basis allowable is given as

$$\tau_{B-basis} = \mu_{c,test} - k_B \sigma_{c,test} \tag{2-26}$$

where k_B is given as a function of the number of coupon in Table 8.5.10 of the Composite Material Handbook [2].

We again use the parameters, $\mu_{c,true}$ = 1.0, $\sigma_{c,true}$ =0.07 (COV 7%), $\mu_{e,true}$ =1.05, and $\sigma_{e,true}$ =0.0315 (COV 3%), to generate coupon test results and calculate a required area to sustain a unit force with B-basis allowable as shown in Eq. (2-27).

$$A_{design} = \frac{1}{\tau_{B-basis}} \tag{2-27}$$

We calculate average required area as function of the number of tests with 1 million repetitions of tests results.

Table 2-13 shows that the mean of calculated design area with 90 coupon tests is 6.2% lower than the mean of calculated design area with 10 coupon tests. Another adverse aspect of a small number of coupon tests on design is variability of the design. As seen in Table 2-13, design based on 10 coupon tests has 5 times larger standard deviation than design with 90 tests. If we take the 99th percentile of the 1 million samples, as a worst case representative, we obtain 1.343, 1.173, and 1.150 for 10, 50, and 90 tests, respectively.

Summary

In this chapter, the effect of the number of coupon and element tests on reducing conservativeness and weight penalties due to the uncertainty in structural element strength was studied. Two sources of epistemic uncertainties were considered: (a) the sampling uncertainty in measuring material variability and (b) the uncertainty in the failure theory. A large number of coupons reduce the uncertainty in measuring material variability, while element tests reduce the uncertainty in the failure theory. These uncertainties were combined using the convolution integral, which is more accurate and robust than MCS. Then, Bayesian inference was used to update this uncertainty with element test results. Because test results can vary, a large number of simulations were used to obtain mean performance and distributions.

For a typical case of ±10% uncertainty bounds on the failure theory, 5% actual error, 7% and 3% coefficient of variation in material strength and element strength,

element tests were found to be very important in reducing weight penalties from about 15% with no tests, to about 2% with five element tests. The effect of the number of coupon tests was much smaller because sampling uncertainty was much smaller than the uncertainty in the failure theory. When the failure theory was much more accurate (±2% confidence bounds and 1% actual error), the effect of the number of coupons became comparable to that of element tests. The methodology developed would thus allow designers to estimate the weight benefits of tests and improvements in failure predictions.

Table 2-1. Sources of uncertainty in estimating element strength with building-block test process.

Test stage	Objectives	Uncertainty sources
Coupon test	Estimate nominal value and variability of material failure strength	Variability in material strength and sampling error due to a finite number of coupons
Element design	Estimate nominal multi-axial failure strength based on a failure theory	Incomplete knowledge of failure mechanism: error in failure theory
Element test	Reduce uncertainty in the multi-axial strength	Sampling error due to a finite number of elements

Table 2-2. True distributions of coupon and element tests

Test	Distribution	Parameters
Coupon test	Normal	$\mu_{c,true}$ = 1.0, COV 7%
Element test	Normal	$\mu_{e,true}$ = 0.95, COV 3%

Table 2-3. Statistics for coupon and element tests

No. of coupon tests	Coupon test	Element tests (order by sequence)
10	$\mu_{c,test}$ = 0.972 , $\sigma_{c,test}$ = 0.091	0.945, 0.955, 0.987, 0.953, 0.935 $\mu_{e,test}$ = 0.955 , $\sigma_{e,test}$ = 0.0193
50	$\mu_{c,test}$ = 1.004 , $\sigma_{c,test}$ = 0.073	0.896, 0.981, 0.939, 0.998, 0.957 $\mu_{e,test}$ = 0.954 , $\sigma_{e,test}$ = 0.039
90	$\mu_{c,test}$ = 1.001 , $\sigma_{c,test}$ = 0.070	0.917, 0.989, 0.954, 0.939, 0.948 $\mu_{e,test}$ = 0.949 , $\sigma_{e,test}$ = 0.026

Table 2-4. Error distributions of element tests

Error	Distribution	Bounds
b_e	Uniform	$\pm 10\%$
$\left[\sigma_e^{lower}, \sigma_e^{upper}\right]$	Uniform	$[0, 0.04]$

Table 2-5. Estimates of the conservative element strength and the resulting weight penalty (compared to infinite number of tests) from a single set of test results ($\mu_{e,true}$ =0.95: Unconservative 5% error in failure theory)

		Ne=0	Ne=1	Ne=3	Ne=5
5th percentile	Nc=10	0.872	0.910	0.936	0.936
Weight penalty		8.8%	4.3%	1.4%	1.4%
5th percentile	Nc=50	0.911	0.893	0.912	0.929
Weight penalty		4.1%	6.2%	4.0%	2.2%
5th percentile	Nc=90	0.910	0.903	0.923	0.927
Weight penalty		4.3%	5.1%	2.8%	2.3%

Table 2-6. Four scenarios associated with epistemic uncertainty in failure theory and corresponding example settings (COV of 7% in material strength is assumed)

Magnitude of error in failure theory	Failure theory	True mean of element test	Error bound
Large epistemic uncertainty in failure theory	Unconservative	$\mu_{e,true}$ = 0.95	$b_e = \pm 10\%$ (standard deviation of 5.8%)
	Conservative	$\mu_{e,true}$ = 1.05	
Small epistemic uncertainty in failure theory	Unconservative	$\mu_{e,true}$ = 0.99	$b_e = \pm 2\%$ (standard deviation of 1.2%)
	Conservative	$\mu_{e,true}$ = 1.01	

Table 2-7. Mean, 95th percentile of weight penalties and probability of unsafe design (PUD) ($\mu_{e,true}$ =0.95: Unconservative 5% error in failure theory)

Measures		Ne=0	Ne=1	Ne=3	Ne=5
Mean	Nc=10	5.2%	3.1%	2.5%	2.1%
	Nc=50	4.5%	3.1%	2.5%	2.1%
	Nc=90	4.5%	3.1%	2.5%	2.1%
95th perc. of weight penalty factor	Nc=10	9.3%	7.1%	5.2%	4.3%
	Nc=50	6.2%	6.1%	5.0%	4.3%
	Nc=90	5.7%	5.9%	5.0%	4.3%
Probability of unsafe design (PUD)	Nc=10	2%	10%	8%	7%
	Nc=50	0%	9%	7%	6%
	Nc=90	0%	9%	7%	6%

Table 2-8. Mean, 95th percentile of weight penalties and probability of unsafe design (PUD) ($\mu_{e,true}$ =1.05: Conservative 5% error in failure theory)

Measures		Ne=0	Ne=1	Ne=3	Ne=5
Mean	Nc=10	16.3%	4.3%	2.7%	2.2%
	Nc=50	15.5%	4.2%	2.6%	2.1%
	Nc=90	15.4%	4.2%	2.6%	2.1%
95th perc. of weight penalty factor	Nc=10	20.8%	9.3%	5.8%	4.5%
	Nc=50	17.4%	9.5%	5.7%	4.5%
	Nc=90	16.8%	9.5%	5.7%	4.5%
Probability of unsafe design (PUD)	Nc=10	0%	5%	6%	6%
	Nc=50	0%	5%	7%	6%
	Nc=90	0%	5%	7%	6%

Table 2-9. Mean, 95th percentile of weight penalties and probability of unsafe design (PUD) ($\mu_{e,true}$ =0.99: Unconservative 1% error in failure theory)

		Ne=0	Ne=1	Ne=3	Ne=5
Mean	Nc=10	3.2%	3.0%	2.4%	2.0%
	Nc=50	1.5%	1.5%	1.4%	1.3%
	Nc=90	1.3%	1.2%	1.2%	1.1%
95th perc. of weight penalty factor	Nc=10	7.4%	6.8%	5.4%	4.3%
	Nc=50	3.2%	3.1%	2.9%	2.7%
	Nc=90	2.5%	2.5%	2.4%	2.3%
Probability of unsafe design (PUD)	Nc=10	10%	9%	8%	7%
	Nc=50	7%	6%	7%	7%
	Nc=90	5%	5%	6%	6%

Table 2-10. Mean, 95th percentile of weight penalties and probability of unsafe design (PUD) ($\mu_{e,true}$ =1.01: Conservative 1% error in failure theory)

		Ne=0	Ne=1	Ne=3	Ne=5
Mean	Nc=10	5.3%	4.9%	3.8%	2.9%
	Nc=50	3.6%	3.4%	3.0%	2.5%
	Nc=90	3.3%	3.2%	2.8%	2.5%
95th perc. of weight penalty factor	Nc=10	9.6%	8.9%	7.3%	5.8%
	Nc=50	5.3%	5.1%	4.6%	4.1%
	Nc=90	4.6%	4.4%	4.1%	3.7%
Probability of unsafe design (PUD)	Nc=10	2%	2%	2%	3%
	Nc=50	1%	1%	1%	2%
	Nc=90	0%	0%	1%	1%

Table 2-11. Probability of unsafe design (PUD), 95th percentile of weight penalties and magnifier

Case	Proposed method Nc=10	Nc=50	Nc=90	Current method
	Probability of unsafe design (PUD)			
Unconservative 5% error	6.1%	6.4%	6.4%	12.5%
Conservative 5% error	6.7%	7.3%	7.3%	12.5%
Unconservative 1% error	5.8%	0.4%	0.0%	12.5%
Conservative 1% error	7.8%	0.6%	0.2%	12.5%
	95th perc. of weight penalty factor (extreme design weight)			
Unconservative 5% error	5.4%	5.2%	5.1%	6.8%
Conservative 5% error	5.7%	5.7%	5.7%	6.8%
Unconservative 1% error	5.6%	4.2%	3.9%	6.8%
Conservative 1% error	6.1%	4.3%	3.9%	6.8%

Table 2-12. Probability of *Z* at two different values

Z value		0.955	0.975
MCS	Mean	2.34×10^{-7}	6.77×10^{-4}
	COV	210.7%	3.9%
Convolution integral		2.40×10^{-7}	6.78×10^{-4}

Table 2-13. Statistics for the calculated design areas with different number of coupon tests (True mean and standard deviation of material strength are 1.0 and 0.07, respectively).

# of coupon tests	Design area		B-basis allowable	
	Mean	Std.	Mean	Std.
10	1.194	0.064	0.840	0.044
50	1.129	0.019	0.885	0.015
90	1.120	0.013	0.892	0.011

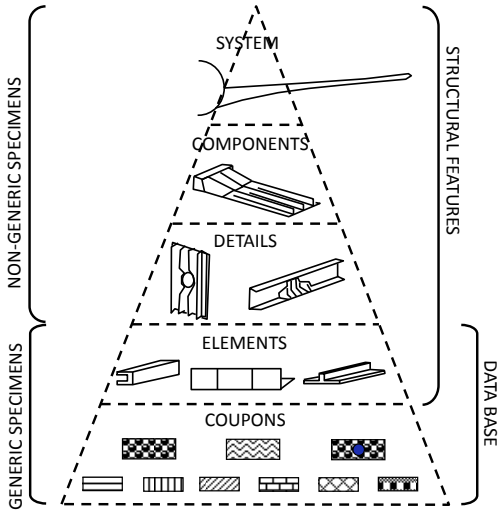

Figure 2-1. Building-block test process for aircraft structural components.

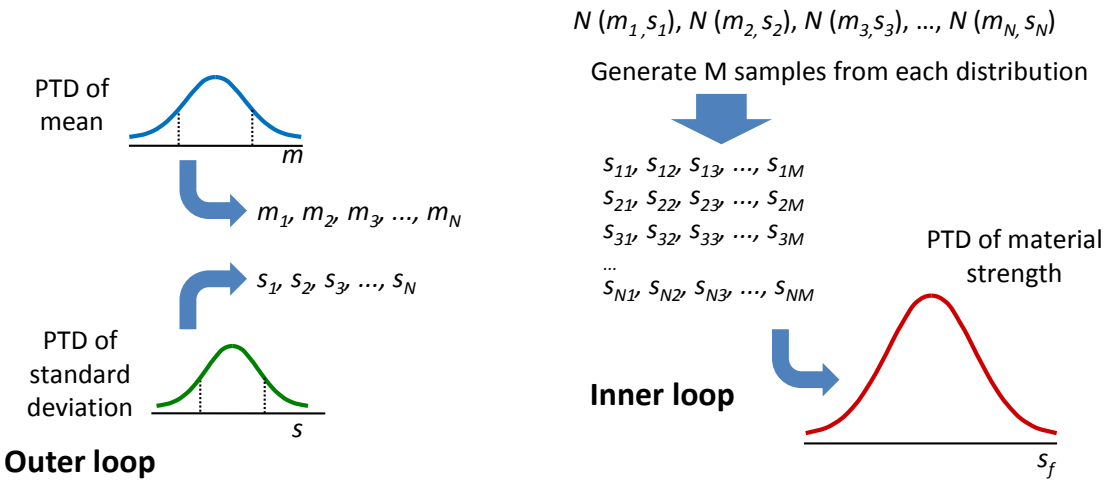

Figure 2-2. Double-loop Monte Carlo simulation to obtain the PTD of failure strength.

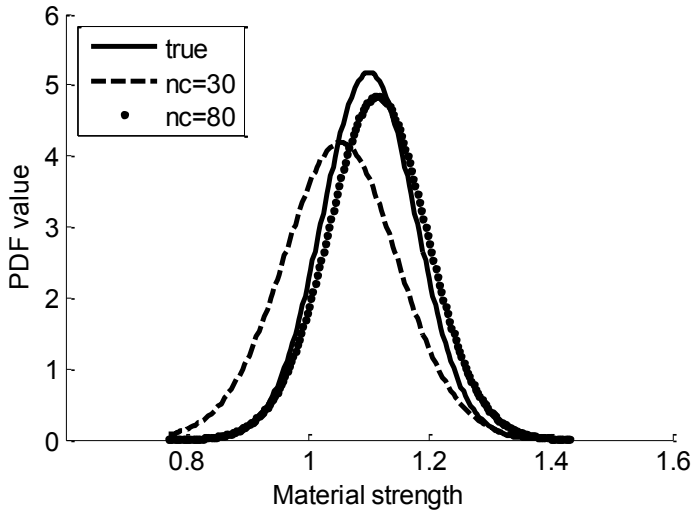

Figure 2-3. The distributions of element mean failure strength and its dependence on the number of coupons prior to the element tests. The error bounds are 10%, $\mu_{c,true}$ =0.85, $\sigma_{c,true}$ =0.068, and $k_{3d,calc}$ =1.

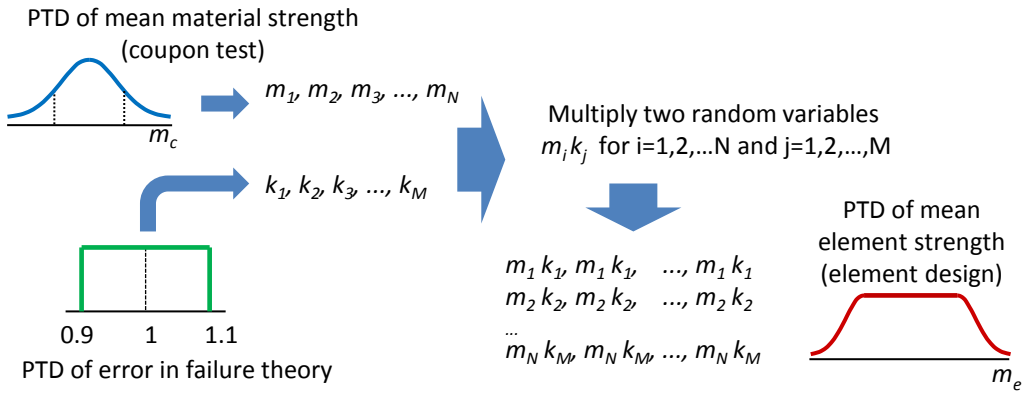

Figure 2-4. Process of estimating element mean failure strength.

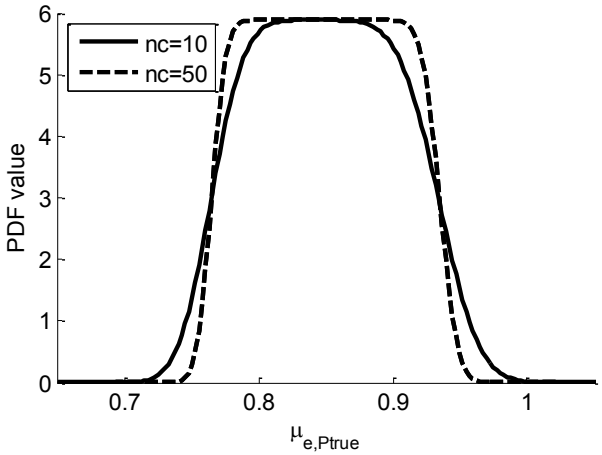

Figure 2-5. The distributions of element mean failure strength and its dependence on the number of coupons prior to the element tests. The error bounds are 10%, $\mu_{c,true}$=0.85, $\sigma_{c,true}$=0.068, and $k_{3d,calc}$=1.

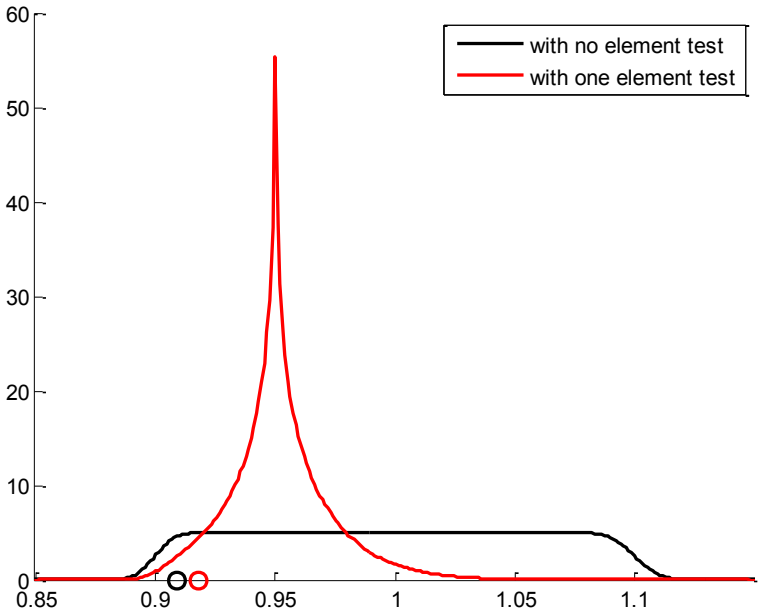

Figure 2-6. Comparison of the uncertainty in mean element strength before the first element test and after. The distribution before corresponds to 50 coupon tests that happen to have the correct mean (1.0). The true strength is 0.95, and the updated distribution is given for an element test that has no error.

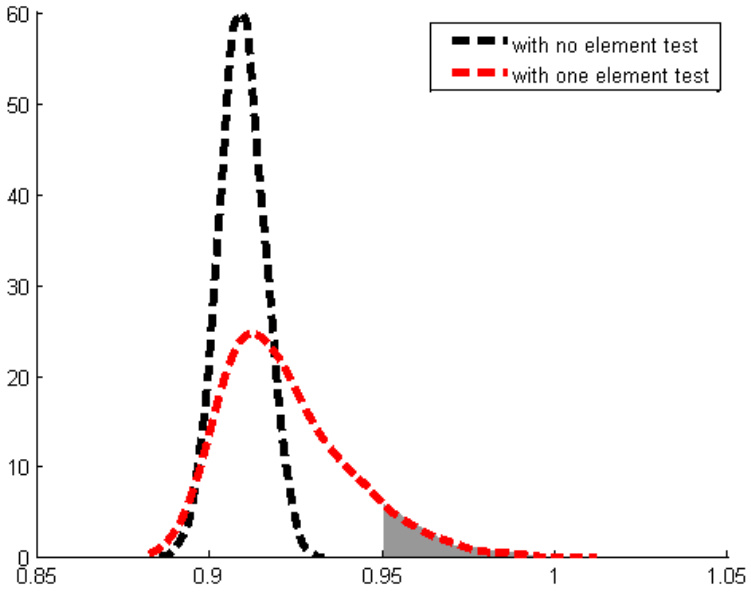

Figure 2-7. Distributions of 5th percentiles with no element test and one element tests while the true mean element strength is 0.95.

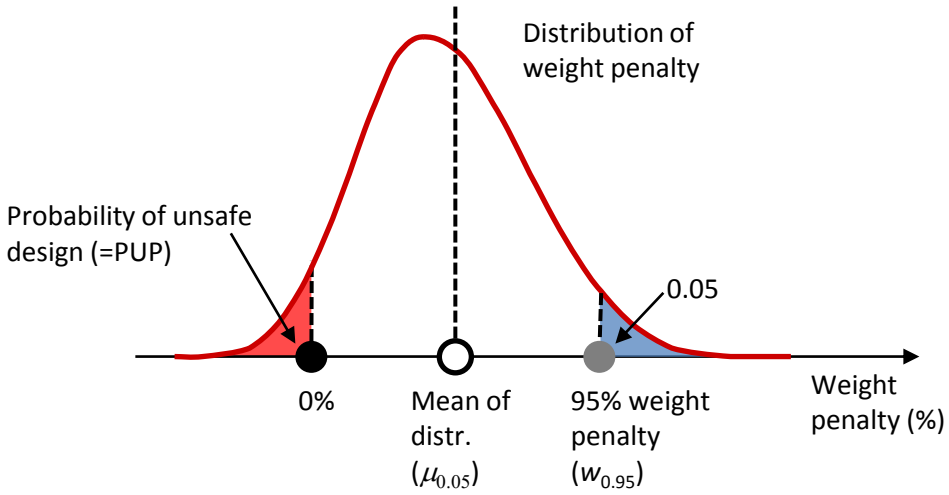

Figure 2-8. Distribution of weight penalty due to the variability in tests.

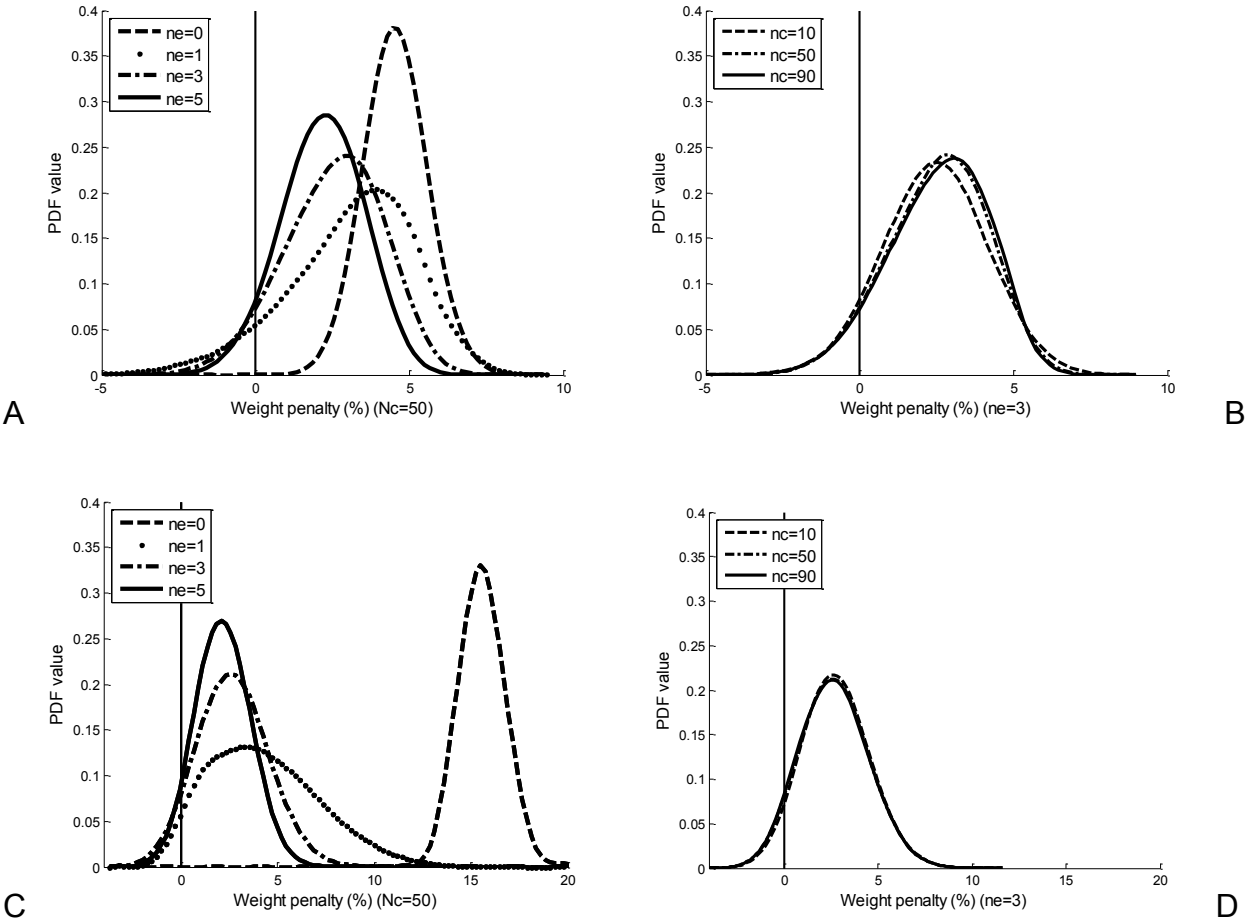

Figure 2-9. Distributions of weight penalties for comparison between the number of coupon tests and the number of element tests. A) n_e = 0,1,3,5 with n_c = 50 ($\mu_{e,true}$= 0.99 and b_e=±10%), B) n_e = 3 with n_c = 10,50,90 ($\mu_{e,true}$ = 0.99 and b_e=±10%), C) n_e = 0,1,3,5 with n_c = 50 ($\mu_{e,true}$ = 1.01 and b_e=±10%), and D) n_e = 3 with n_c = 10,50,90 ($\mu_{e,true}$ = 1.05 and b_e=±10%).

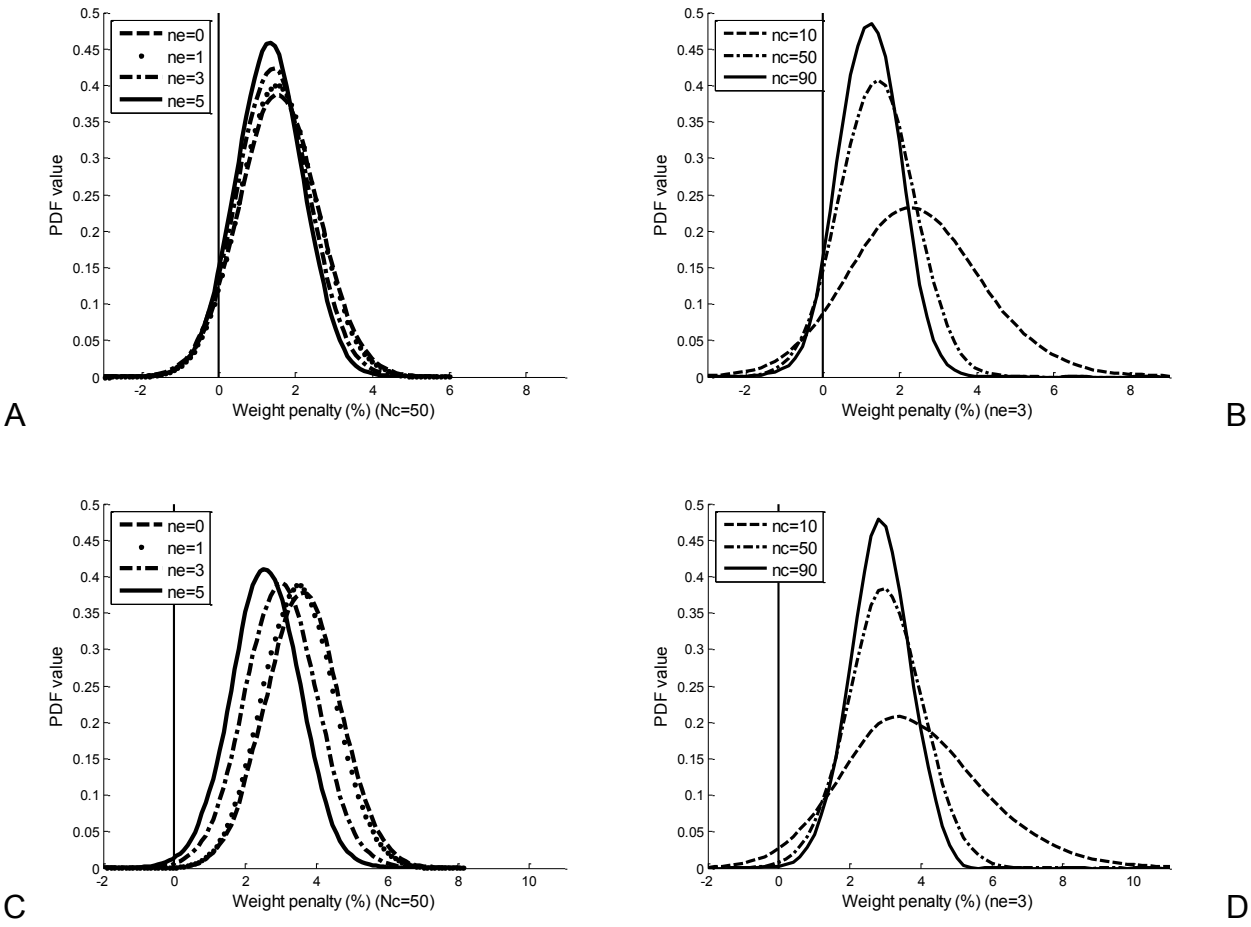

Figure 2-10. Distributions of weight penalties for comparison between the number of coupon tests and the number of element tests. A) n_e = 0,1,3,5 with n_c = 50 ($\mu_{e,true}$ = 0.99 and b_e=±2%), B) n_e = 3 with n_c = 10,50,90 ($\mu_{e,true}$ = 0.99 and b_e=±2%), C) n_e = 0,1,3,5 with n_c = 50 ($\mu_{e,true}$ = 1.01 and b_e=±2%), and D) n_e = 3 with n_c = 10,50,90 ($\mu_{e,true}$ = 1.05 and b_e=±2%).

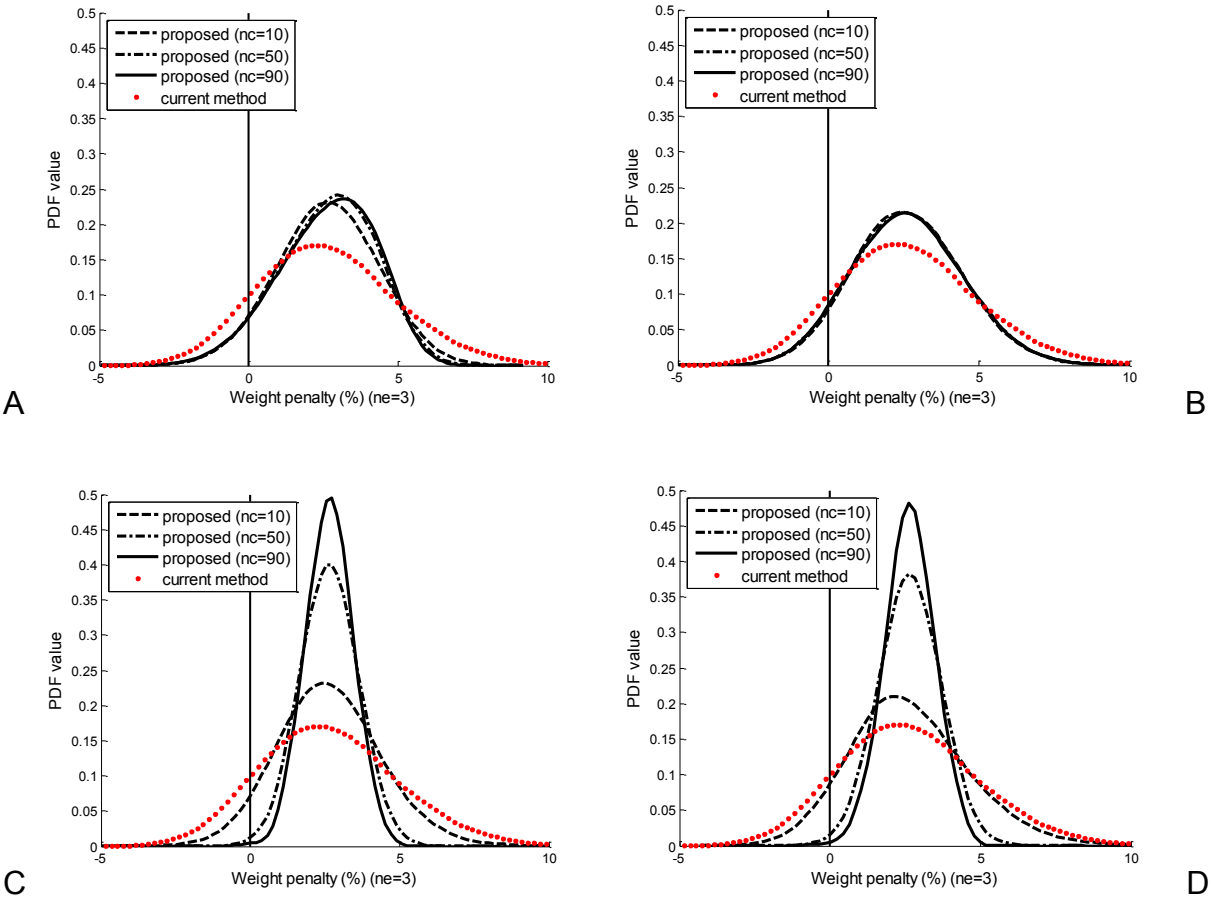

Figure 2-11. Distributions of weight penalties for comparison between the proposed method and current method (taking the lowest element strength among three). A) Unconservative 5% error ($\mu_{e,true}$ = 0.95 and $b_e = \pm 10\%$), B) Conservative 5% error ($\mu_{e,true}$ = 1.05 and $b_e = \pm 10\%$), C) Unconservative 1% error ($\mu_{e,true}$ = 0.99 and $b_e = \pm 2\%$), and D) Conservative 1% error ($\mu_{e,true}$ = 1.01 and $b_e = \pm 2\%$).

CHAPTER 3
EFFECT OF TESTS ON STRUCTURAL SAFETY WITH CORRELATED MULTIPLE FAILURE MODES

Motivation and Scope

In complex system design, each structural element is required to ensure the required safety for a given load level to prevent failure of whole structure, which is possibly triggered by the failure of an element. Estimating the probability of failure (PF) of the structure for the required load level becomes important to ensure the safety. In this study, we consider multiple failure modes due to various sources of uncertainty, such as variability in manufacturing process. In such a case, it is possible that some of them are affected by the same source of uncertainty, and so they are often correlated. Considering the presence of correlated multiple failure modes is an important issue for ensuring the safety of structural elements.

To estimate PF of a structural element with multiple failure modes, two things have to be properly considered. Firstly, the effects of error in numerical models and structural tests to reduce it have to be appropriately reflected on the PF estimation. The correlation brings two issues. Since errors in numerical models for predicting failures by different modes are correlated, the uncertainty model has to reflect the correlation between errors in failure predictions. Also the correlation among failure modes leads to correlated variability of limit state functions, which makes it difficult to estimate PF.

To incorporate test results into numerical model, uncertainty in test process needs to be quantified and included. Tests usually have uncertainties in both input and output parameters. Thus the uncertainties in input parameters have to be propagated to uncertainty in outputs so that the effect of uncertainty in tests can be properly taken into account.

Advanced composite materials have become key ingredients in modern aircraft structures due to their superior strength to weight ratio, stiffness tailorability, fatigue and corrosion properties. Hence, the composite material has been widely used for aircraft structure designs. To ensure safety of composite structures, designers rely on building-block testing, but the effect of tests has been rarely quantified. Here, we make an uncertainty model to show the effect of tests on safety of composite structures. In this study, uncertainty in geometric imperfection and correlated uncertainties in laminate material properties are incorporated in the uncertainty model, and two correlated failure modes, buckling and strength failure modes, are considered. Abaqus is used to predict buckling load and strength failure load using static nonlinear analysis with Riks method to catch snap-through instability.

This chapter is composed of six sections. First section is to show how to model uncertainties to incorporate contribution of tests to reduce uncertainty on estimating PF, especially for a case of having correlated multiple failure modes. Second section is to show how to construct likelihood function with uncertainty in input parameters in test data. Third section is to present the way of calculating system PF with considering correlated failure modes. Fourth section has illustrative examples. In the illustrative examples, a simple beam model is used to demonstrate the presented uncertainty model and the effect of tests. And PF of a curved composite panel model is estimated with actual test results collected from one literature and the effect of a single test on uncertainty in PF estimation is shown.

Modeling Uncertainty

Modeling Uncertainty in Numerical Model for Estimating PF

Estimating PF starts with quantifying uncertainty in structural capacity, such as buckling load and strength failure load, which is triggered by input uncertainties, such as variability in material properties and manufacturing imperfection (alreatory uncertainty). Then conditional expectation of probability that capacity is less than required design load is calculated.

If there is no error in measuring input uncertainties, error in the numerical model (epistemic uncertainty) is the only uncertainty source in PF estimate. By applying all possible errors in numerical model, PF distribution can be obtained, which models uncertainty in PF calculation due to the epistemic uncertainty.

Figure 3-1A shows a PF calculation process for a given error in the numerical model. This is different from the conventional approach in which the error is also considered as a random variable in calculating PF. In this process, contribution of error in numerical model is separated from calculating PF so that the effect of the error can be clearly seen. There are three variabilities: variabilities in geometric dimension $f_{inp}(d)$, material property $f_{inp}(m)$ and required load $f_P(P)$. We then calculate the distribution of the buckling load $f_{calc}(\lambda \mid e_{calc})$ which is expressed as a conditional probability density function (PDF) of buckling load for given calculation error e_{calc}. Finally PF is calculated using $f_{calc}(\lambda \mid e_{calc})$ and $f_P(P)$. The PF is a conditional expectation of probability that the required load is less than the buckling load.

Once the PF is estimated for a given value of error, the distribution of error is used to estimate the distribution of PF. Figure 3-1B shows the process of calculating PF

distribution. The PF calculation process is a function of the error as shown in Figure 3-1A so that the PF distribution can be obtained from transformation of error distribution with the PF calculation function. Therefore, the uniqueness of the proposed approach is that the PF is estimated as a distribution, not a value as in the conventional approach.

Once the distribution of PF is estimated, structural tests are used to narrow the distribution in PF. Since the uncertainty in PF is caused by error distribution, structural tests reduce the error distribution, which is used to reduce the distribution of PF. Figure 3-2 shows the effect of reducing uncertainty in the error distribution $f_{e,calc}(e_{calc})$ with tests on the uncertainty in PF estimation. The distributions with dotted line and solid line represent before and after tests. The effect of the tests on PF estimation can be seen through the narrowed PF distribution and can be quantified by measuring the change of standard deviations.

Modeling Uncertainty in Estimating Structural Capacities for Multiple Failure Modes

In this section, we assume a scenario of estimating PF of a structural element which has two correlated failure modes, buckling and strength failures. Modeling uncertainties in the numerical models for predicting buckling load and strength failure load is described.

Buckling load is estimated for given dimension *d* and material property *m*. The relationship between the true buckling load and calculated value for buckling load are expressed as

$$C^{\lambda}_{true} = \left(1 - e^{\lambda}_{calc,true}\right)\lambda_{calc} \tag{3-1}$$

where C^{λ}_{true} is the true buckling load for given dimension and material property *d* and *m*, λ_{calc} is the calculated buckling load and the $e^{\lambda}_{calc,true}$ is unknown true error in buckling load capacity calculation.

To estimate the strength failure load, we are in need of using failure theory to determine structural failure. For example, we can determine failure load of a tension problem with the maximum strain criterion by determining the load which reaches axial strain (structural response) to the ultimate strain. In this example, we have two uncertainty sources in estimating strength failure: uncertainty in predicting structural response and uncertainty in the failure theory as shown in the previous chapter. The former is associated with the error in the numerical model.

If there is no error in numerical model, we only have the error in the failure theory as

$$C^{s}_{true} = \left(1 - e^{f}_{true}\right) S_{true} \tag{3-2}$$

where C^{s}_{true} is the true failure strength for given dimension *d* and material property *m*, S_{true} is the failure load which is determine by failure criterion, and e^{f}_{true} is the true error in estimating strength failure load using the failure theory. The numerical model, however, also has error to estimate structural response with respect to the load (e.g. error in a load-strain curve). If we have no error in our numerical model to evaluate the relation between load and structural response, we can express the true load S_{true} as a function of the structural response. Using strain as the structural response, the load-strain relation is defined as

$$S_{true} = f^{s}_{true}\left(\varepsilon_{true}\right) \tag{3-3}$$

Equation (3-3) generally has a form of load-strain curve, and the error in the curve has to be considered. In this study, we propose a simple method to parameterize errors in the curve.

Parameterization of a Load-Strain Curve for Modeling Uncertainty in Strength Failure Load Prediction

The strength failure load is estimated at the maximum strain point of the load-strain curve. Figure 3-3 is a conceptual figure to show a discrepancy between the calculated load-strain curve and the true curve. It is assumed that the snap through behavior is observed because of the presence of buckling.

In this study, we propose parameterization of the curve with the buckling load and buckling strain. Reducing error in the curve can be achieved by reducing error in the parameters. However, the errors for both buckling load and buckling strain are coupled in the numerical model. We propose a simple method for decoupling the parameters by normalizing the true curve in terms of parameters and their errors. It is assumed that normalized true curve and normalized curve from numerical model follow the same functional relationship. The normalized curve can be expressed as

$$\frac{P}{\lambda_{calc}\left(1-e^{\lambda}_{calc,true}\right)} = f_{P\varepsilon}\left(\frac{\varepsilon}{\varepsilon_{calc}\left(1-e^{\varepsilon}_{calc,true}\right)}\right) \tag{3-4}$$

where $e^{\lambda}_{calc,true}$ and $e^{\varepsilon}_{calc,true}$ are true error in buckling load prediction and the true error in calculation of buckling, respectively. $f_{P\varepsilon}$ is the normalized curve from numerical model. Equation (3-4) provides a relationship for load *P* and strain *ε* in terms of parameter errors. When we know the true errors, $e^{\lambda}_{calc,true}$ and $e^{\varepsilon}_{calc,true}$, the true strength failure capacity can be determined with the ultimate strain as

$$S_{true} = \lambda_{calc}\left(1 - e^{\lambda}_{calc,true}\right) f_{P\varepsilon}\left(\frac{\varepsilon_u}{\varepsilon_{calc}\left(1 - e^{\varepsilon}_{calc,true}\right)}\right) \tag{3-5}$$

By replacing S_{true} in the Eq. (3-2) with that of Eq. (3-5), uncertainties in the strength failure is modeled with the parameterized load-strain curve.

Incorporating the Effect of Tests in Numerical Model using Bayesian Inference

From the previous section, it is shown that errors in predicting buckling load and strength failure load are formulated with errors. However, since the true errors are unknown, we have to estimate the errors. It is assumed that the estimated errors are defined as uniform distributions as follows

$$\begin{aligned} f^{init}_{e,\lambda}\left(e^{\varepsilon}_{calc}\right) &= \frac{1}{\left(u^{\lambda}_{e} - l^{\lambda}_{e}\right)} I\left(e^{\lambda}_{calc} \in [l^{\lambda}_{e}, u^{\lambda}_{e}]\right) \\ f^{init}_{e,\lambda}\left(e^{\varepsilon}_{calc}\right) &= \frac{1}{\left(u^{\varepsilon}_{e} - l^{\varepsilon}_{e}\right)} I\left(e^{\varepsilon}_{calc} \in [l^{\varepsilon}_{e}, u^{\varepsilon}_{e}]\right) \end{aligned} \tag{3-6}$$

where $I(x \in [l,u])$ is an indicator function that gives 1 when *x* belongs to the range [*l*,*u*] and 0 for otherwise. In the above equation, *u* and *l* represent the upper and lower bounds, respectively. The superscript *λ* and *ε* represent buckling load and buckling strain, respectively.

The initial error distributions (prior) in Eq. (3.6) are reduced based on the test observations. Bayesian inference is used with the prior distribution in Eq. (3-6) and the likelihood functions from tests. Since there is no information for the relationship between the two errors, the prior distribution is modeled as independent uniform distributions. The likelihood function reflects uncertainty in test process and is modeled with copulas to reflect correlations between two errors. Appendix B explains the detailed information of copulas. Detailed derivation for the likelihood function and relevant issues are

described in the next section. Finally the updated joint distribution of errors (posterior distribution) is expressed as follows

$$f_e^{upd}\left(e_{calc}^{\lambda}, e_{calc}^{\varepsilon}\right) = \frac{f_{e,\lambda}^{init}\left(e_{calc}^{\lambda}, e_{calc}^{\varepsilon}\right) l_{e,\lambda}\left(e_{calc}^{\lambda}, e_{calc}^{\varepsilon}\right)}{\int_{l_e^{\lambda}}^{u_e^{\lambda}} \int_{l_e^{\varepsilon}}^{u_e^{\varepsilon}} f_{e,\lambda}^{init}\left(e_{calc}^{\lambda}, e_{calc}^{\varepsilon}\right) l_{e,\lambda}\left(e_{calc}^{\lambda}, e_{calc}^{\varepsilon}\right) de_{calc}^{\lambda} de_{calc}^{\varepsilon}} \tag{3-7}$$

Note that the errors in calculation for the buckling load and buckling strain are correlated even the correlation is not explicitly expressed in Eq. (3-7).

Constructing Likelihood Function with Uncertainty in Input Parameters

Likelihood Functions due to Uncertainty in Input Parameters

When there are no errors in test, we can obtain a true observation. However, this is not the case. In structural tests, there are many sources of errors, such as measurement errors and errors in boundary conditions and applied loads. To compare test observation with predictions from numerical model, input parameters of the test and that of the predictions have to be the same. However in case of a thin composite panel, measurement errors in output parameters, such as surface strain, buckling load and buckling strain, are very small, less than 0.1%, whereas measurement errors in input parameters, such as material properties and thickness, are approximately 3 to 4% [14].

That implies that a comparison between a predicted buckling load and a test observation does not give a correct error in calculation. For example, predicted buckling load is based on a numerical model and measured input parameters. However, the true input parameters, which draw a test observation, are different from the measured input parameters while numerical test uses measured input parameters to identify the calculation error by comparing predicted buckling load and observed buckling load from test.

Since the true input parameters are not obtainable, we need obtain a likelihood function of the true prediction for the measured input parameters. To establish a proper likelihood function with the measurement errors in input parameters, the effect of input parameter uncertainty on output parameter uncertainty has to be quantified.

Here we have a simple example that uncertainty in input parameters of test data causes problem to obtain error in output from a numerical model. If we predict an output using a prediction function g_{pred} and measured input x_{meas}, the true prediction error e_{pred} can be obtained from

$$g_{true}(x_{meas}) = (1 - e_{pred}) g_{pred}(x_{meas}) \tag{3-8}$$

where g_{true} is a true function which provides test results for given input and g_{pred} is a function with error to predict output. Note that $g_{true}(x_{meas})$ is not the test observation $g_{true}(x_{true})$. As mentioned earlier, the measurement error in output is negligibly small, the measured output parameter for the true input parameters is equal to $g_{true}(x_{true})$ Figure 3-4A shows an ideal case that there is no measurement error. Fig. 3-4B shows the case that measurement error in output parameters are ignorable but that in input parameters are large that the situation this section deals with. Figure 3-4C shows that a likelihood function for $g_{true}(x_{meas})$ and the likelihood function can be obtained through quantifying the effect of uncertainty in input parameter on the output parameter by applying all possible true input parameters around measured input parameters.

Effect of Uncertainty in Input Parameter on the Output Parameter

In this section, the process to obtain likelihood function of buckling load and surface strain for measured input parameters is explained.. Likelihood function is

obtained using a numerical model. It is assumed that the effect of errors in boundary condition and measured strain and buckling load are negligibly small.

If we can obtain the true buckling load and strain for measured dimension and material property, we can quantify the effect of the measurement errors in the input parameters on output parameters by calculating distributions in strain and buckling load according to the measurement errors as

$$\begin{aligned} \hat{\lambda}_{test} &= g^{\lambda}_{true}\left(\hat{d}_{meas}, \hat{m}_{meas}\right) \\ \hat{\varepsilon}_{test} &= g^{\varepsilon}_{true}\left(\hat{d}_{meas}, \hat{m}_{meas}\right) \end{aligned} \tag{3-9}$$

where variables with a hat are random variables and the *g* represents the true function. The random variables on the left-hand side can be modeled as likelihood functions. However since the true function is unknown, the numerical models g^{λ}_{calc} and g^{ε}_{calc} have to be alternatively used as in Eq. (3-10) with errors in the numerical model.

$$\begin{aligned} \hat{\lambda}_{test} &= \left(1 - e^{\lambda}_{calc}\left(\hat{d}_{meas}, \hat{m}_{meas}\right)\right) g^{\lambda}_{calc}\left(d_{meas}, m_{meas}\right) \\ \hat{\varepsilon}_{test} &= \left(1 - e^{\varepsilon}_{calc}\left(\hat{d}_{meas}, \hat{m}_{meas}\right)\right) g^{\varepsilon}_{calc}\left(d_{meas}, m_{meas}\right) \end{aligned} \tag{3-10}$$

The true errors, e^{λ}_{calc} and e^{ε}_{calc}, in calculations vary for different dimensions and material properties in reality. It is assumed that the variation of error due to change of input parameters is negligibly small because variation in dimensions and material properties are 2% to 3%. Since the errors are no longer functions of input parameters, the error function is replaced with constants. Equation (3-10) can then be approximated as

$$\begin{aligned} \hat{\lambda}_{test} &\approx \left(1 - e^{\lambda}_{calc}\right) g^{\lambda}_{calc}\left(\hat{d}_{meas}, \hat{m}_{meas}\right) \\ \hat{\varepsilon}_{test} &\approx \left(1 - e^{\varepsilon}_{calc}\right) g^{\varepsilon}_{calc}\left(\hat{d}_{meas}, \hat{m}_{meas}\right) \end{aligned} \tag{3-11}$$

where e^{λ}_{calc} are e^{ε}_{calc} the constant errors.

Since measurement errors in output parameters are small while that in input parameters are large, test errors are defined as discrepancy between measured outputs that have true input parameters that are different from measured input parameters and true outputs corresponding to measured inputs, which we need to calculate the errors in calculation, as

$$\begin{aligned} g_{true}^{\lambda}\left(d_{meas}, m_{meas}\right) &= \left(1-e_{test}^{\lambda}\right) g_{true}^{\lambda}\left(d_{true}, m_{true}\right) \\ g_{true}^{\varepsilon}\left(d_{meas}, m_{meas}\right) &= \left(1-e_{test}^{\varepsilon}\right) g_{true}^{\varepsilon}\left(d_{true}, m_{true}\right) \end{aligned} \tag{3-12}$$

By replacing the true functions with numerical models with errors, and again, Eq. (3-12) is reformulated as

$$\begin{aligned} \left(1-e_{calc}^{\lambda}\right) g_{calc}^{\lambda}\left(d_{meas}, m_{meas}\right) &= \left(1-e_{test}^{\lambda}\right)\left(1-e_{calc}^{\lambda}\right) g_{calc}^{\lambda}\left(d_{true}, m_{true}\right) \\ \left(1-e_{calc}^{\lambda}\right) g_{calc}^{\varepsilon}\left(d_{meas}, m_{meas}\right) &= \left(1-e_{test}^{\varepsilon}\right)\left(1-e_{calc}^{\lambda}\right) g_{calc}^{\varepsilon}\left(d_{true}, m_{true}\right) \end{aligned} \tag{3-13}$$

Since the errors are constants, the errors in the both sides are compensated each other. However since the true dimensions and material properties are unknown, possible true input parameters, distributions of input parameters for the true parameters are substitute instead of the true input parameters. Finally the errors in measured outputs for the true outputs for the measured input parameters are calculated as

$$\begin{aligned} \hat{e}_{test}^{\lambda} &= 1-\frac{g_{calc}^{\lambda}\left(d_{true}, m_{true}\right)}{g_{calc}^{\lambda}\left(\hat{d}_{meas}, \hat{m}_{meas}\right)} \\ \hat{e}_{test}^{\varepsilon} &= 1-\frac{g_{calc}^{\varepsilon}\left(d_{true}, m_{true}\right)}{g_{calc}^{\varepsilon}\left(\hat{d}_{meas}, \hat{m}_{meas}\right)} \end{aligned} \tag{3-14}$$

Based on the test errors, we can estimate the true outputs for the measured input parameters from measured outputs. The calculation errors are estimated based on the test errors in next section.

Calculating Likelihood Functions for Errors in Numerical Model

The likelihood function for errors in numerical model is defined as a conditional PDF for measured test observations. To make a connection between the errors in numerical model and the errors in test, the LHS of Eq. (3-12) is rewritten using numerical model as

$$\begin{aligned}\left(1-e_{calc}^{\lambda}\right)g_{calc}^{\lambda}\left(d_{meas},m_{meas}\right)&=\left(1-e_{test}^{\lambda}\right)g_{true}^{\lambda}\left(d_{true},m_{true}\right)\\ \left(1-e_{calc}^{\varepsilon}\right)g_{calc}^{\varepsilon}\left(d_{meas},m_{meas}\right)&=\left(1-e_{test}^{\varepsilon}\right)g_{true}^{\varepsilon}\left(d_{true},m_{true}\right)\end{aligned} \tag{3-15}$$

From the assumption of very small measurement error in outputs, $g_{true}^{\lambda}\left(d_{true},m_{true}\right)$ and $g_{true}^{\varepsilon}\left(d_{true},m_{true}\right)$ can be replaced with λ_{meas} and ε_{meas}.

$$\begin{aligned}\left(1-e_{calc}^{\lambda}\right)g_{calc}^{\lambda}\left(d_{meas},m_{meas}\right)&=\left(1-e_{test}^{\lambda}\right)\lambda_{meas}\\ \left(1-e_{calc}^{\varepsilon}\right)g_{calc}^{\varepsilon}\left(d_{meas},m_{meas}\right)&=\left(1-e_{test}^{\varepsilon}\right)\varepsilon_{meas}\end{aligned} \tag{3-16}$$

By substituting Eq. (3-14) (the estimated test errors) into Eq. (3-16), the errors in numerical model are estimated as

$$\begin{aligned}\hat{e}_{calc}^{\lambda}&=1-\frac{\lambda_{meas}}{g_{calc}^{\lambda}\left(\hat{d}_{meas},\hat{m}_{meas}\right)}\\ \hat{e}_{calc}^{\varepsilon}&=1-\frac{\varepsilon_{meas}}{g_{calc}^{\varepsilon}\left(\hat{d}_{meas},\hat{m}_{meas}\right)}\end{aligned} \tag{3-17}$$

Note that since the random variables $\hat{e}_{calc}^{\lambda}$ and $\hat{e}_{calc}^{\varepsilon}$ are correlated, the likelihood function $l_{e,\lambda}\left(e_{calc}^{\lambda},e_{calc}^{\varepsilon}\right)$ can be modeled as a copula that defines statistical correlation between the random variable in Eq. (3-17), $\hat{e}_{calc}^{\lambda}$ and $\hat{e}_{calc}^{\varepsilon}$.

Examples for Likelihood Functions

Likelihood function can be interpreted as probability density function of true errors for given errors in numerical model. Here two likelihood functions are shown after a test using the simple beam example. In Figure 3-5, the plots have two symbols, true errors

(red circle) and calculated errors (green triangle) based on measured output parameters in buckling load and strain calculations, and a likelihood function (blue scattered plot).

Figure 3-5 shows that an illustration of a scattered plot of the likelihood with 1000 randomly generated samples and true errors and calculated errors. The horizontal axis is error in buckling load calculation and the vertical axis is error in strain calculation. Distance between the two symbols represents the error in measuring input parameters. Difference between two plots represents variability in tests. Also it is shown that the errors in numerical models are correlated.

Estimating Probability of Failure with Multiple Failure Modes

In the previous sections, we model the uncertainty in numerical models. Also a likelihood function is derived to reflect contribution of tests to reducing uncertainty in the PF estimation. To estimate PF, variability in structural capacities has to be calculated. For multiple failure mode cases, statistical correlation in the variability of structural capacities has to be considered. MCS is a very general method and has no limitation to calculate PF. However, MCS requires high computational resources, especially for small PF, such as reliability index of β=4 or 5.

Here, we propose a strategy to calculate PF using MCS with less computational burden than the traditional MCS. Correlation among multiple failure modes is considered by decomposing failure modes with a condition. Computational efficiency is increased by decreasing the number of parameters that have to be estimated.

Conditional Failure Mode Decomposition

PF of a structural element with a compressive load with two failure modes is defined as

$$PF = \Pr\left(\min\left(\hat{C}^{\lambda}_{calc}, \hat{C}^{s}_{calc}\right) < \hat{P}\right) \tag{3-18}$$

In this study, there are two critical failure modes. The critical failure modes are determined by the one with smaller capacity. Based on the condition of the critical failure mode, PF equation can be re-written as

$$PF = \Pr\left(\hat{C}^{\lambda}_{Ptrue} \mid \left(\hat{C}^{\lambda}_{Ptrue} < \hat{C}^{s}_{Ptrue}\right) < \hat{P}\right)\mathrm{P}_b + \Pr\left(\hat{C}^{s}_{Ptrue} \mid \left(\hat{C}^{s}_{Ptrue} < \hat{C}^{\lambda}_{Ptrue}\right) < \hat{P}\right)\mathrm{P}_s \tag{3-19}$$

where P_b is probability that buckling failure mode becomes critical, and P_s is probability of the other case. Because $\hat{C}^{\lambda}_{Ptrue} \mid \left(\hat{C}^{\lambda}_{Ptrue} < \hat{C}^{s}_{Ptrue}\right) < \hat{P}$ and $\hat{C}^{s}_{Ptrue} \mid \left(\hat{C}^{s}_{Ptrue} < \hat{C}^{\lambda}_{Ptrue}\right) < \hat{P}$ are two disjointed events, these two random variables can be considered as independent. Hence Eq. (3-18) can be simply reformulated to Eq. (3-19) as a sum of two probabilities which can be independently determined.

We use MCS for generating capacity samples of buckling load and strength failure load with uncertainty in dimensions and material properties. Then, we categorize the generated samples into two groups: one group of samples which satisfies $\hat{C}^{\lambda}_{Ptrue} < \hat{C}^{s}_{Ptrue}$ and the other group of samples, and fit a CDF for each group. K-S goodness of fit test is used for fitting each group of samples. The fitted CDFs are approximated distribution of these two conditional random variables. Table 3-1 shows detailed process to calculate PF using this presented method.

Illustrative Examples

In this section, two examples, a simple beam model and a composite panel with a hole model, are shown. For the simple beam example, it is assumed that true variability in tests, true uncertainty in measured data, true errors in numerical model and true PF are assumed to be given for the purpose of generating samples and validating the

model. Process of estimating PF is repeatedly simulated with the uncertainty model to show the effect of variability in tests and to validate the uncertainty model. Tests are randomly generated for each simulation using the true variability. In this simulation, PF estimations based on the randomly generated tests vary and the estimated PF can be compared to the true PF. Average value of PF estimations is used for the expected PF. Also the effect of correlation is demonstrated.

For the second example, PF of a composite panel with a hole is estimated with test data collected from a literature based on actual structural tests. Correlated uncertainty of laminate material properties and uncertainty in geometric imperfection are taken into account.

Example 1: A Simply Supported Beam

For the simply supported beam in Figure 3-6, there are two failure modes, buckling and strength failure modes, and it is assumed that a single element test is available. Two equations for buckling load and strength failure load are used to make simulation environment: true equations and equations with error. The true equation gives the true buckling load and strain, but errors are deliberately put into the equations with error to reflect numerical model errors. To simulate structural tests, test data is generated with the true equations, adding randomly generated material properties and specimen geometry. The measured material properties, geometries and test results, buckling load and strain at the buckling point, have measurement errors. Then, we estimate PF using the equations with error, the simulated test results and measured material properties and geometries. Since we know the true equations and true errors in the simulation, the estimated PF will be verified against the true PF. To see the effects of test variability,

the simulation is repeated 1,000 times and collect the statistical characteristics of the presented uncertainty model to estimate PF.

Dimensions and boundary conditions of the beam model are shown in Figure 3-6. Couple *C* and axial forces *P* with roller boundary conditions are imposed on the two ends.

The couple *C* and the axial load *P* have variability. Hence PF of the structure is a function of the axial force *P* and the couple *C*, equations with error for calculated buckling load P_{calc}^{λ} and strength failure load P_{calc}^{s} and corresponding true values P_{true}^{λ} and P_{true}^{ε} are expressed in Table 3-2.

To simulation PF estimation process, Table 3-1 is used. Two different loading conditions, with and without including the couple *C* are considered. It will be shown that the loading condition affects correlation between the two failure modes. The correlation brings dominant failure mode switching as the load level changes and possibly bring large error in PF calculation when one failure mode is neglected.

Beam with an Axial Load

Table 3-3 shows uncertainty sources for material properties and dimensions of the beam. The uncertainties in manufacturing process are variabilities in input parameters and errors in measuring input and outputs during test data. It is assumed that test is well controlled, such that the standard deviations of test variabilities are 1/5 of the manufacturing variabilities.

Without a couple *C*, the PF is estimated in terms of the magnitude of nominal *P*. For *N*, *M* and *Q* in Table 3-1, the number of function evaluations to obtain samples for capacities is *N*=200. After test, *M*=100 function evaluations are needed to establishing

likelihood function. Finally, Q=100×N capacity samples are calculated and separated into two cases, $\hat{C}^{\lambda}_{Ptrue} \mid \left(\hat{C}^{\lambda}_{Ptrue} < \hat{C}^{s}_{Ptrue}\right)$ and $\hat{C}^{s}_{Ptrue} \mid \left(\hat{C}^{s}_{Ptrue} < \hat{C}^{\lambda}_{Ptrue}\right)$. The separated samples are fitted to two CDFs. R=10 Millions samples are generated from the fitted CDFs and a CDF for load P to calculate PF. Error bounds for buckling load, strain and failure theory are given in Table 3-4.

Since we have the uncertainties due to MCS and test variability, the PF estimation process is repeated 1,000 times. Statistics are compared to the true PF in Table 3-5.

From Table 3-5, we can see the effects of a single test. When P=19 MN, we expect PF of 2.61×10^{-4} before test, but expected PF becomes 1.18×10^{-4} after using test result for reducing the error in failure prediction. The effects of test is significant in terms of design weight because the error in PF calculation has to be compensated by additional design weight. The standard deviation of PF without test represents error in MCS. We can observe that the standard deviation with test becomes larger than the standard deviation without test. This happened because the additional uncertainty comes from test variability.

Beam with a Couple

Next, we consider the case when both the axial force and the couple are applied to the beam. Different from the previous case, the dominant failure mode switches due to the existence of a couple. In order to illustrate this switch, the nominal values of h = 0.08 m and C=105 kN-m are used. All other parameters are the same as in Tables 3-3 and 3-4. The PF is estimated in terms of the magnitude of nominal P and the nominal value of C which is fixed. The number of function evaluations is N=200. For after test case, M=100 is used. Q=100×N and R=10 Million. Same error bounds with the previous

example are used. PF estimation process is repeated 1,000 times. Statistics are compared to the true PF in Table 3-6.

A notable observation from this example is the observation that dominant failure mode is switched as axial load increases. For example, the strength failure mode is dominant when nominal *P* is 2.1MN but buckling failure mode is dominant when nominal P is 2.3MN. With a small change in axial load, dominant failure mode is changed. In other words, when design requirement for axial load is 2.1MN, ignoring the effect of strength failure mode is not influential for system PF calculation but strength failure mode is no longer ignorable when the design requirement for axial load is changed to 2.3MN.

Example 2: A Composite Panel with a Hole

In this section, the PF of curved composite panel is estimated with the proposed method. Uncertainties that reflect features of composite materials have to be taken into account. Correlation between material properties due to the fiber volume fraction is the one that has to be considered in the uncertainty model. Ignoring the correlation of the material properties may induces a large error in predicting PF [16]. Geometric imperfection is another major source of uncertainty for composite structures. The effect of the imperfection for the curved panel example is shown in a later section. Hilburger and Starnes [17] investigated the effects of imperfections on the non-linear response and buckling loads of un-stiffened thin-walled compression-loaded graphite-epoxy cylindrical shells. They categorized two imperfection types as traditional imperfection and non-traditional imperfection. Here, the traditional Imperfection is considered as variability in geometry.

Comparison of Experimental and Analytical Results

The composite panel was fabricated from commercially available unidirectional Thornel 300 graphite fiber tapes pre-impregnated with 450K cure Narmco 5208 thermosetting epoxy resin fixture [15].

The geometry of the test specimen, loading and boundary conditions are schematically shown in Figure 3-7. The appropriate boundary conditions for the cylindrical panel are (i) fully clamped on the bottom edge, (ii) clamped except for axial motion on the top edge (potted end), and (iii) simply-supported on the vertical edges (knife-edge restraints). The test consists of statically imposing a uniform end-shortening, δ, until the specimen reaches buckling point. Electrical strain gages were used to monitor surface strains near the hole in the axial direction. A single test was performed and the buckling failure occurred.

In this study, we assume that we have two potential modes, buckling failure and strength failure. Also it is assumed that the strength failure will be occurred by a failure of a single ply instead of a progressive damage model.

We use nonlinear finite element analysis using Abaqus to predict strength failure and buckling failure as for anticipated severe deflection around the hole. The Riks method is used to capture the snap-through behavior. The composite panel in Figure 3-7A is modeled with 9 node shell elements (S9R5 element in Abaqus). The panel section is defined as a composite general section with the stacking sequence and the ply thickness as shown in Table 3-7. After the analysis, the load-displacement curve is used to determine buckling point. Load-ply strain curves are analyzed to determine strength failure load of a ply.

Figure 3-8 shows comparisons between predicted load-displacement curve and load-surface strain curve from simulation and an experiment. The curves are plotted up to buckling point. The surface strain is measured from two strain gages on the top and bottom surfaces of the panel near the hole boundary. Table 3-8 has measured buckling load and surface strain at the buckling point from the test.

Geometric Imperfection

In this composite laminate panel, buckling load is very sensitive to the geometric imperfection, but the test specimen's imperfection data is not available. We used the imperfection that provides the best prediction as the actual imperfection of the specimen. Figure 3-9 shows the effect of the imperfection with various perturbation magnitudes. It shows that the effects of imperfection on buckling load and nominal strain are substantial. Based on numerical tests, it is concluded that -10% to 10% of thickness perturbations are reasonable for the geometric imperfection range of the panel. Eigenvectors of modes 1 to 4 are multiplied with the thickness perturbations and added on nodal coordinates. There are two perturbation directions, positive and negative to the normal direction of the curved surface. The eigenvectors are obtained from the linear buckling analysis. Simulation result indicates that -10% thickness perturbation with mode 3 eigenvector provides the best predictions for buckling load and surface strain. Hence we assume that the specimen's actual imperfection is approximately mode 3 eigenvector shaped with the thickness perturbation of -10%.

Uncertainty Modeling of Curved Composite Panel

In this section, variabilities in buckling load and strength failure load, capacities of the curved composite panel, are estimated using ABAQUS. Table 3-9 shows variabilities in material properties and geometries. In Table 3-9, ply material properties,

E_1, E_2, G_{12} and v_{12}, are modeled as correlated random variables using copula. It is assumed that the fiber volume fraction is the dominant factor to make the correlation. Using the relationship between the elastic constants in terms of volume fraction from mixture rule, the correlation between material properties are calculated [16]. We assume that the material properties in Table 3-7 are the nominal values and the coefficient of variance for the nominal values are shown in Table 3-9. Covariance matrix that defines the correlation between material properties is calculated based on the coefficient of variations (See detailed information in Ref. [16]). It is assumed that the ultimate strains are independent each other. Variability in thickness and imperfection are also provided with Table 3-9. It is assumed that all the plies have the same variability in thickness. For the variability in imperfection, we randomly select an eigenvector and multiply the perturbation factor which is generated from the uniform distribution.

Variabilities of capacities are estimated using the uncertainty sources and ABAQUS model with MCS. Strength failure is estimated using load-strain curve and the maximum strain criterion. Strength failure beyond the buckling point is estimated using post buckling analysis. 200 samples are generated using ABAQUS. As it is assumed that there are errors in measurements of dimensions and material properties of the test specimen, the errors in test measurements are considered to estimate PF.

Table 3-10 shows the uncertainty in the test measurements and assumed values. Note that the effect of error in boundary condition is ignored since the effect of error in boundary conditions is very limited for this curved panel.

From the test measurements and error in measurements, the errors in measurements for buckling load and strain are obtained using Eq. (3-14). 100 samples are generated using ABAUQUS with the uncertainty sources in structural test. Best marginal distributions are fitted using K-S goodness of fit test, and Kendal's tau rank correlation coefficient is calculated. The best fit distributions for the test errors are normal distributions.

Correlation between the test errors is modeled using Frank copula and Kendal's tau. The parameters of the fitted distributions and Kendal's tau are shown in Table 3-11.

Using Eq. (3-17), a likelihood function for error in numerical model, $\hat{e}^{\lambda}_{calc}$ and $\hat{e}^{\varepsilon}_{calc}$ is obtained. Table 3-12 shows the type of best marginal CDFs and statistics of the errors in numerical model are shown. Correlation between two errors is also modeled with Frank copula and Kendal's tau. Error bounds in Table 3-4 are used for establishing prior distribution.

Estimating PF Based on a Single Test

PFs and their corresponding reliability indices of the composite panel are estimated in terms of different load levels. The updated distribution of the calculation errors is used to estimate PF with a test, and the prior is used for PF without test.

With the test, conservativeness in the PF estimate can be significantly reduced as shown in Table 3-13. In this study, the effect of errors in numerical model is considered to estimate PF. The change in PF after test represents uncertainty reduction in errors of numerical model. Also there is an observation that PF is increased exponentially proportional to the load.

Summary

In this chapter, an uncertainty model to incorporate the effect of tests on reducing uncertainty in estimating PF with multiple failure modes is proposed. In the model, the errors in numerical model are considered separately for estimating PF to show the effect of errors on estimating PF, and correlation between the errors is considered. Also a scheme of reducing uncertainty in predicting multiple failure modes with a single test is taken into account in the model. Statistical decomposition technique for correlated failure modes is also proposed to estimate PF without breaking their correlation. The proposed method is applied to a curved composite panel with a hole. Two correlated failure modes, buckling failure and strength failure, are considered. Typical uncertainties with composite materials, correlated variability in material properties and geometric imperfection, are also taken into account and considered to estimate PF of the panel.

The proposed method for estimating PF is demonstrated with a beam example. In this example, the effect of uncertainty in numerical error is quantified. The numerical example shows that performing a single test can significantly reduce the uncertainty in numerical model. For the curved composite panel, ABAQUS is used for non-linear analysis to predict buckling and strength failures. PF of the curved panel according to the load level is estimated with the proposed method and presented.

Table 3-1. Probability of failure calculation process.

1. Generating *N* random sets of input parameters, dimension *d* and material property *m*
2. Calculating *N* capacities with respect to the generated *N* sets of *d* and *m* using an analysis code (If test is performed go to step 3, otherwise go to step 6)
3. Generating *M* sample sets of $\hat{d}_{meas}$ and $\hat{m}_{meas}$ as for uncertainty in input parameters
4. Calculating *M* sample sets of $\hat{e}^{\lambda}_{calc}$ and $\hat{e}^{\varepsilon}_{calc}$ using test results which presented in ref [15] and $f_{\lambda,calc}\left(\hat{d}_{meas},\hat{m}_{meas}\right)$ and $f_{s,calc}\left(\hat{d}_{meas},\hat{m}_{meas}\right)$ with respect to the generated $\hat{d}_{meas}$ and $\hat{m}_{meas}$ using the analysis code
5. Fitting the *M* sample sets of $\hat{e}^{\lambda}_{calc}$ and $\hat{e}^{\varepsilon}_{calc}$ using copula and marginal PDFs.
6. Generating *M* errors using error bounds of buckling load and strain calculations
7. Generating *Q* errors in buckling load and strain using the fitted copula model
8. Combining the *N* sets from the step 2 and *Q* samples from step 6 and generate *N* sets of structural capacity samples
9. Categorizing those generated capacity samples from step 8 into two failure cases of buckling failure and strength failure and fit those samples to two CDFs (K-S goodness of fit test is used for fitting the samples)
10. Generating a large number of *R* samples from the two CDFs and *R* samples from random design load distribution and calculate PF
11. Repeating the step 10 by *N* times to obtain PF distribution

Table 3-2. Equations with error and true equation for the simple beam model.

	Buckling load	Strength failure load
True equation	$P^{\lambda}_{calc}=\frac{\pi^2 EI}{l^2}-\frac{C^2}{4EI}$	$\lvert\varepsilon_{calc}\rvert\le\varepsilon_u$ $\varepsilon_{calc}=-\left(\frac{P^s_{calc}}{EA}+\frac{0.5hC}{EI}\right)$
Equation with error	$P^{\lambda}_{true}=0.97\left(\frac{\pi^2 EI}{l^2}-\frac{C^2}{4EI}\right)$	$1.02\lvert\varepsilon_{true}\rvert\le\varepsilon_u$ $\varepsilon_{true}=-1.05\left(\frac{P^s_{true}}{EA}+\frac{0.5hC}{EI}\right)$

Table 3-3. Nominal values and variabilities from uncertainty sources.

	Uncertainty source	Nominal value	Variability	Distribution
Material properties	Manufacturing process	E: 200 GPa ε_u: 0.0025	CV=3% for E CV=1% for ε_u	Normal
	Measurement error	E: 0% ε_u: 0%	Std. of 1% for E No error for ε_u	Normal
Dimensions	Manufacturing process	b: 0.3 m h: 0.165 m	±1% for b and h	Uniform
	Measurement Error	b: 0% h: 0%	Std. of 0.5% for b and h	Normal
Axial force	Operating condition	TBD	CV=3% for P	Normal
Moment	Operating condition	TBD	CV=1% for C	Normal

Table 3-4. Error bounds for errors in numerical model.

Error types	Error bounds
Error in buckling load calculation $e^{\lambda}_{calc,Ptrue}$	[-0.05,0.05]
Error in strain calculation $e^{\varepsilon}_{calc,Ptrue}$	[-0.08,0.08]
Error in failure theory e^{f}_{Ptrue}	[-0.05,0.05]

Table 3-5. PF estimations with 1000 repetitions without couple.

	Load (P)	19 MN	19.5 MN	20 MN
w/ test (N=200 M=100)	Mean PF	1.18×10^{-4}	5.91×10^{-4}	2.42×10^{-3}
	Std. PF	5.85×10^{-5}	2.27×10^{-4}	7.34×10^{-4}
	COV	0.5	0.38	0.3
w/o test (N=200)	Mean PF	2.61×10^{-4}	1.01×10^{-3}	3.22×10^{-3}
	Std. PF	5.24×10^{-5}	1.73×10^{-4}	4.65×10^{-4}
	COV	0.2	0.17	0.14
True PF (system)		4.68×10^{-5}	2.96×10^{-4}	1.42×10^{-3}
True PF (buckling)		4.32×10^{-5}	2.68×10^{-4}	1.30×10^{-3}
True PF (strength)		1.86×10^{-5}	1.35×10^{-4}	0.7×10^{-4}

Table 3-6. PF estimations with 1000 repetitions with couple.

	Load (P)	2.1 MN	2.2 MN	2.3 MN
	Couple (C)		105 kN-m (fixed)	
w/ test (N=200 M=100)	Mean PF	1.72×10^{-4}	5.72×10^{-4}	3.24×10^{-3}
	Std. PF	1.44×10^{-4}	3.97×10^{-4}	1.62×10^{-3}
	COV	0.84	0.69	0.5
w/o test (N=200)	Mean PF	1.97×10^{-3}	3.17×10^{-3}	6.00×10^{-3}
	Std. PF	3.81×10^{-4}	5.84×10^{-4}	1.01×10^{-3}
	COV	0.19	0.18	0.17
True PF (system)		8.8×10^{-5}	3.63×10^{-4}	2.54×10^{-3}
True PF (buckling)		4.8×10^{-6}	1.45×10^{-4}	2.19×10^{-3}
True PF (strength)		8.6×10^{-5}	2.51×10^{-4}	6.0×10^{-4}

Table 3-7. Ply material properties / Ply section properties.

Material property	
E_1	135 GPa (19600 ksi)
E_2	13.0 GPa (1890 ksi)
G_{12}, G_{13}	6.4 GPa (930 ksi)
G_{23}	$E_2/3$
Poisson's ratio	0.38
Ply thickness	0.142 mm (0.0056 inch)
Stacking sequences	$[\pm 45/90/0_2/90/\mp 45]_s$

Table 3-8. Experiment results.

Buckling load	101.6 kN (22840 lb)
Surface strain	-0.0128

Table 3-9. Experimental results.

	Causes	Experimental variability	Modeling
Material properties	Variability	CV=4.25% for E_1, 2.75% for E_2, 1.5% for G_{12} and 5.25% for v_{12} (correlated) CV=6% for ε_{1u}, and ε_{1l}, 10% for ε_{2l}, ε_{2u} and ε_{12u}* (independent)	Considering correlation between the parameters using Gaussian copula
Thickness	Variability	±3% of thickness (0.0056×0.03=0.00269in)	Uniform distribution for individual ply thickness
Imperfection	Variability	±10% of thickness (0.0056×16×0.1=0.00896 in)	Uniform distribution Imperfection mode is randomly selected among mode 1, 2, 3, and 4

Table 3-10. Uncertainty sources in structural test.

	Causes	Experimental variability	Modeling
Material properties	Measurement	CV=1% for E_1, 3% for E_2, G_{12} and v_{12}	Independent normal distributions
Thickness	Measurement	±0.08% of thickenss (panel thickness: 0.0056×16=0.0896 in)	Unifrom distribution
Imperfection	Measurement	±0.08% of thickenss	Uniform distribution
Boundary condition	Imperfect BC	Torsional springs on nodes applying BC	Ignored as for little effect
Load	Measurement	0.256 lb (experimental buckling load: 22840 lb)	Ignored as for little effect

Table 3-11. Uncertainty sources on experiment.

(200 samples)	Buckling load	Surface strain
Mean	22801.01	0.0132
Standard deviation	214.07	0.000063
COV (std. of error)	0.93%	0.47%
Kendal's tau	0.15	

Table 3-12. K-S test to identify the best fit CDF for buckling load and surface strain.

	Error in buckling load	Error in surface strain
CDF type	Logn	Gamma
Mean	1.0041	0.975
Standard deviation	0.0094	0.0046
COV (std. of error)	0.93%	0.47%
Kendal's tau	0.15	

Table 3-13. Estimated PF with various load levels.

Load P	After test		Before test	
(lb)	PF	β	PF	β
2.0×10^{4}	1.14×10^{-1}	-1.21	1.49×10^{-2}	-1.04
1.9×10^{4}	4.78×10^{-2}	-1.67	6.89×10^{-2}	-1.48
1.8×10^{4}	1.61×10^{-2}	-2.14	2.56×10^{-2}	-1.95
1.7×10^{4}	4.12×10^{-3}	-2.64	7.04×10^{-3}	-2.46

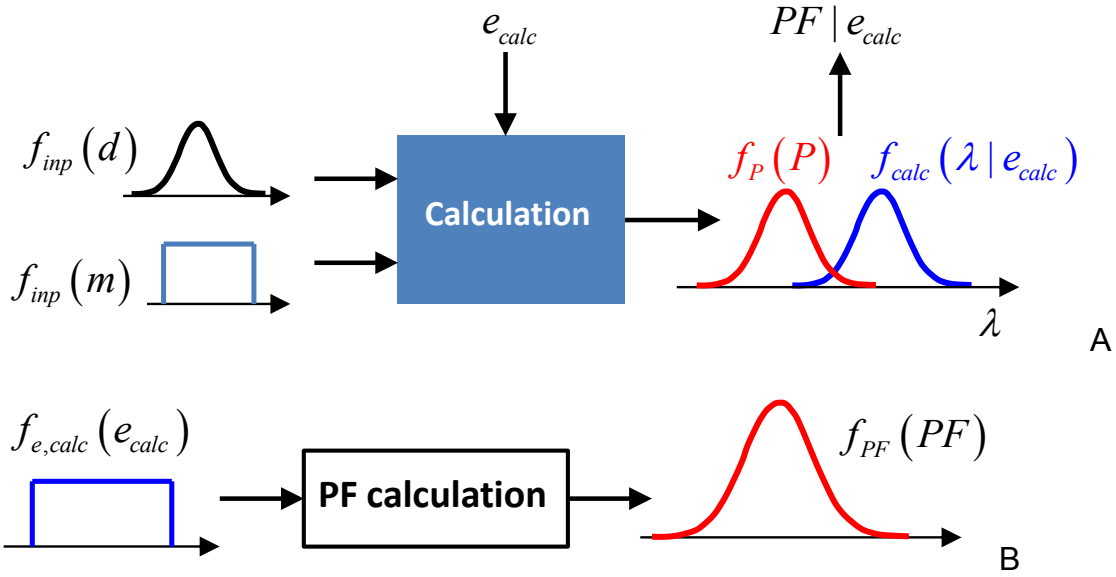

Figure 3-1. Illustration of estimating PF distribution. A) calculating PF for the input uncertainties, geometric dimensions *d* and material properties *m*, with respect to the error values e_{calc} in numerical model, and B) calculating PF distribution based on the error distribution.

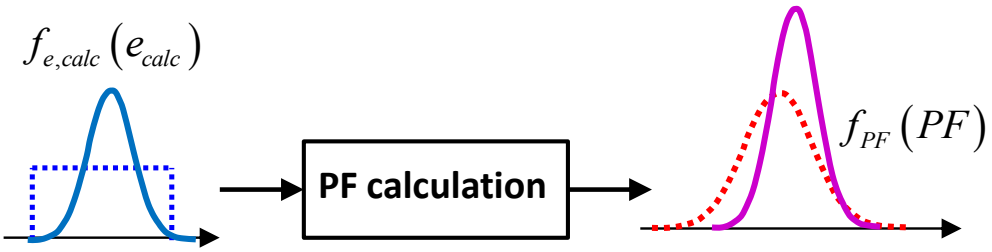

Figure 3-2. Illustration of the effect of tests on uncertainty in PF estimation by reducing uncertainty in numerical error by carrying out tests.

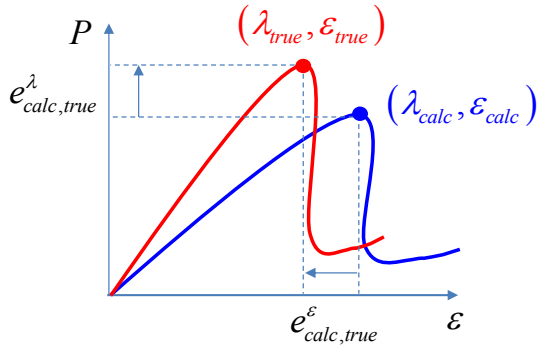

Figure 3-3. Illustration of errors in the load-strain curve.

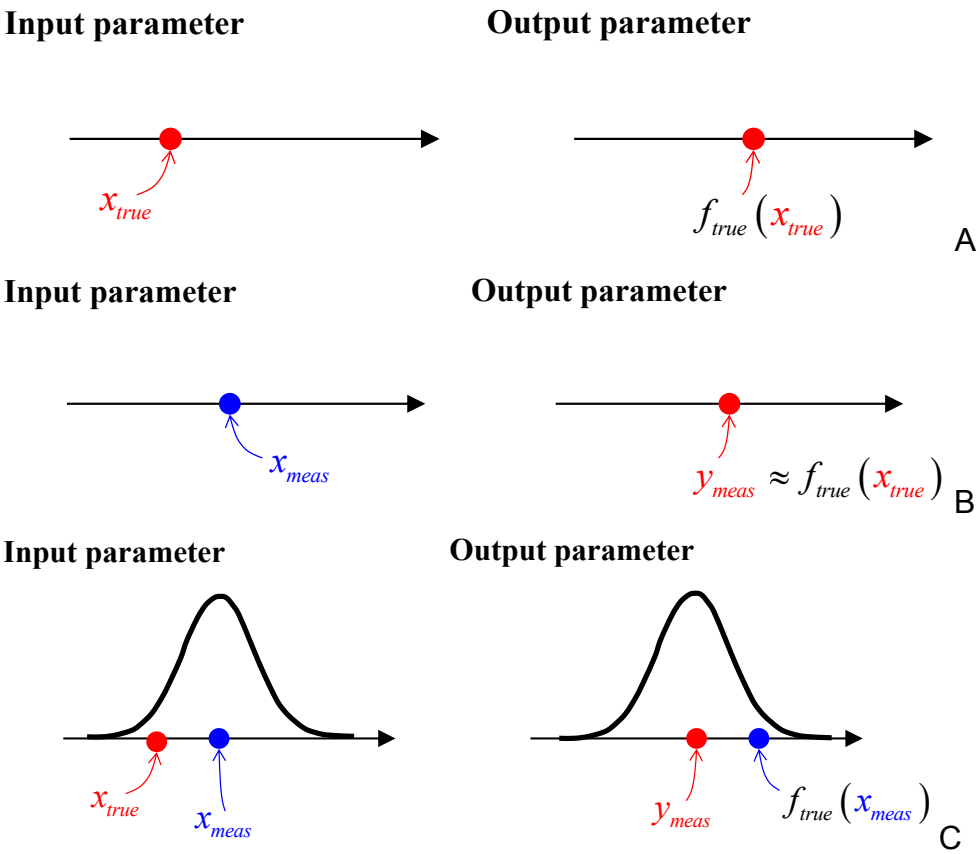

Figure 3-4. Illustration for the effect of errors in input parameters. A) test observation for input and output parameters without measurement errors (ideal case) and B) test observation for input and output parameters with measurement errors (real case), C) uncertainty in output parameters for the measurement error in input parameters.

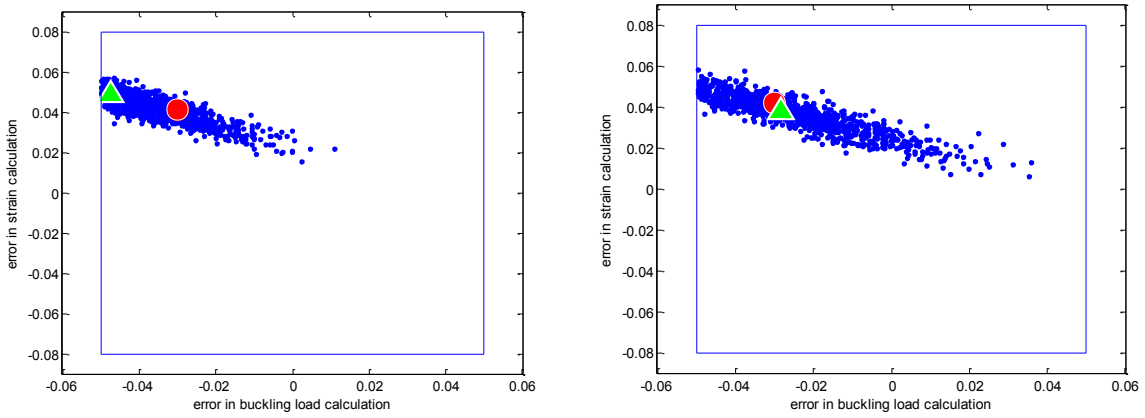

Figure 3-5. A scattered plot of the likelihood function (1000 samples), true error (red circle) and measured error (green triangle). A) Large error in test and B) Small error in test.

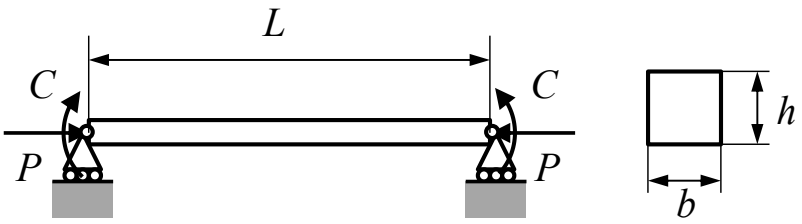

Figure 3-6. Simple beam model.

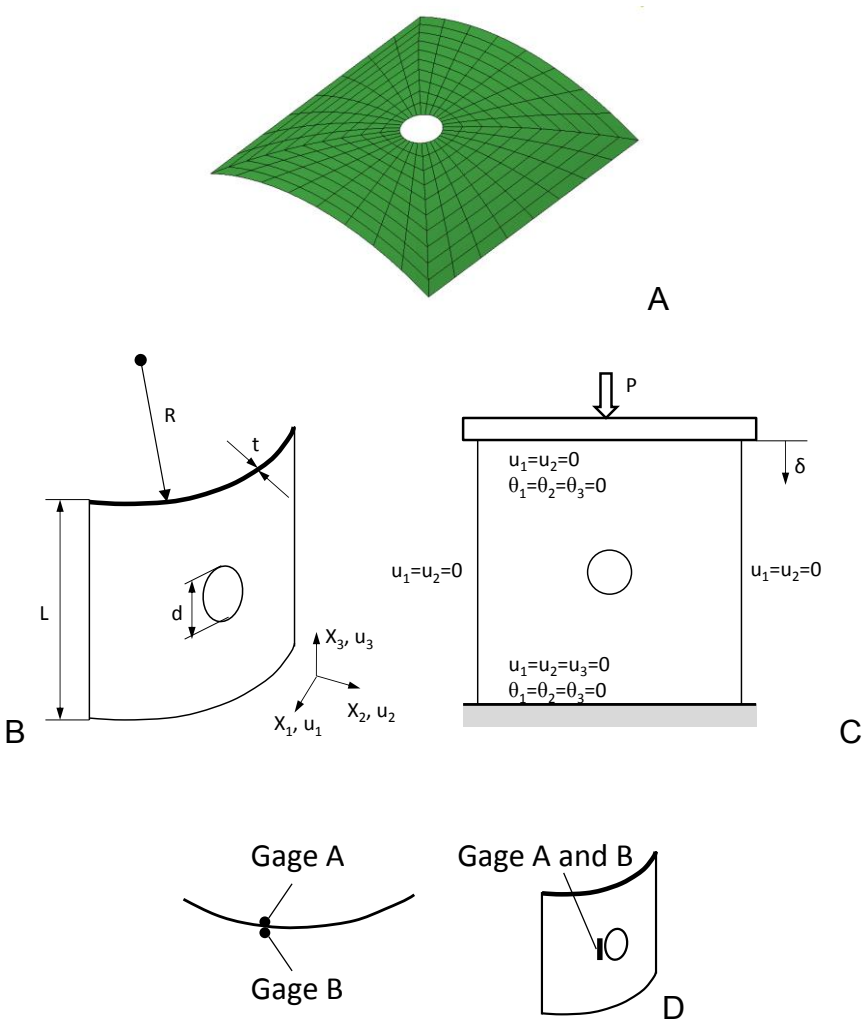

Figure 3-7. Curved composite laminate panel. A) Abaqus Model, B) geometry, C) boundary conditions and D) strain gage locations for test.

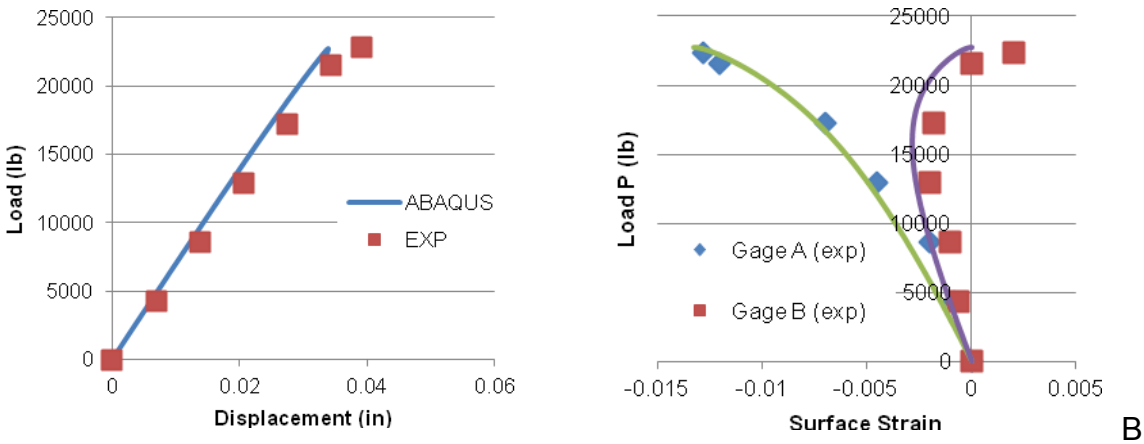

Figure 3-8. Curved composite laminate panel modeling with ABAQUS. A) Load-Displacement (P-δ) curve (up to buckling point) and B) Load-Surface strain curve.

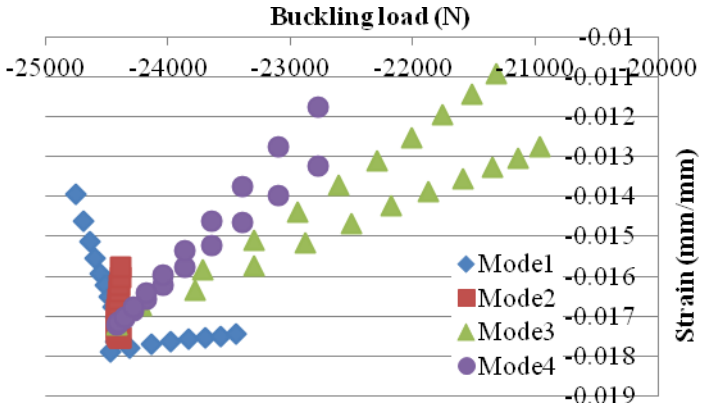

Figure 3-9. Effects of various imperfections (estimated simulation error).

CHAPTER 4
THE EFFECT OF IGNORING DEPENDENCE BETWEEN FAILURE MODES ON EVALUATING SYSTEM RELIABILITY

Motivation and Scope

System reliability is often evaluated with the assumption of independence to make calculation simple by ignoring dependence between failure modes. This chapter is to investigate the effect of ignoring dependence between failure modes on evaluating system reliability. The error in calculating system reliability is investigated with respect to the strength of dependence between two failure modes and the ratio between two marginal failure modes for varied system reliability.

Tail dependence, which is different from the strength of dependence, is introduced to explain the behavior of the error in system reliability by ignoring dependence. Since failure is occurred in the tail of a limit state distribution, tail dependence is actually influential to the error rather than the general dependence measures, such as the linear correlation coefficient and the Kendall's tau. To study the effect of dependence model, the error in terms of various dependence models is determined using the famous bivariate normal distribution and copulas.

The chapter is composed of five sections. First section is to introduce the error due to ignoring dependence on calculating system reliability. A structural example of two trusses having two dependent component failure modes is presented to facilitate understanding of dependence between failure modes and the error due to ignoring dependence. Second section is to investigate the error using examples that have the widely known bivariate normal distribution (BVN) as for their dependence model. The concept of tail dependence is introduced with the L function as a measure of the tail dependence. The error by ignoring dependence with a strong tail dependence is

compared to that of BVN, which does not have a strong tail dependence. Third section is to introduce copulas to investigate the effect of different dependence models. Fourth section demonstrates that ignoring dependence leads to only small error in an optimal solution and the corresponding design weight for a reliability based optimization of the two trusses. Finally, summary of this chapter is presented.

Error due to Ignoring Dependence on Calculating System Reliability

In this section, the error due to ignoring dependence on calculating system reliability is quantified with structural examples with two dependent failure modes.

Dependence between Failure Modes and Calculating Reliability

Structural failure with multiple failure modes is modeled with uncertainties in limit states, which are also called output uncertainties. Dependence between failure modes is equivalent to dependence between output uncertainties. If there is a system with N failure modes, limit states are defined such that the i^{th} failure event occurs when

$$G_i \le 0,\ i = 1,...,N \tag{4-1}$$

while the system is intact when

$$G_i > 0,\ i = 1,...,N \tag{4-2}$$

PF of only one failure mode is referred as a marginal PF that is defined as

$$P_{fi} = \Pr\left(G_i \le 0\right) \tag{4-3}$$

Two commonly used concepts for multiple failure modes are a series and parallel failure models. For the series failure model, the system fails if any of its failure modes is activated. For the parallel model, the system fails if all of its failure modes are activated [48]. The series failure model takes account of union of failures, and the parallel model takes account of intersection of failures. Both models are affected by dependence of

failure modes. In this chapter, the effect of ignoring dependence is discussed with the series model, since it is a common failure scenario in structural design.

A series model composed of two failure modes are defined using two limit states. System PF with dependent two failure modes (or exact system PF) is expressed as

$$P_{f\,sys} = \Pr\left(\{G_1 \le 0\} \bigcup \{G_1 \le 0\}\right) \tag{4-4}$$

Using the well-known expansion theorem [47], the probability of the union of two events is decomposed as

$$P_{f\,sys} = \Pr\left(G_1 \le 0\right) + \Pr\left(G_2 \le 0\right) - \Pr\left(\{G_1 \le 0\} \bigcap \{G_1 \le 0\}\right) \tag{4-5}$$

Approximate analytical methods have been developed to evaluate the system PF without integrating the joint PDF over the failure region [47-49]. However, if the error is not significant, assuming independence is more attractive since it makes the problem simple without any specialized methods. With the independence assumption, the system PF can be calculated based on the marginal PFs and the probability of the intersection with the independence assumption is expressed withEq. (4-5) and

$$P_{f\,sys}^{idp} = \Pr\left(G_1 \le 0\right) + \Pr\left(G_2 \le 0\right) - \Pr\left(G_1 \le 0\right)\Pr\left(G_2 \le 0\right) \tag{4-6}$$

where the superscript idp represents the independence assumption.

Illustrative Truss Example

A simple two-member truss shown in Fig. 4-1 is used to illustrate the dependence between limit states. A horizontal force *h* and vertical force *v* are applied at the joint of two members. The truss structure has two failure modes due to the resulting stresses: failure of elements 1 and 2 when the corresponding stresses exceed the ultimate stress, σ_{u1}, that the material can sustain.

The limit state and the member force of element 1 are defined as

$$G_1 = A_1\sigma_{u1} - F_1$$
$$F_1 = \frac{1}{2}\left(\frac{v}{\cos\alpha} + \frac{h}{\sin\alpha}\right) \quad (4\text{-}7)$$

The limit state and the member force of element 2 are defined as

$$G_2 = A_2\sigma_{u2} - F_2$$
$$F_2 = \frac{1}{2}\left(\frac{v}{\cos\alpha} - \frac{h}{\sin\alpha}\right) \quad (4\text{-}8)$$

It is assumed that the ultimate strength and two external forces are input uncertainties, and the height of the structure and angle are deterministic. The values and distributions of these variables will be given in the reliability-based optimization example section.

Figure 4-2A shows a scatter plot of 10,000 randomly generated limit state pairs, G_1 and G_2, which shows dependence between two failure modes. The linear correlation coefficient between G_1 and G_2, is 0.79. Because the limit states are linear with respect to random variables and because these random variables are normally distributed, the joint probability density function (PDF) is bivariate Gaussian (normal). The system PF, P_{fsys}, is estimated as the ratio of the number of samples in the shaded area in Figure 4-2A to the total number of samples. The histograms shown on both axes are marginal histograms representing the marginal PDF of limit states. Figure 4-2B is a contour plot of the joint PDF of limit states G_1 and G_2, based on the 10,000 samples.

Error due to Ignoring Dependence for Bivariate Gaussian Joint Distribution

It is easy to calculate the system PF if the two failure modes are assumed to be independent, but this incurs an error. Figure 4-3 shows the difference in intersection probability with and without considering dependence between the two failure modes.

Figure 4-3A shows 10,000 samples of the two dependent limit states. The samples are generated from the bivariate normal distribution with mean vector of (1.2,1.2) and the standard deviation vector of (1.0,1.0), and the correlation coefficient of 0.8. The shaded region is the failure region. When the failure modes are assumed to be independent, the joint PDF is equal to the product of two marginal PDFs of limit states, whose corresponding samples are shown in Fig. 4-3B. The numbers of samples in the failure region of G_1, in the failure region of G_2, in the region of intersection and in the region of union are shown in Table 4-1. The numbers reflect the true probabilities and sampling errors due to the finite number of samples (the standard error in each number in Table 4-1 is approximately equal to its square root).

The percent error due to ignoring dependence is calculated as

$$\text{Error} = \left| \frac{P_{f\,sys}^{idp}}{P_{f\,sys}} - 1 \right| \times 100(\%) \tag{4-9}$$

where $P_{f\,sys}$ is the system PF with dependence considered, while $P_{f\,sys}^{idp}$ is the probability assuming independence. The reliability index $\beta = -\Phi^{-1}\left(P_f\right)$ is another widely used measure, where $\Phi^{-1}(\bullet)$ is the inverse of cumulative distribution function (CDF) of standard normal distribution. The error in terms of reliability index is expressed as

$$\text{Error} = \left| \frac{\beta_{sys}^{idp}}{\beta_{sys}} - 1 \right| \times 100 = \left| \frac{-\Phi^{-1}\left(P_{f\,sys}^{idp}\right)}{-\Phi^{-1}\left(P_{f\,sys}\right)} - 1 \right| \times 100\ (\%) \tag{4-10}$$

where β_{sys}^{idp} is reliability index ignoring dependence and β_{sys} is the reliability index with dependence considered.

The Effect of Ignoring Dependence on Error in System Reliability

Error in System Reliability for Bivariate Normal Dependence Model

In this section, the effect of ignoring dependence between failure modes is shown with respect to two parameters; the magnitude of system PF and the strength of dependence given in terms of the linear correlation coefficient ρ. A hypothetical system is assumed with two failure modes and has a bivariate normal distribution (BVN) for a joint PDF of limit states. By changing parameters of BVN, the effect of the level of PF and ρ on the error is studied.

Both failure modes are first assumed to have the same marginal PFs; that is, both have the same PF. The effect of different marginal PFs will be discussed later. The exact system PF is calculated from Eq. (4-5), while the system PF ignoring dependence is calculated from Eq. (4-6).

Since BVN is the joint PDF of limit states, marginal distributions are normal. The mean and standard deviation of the marginal distributions are set to z and 1, respectively. By changing the mean and the correlation coefficient, the magnitude of system PF and the strength of dependence are varied. The joint PDF of limit states and parameters are defined as

$$\begin{bmatrix} G_1 \\ G_2 \end{bmatrix} \sim N_2\left(\begin{bmatrix} z \\ z \end{bmatrix}, \begin{bmatrix} 1 & \rho \\ \rho & 1 \end{bmatrix}\right) \tag{4-11}$$

where $N_2(\bullet,\bullet)$ is BVN of G_1 and G_2. Since the failure is associated with negative values of limit states, the intersection probability of the two failures is obtained with CDF of the BVN. The Error is calculated with Eqs. (4-9) and (4-10). The strength of dependence is usually categorized from very weak to very strong in terms of the linear correlation

coefficient, ρ [55]. The strength of dependence is categorized to moderate, strong and very strong for $0.4 \le \rho \le 0.7$, $0.7 \le \rho \le 0.9$, and $0.9 \le \rho \le 1$, respectively. The error is calculated for strong correlation (0.7-0.9) in terms of the system PF with the range of 10^{-1} to 10^{-6}.

The errors in reliability index and the PF due to ignoring dependence are shown in Figure 4-4 with five different linear correlation coefficients. The errors in reliability index and PF decrease as system reliability index increases regardless the magnitude of the linear correlation coefficient. In Table 4-2, even with strong dependence between failure modes, ρ=0.8, the error in PF is less than 10% for the PF level less than 10-4, and error in reliability is lower than 1% for reliability levels lower than 3.28. The observations imply that the interaction between failures becomes weak when PF is small.

The errors in reliability index and PF due to ignoring dependence are shown in Fig. 4-4 for different linear correlation coefficients. The errors in reliability index and PF decrease as system reliability index increases regardless the level of linear correlation coefficient. In Table 4-2, even with strong correlation between failure modes, ρ=0.8, the error in PF is less than 10% for the PF level less than 10^{-4}, and the error in reliability index is lower than 1% for the level of reliability index lower than 3.28. The observations imply that the interaction between failure modes becomes weak when PF is small.

One can see from Table 4-2 and Fig. 4-4 that the error in reliability index is much smaller than the error in PF. At this point, it is appropriate to note that at low probabilities of failure, small errors in input distributions may lead to small errors in reliability index but large errors in PF. Therefore, striving for very accurate small PF is out of reach anyhow. For example, distributions of failure stresses are typically based

on samples of 100 tests or less. The standard error of a standard deviation of a normal distribution based on a sample of 100 is 7%. At a PF of 10^{-4}, this 7% error would lead to approximately 7% error in reliability index, but more than 50% error in PF.

The Effect of Tail Dependence on the Error in System Reliability

One way of measuring the dependence in the tail region is the shape of distribution. As shown in Fig. 4-3, independent distributions have circular-shaped contour at the failed tail region, while dependent distributions have a sharp contour in this region. For independent modes with a low PF, the low-left region of the contour is locally circular. On the other hand, if we had a distribution that is sharp in that region, as illustrated in Fig. 4-5B, it indicates that the tail dependence between the two failure modes is strong. The linear correlation coefficient is not enough to evaluate the level of tail dependence because the BVN shown in Fig. 4-5A has weaker tail dependence than the other distribution shown in Fig. 4-5B while they have the same correlation coefficient of 0.8.

For distributions with strong tail dependence, we may expect that the error in PF decrease slowly, or will not decrease with decreasing PF. Thus, measuring the degree of tail dependence is important, for which we rely on a statistical measure, denoted by *L* [57], for the lower tails of two distributions. The *L* function is the ratio between probability of intersection and marginal probability. When independence assumption is applied to the PF, it is the ratio between the probability of double failure and the probability of the first mode of failure (or the second since they are the same). More formally, the ratio is defined as a function of marginal PF as

$$L(z) = \Pr\left(G_1 < F_{G_1}^{-1}(z), G_2 < F_{G_2}^{-1}(z)\right) / z \qquad (4\text{-}12)$$

where z is marginal probability. $F_{G_1}^{-1}(z)$ is the inverse CDF of G_1 for given probability z.

The reason that this ratio is relevant to our case is that the system PF is the sum of the two marginal probabilities of failure minus the probability of intersection (see Eq. (4-5)). With the assumption of independence, the L function becomes z because the probability of the intersection is the square of the marginal probability. The error is then about a half of the difference between *L* and z.

Figure 4-6A shows the degree of dependence in the tail of BVN as function of marginal probability and the correlation coefficient. When two limit states are independent, ρ=0, the probability of the intersection is the square of marginal probability, and the ratio is nothing but the marginal probability; i.e., *L*(z) = z. One can read an approximate error for different levels of system PF. For example, when $z=10^{-5}$, the system PF is approximately $2x10^{-5}$, and for ρ =0.8, we see that L=0.14, which estimates about a 7% error in PF.

There are cases that the error does not decrease as the level of system PF decreases because of strong tail dependence. Figure 4-6B shows curves of *L* function for three different degrees of tail dependence. Here, they have the same correlation coefficient and tail dependence of the joint PDF with strong tail dependence is compared to that of BVN in terms of *L* function.

The red *L* function curve in Fig. 4-6B, a weak tail dependence case, converges faster than that of BVN. The error of neglecting dependence is smaller than that of BVN for the same system PF and the error becomes negligible even for a relatively large system PF. However, the green *L* function curve in Fig. 4-6B, a strong tail dependence case, does not decrease; error remains the same even for a very small system PF. The

behavior of *L* function shows that the degree of dependence is very strong even in the extreme tail that there is almost no change in the *L* function.

Figure 4-7A shows the variation of error as a function of the level of system PF for different tail dependences. For a weak tail dependence, even with a strong correlation coefficient, ρ=0.8, the error in PF is less than 10% for the PF level less than 5×10^{-2}. On the other hand, for a strong tail dependence, the error stays high even for a low PF. On the other hand, in terms of the reliability index in Fig. 4-7B, even a strong tail dependence does not change the trend of low errors for high values of reliability index (low values of the PF).

Table 4-3 presents the magnitudes of maximum system PF and minimum reliability index for different target errors. For example, for the weak tail dependence, in terms of reliability index, there is only 1% error when system reliability index is 1.98.

From Table 4-3, we can observe that the error in system PF will not reduce, or reduce more slowly with decreasing PF, while the error in reliability index will still reduce even for distributions with strong tail dependence. A positive side is that the error in reliability index decreases even with strong tail dependence as shown in Fig. 4-7B.

We use the L function as a measure of the degree of tail dependence herein. Another common approach to measure the degree of tail dependence is to estimate TDC [38,58]. The limit of *L* is referred to as tail dependence coefficient (TDC) that represents the strength of tail dependence [38,54].

$$TDC = \lim_{z \to 0} L(z) \tag{4-13}$$

L for BVN converges to zero as z approaches zero that error due to ignoring dependence decreases as system PF decreases. However, distributions with strong tail

dependence have non zero TDC. Unfortunately, accurate TDC estimation to determine the degree of tail dependence requires more than 1,000 samples, which may always not be feasible [58].

Error in System Reliability for Various Dependence Models Defined with Copulas

Copula Theory

The previous sections presented results for BVN and generic strong and weak dependence. In this section, a more general approach will be taken to describe correlation types of distributions. Joint distributions are often modeled by using copulas, and four common copulas in Fig. 4-8 are used to explain the tail dependence and error in neglecting the dependence.

The word 'copula' is a Latin noun which means "a link". The word was employed in a statistical term by Sklar (1959) in the theorem describing the functions that join marginal CDF to form a joint CDF [18]. this context, copula is a function that links a joint CDF to its marginal CDFs [52-54]. Copula is a joint CDF whose one-dimensional margins are uniform in the interval (0,1). Copula is an important concept for modeling a joint CDF that includes dependence.

It is noted that BVN is defined with Gaussian copula with normal marginal distributions but a Gaussian copula is not limited to BVN or multivariate normal distribution. The marginal distributions of Gaussian copula can be any distribution. For example, we will observe the behavior associated with a Gaussian copula when the marginal distributions are Gumbel distributions.

Let $\mathbf{Y}=\{Y_1,Y_2,...,Y_n\}^T$ be a vector of n-dimensional random variables, which are defined with marginal CDFs, $F_{Y_i}(y_i)$. The probability of intersection is a function of dependence.

The probability of intersection of n-dimensional random variables is also called a joint CDF that is defined as

$$F_{Y_1,...,Y_n}(y_1,...,y_n) = \Pr(Y_1 \le y_1,...,Y_n \le y_n) \tag{4-14}$$

Copula functions defines the joint CDF with marginal CDFs

$$F_{Y_1,...,Y_n}(y_1,...,y_n) = C\left(F_{Y_1}(y_1),...,F_{Y_n}(y_n)\right) \tag{4-15}$$

where C is a copula function. Note that copula functions are independent to marginal CDFs and all arguments of copula function have a domain of [0, 1]. Also, due to the property of multivariate CDF, the output of the copula function also has a domain of [0, 1].

Figure 4-9 shows L function for the copulas shown in Fig. 4-8. As expected, the copula with a sharp tail, Clayton, has a very strong tail dependence. Gaussian copula has stronger tail dependence than Gumbel and Clayton copulas.

It is noteworthy that the type of marginal distributions is immaterial as far as the error due to ignoring dependence is concerned. The error is a function of the magnitude of system PF and the type of copula. For example, if the marginal distributions are lognormal and the copula defining the joint distribution is Gaussian, then the error will be the same as in the case of BVN. The readers can refer to Appendix B for detailed explanation.

The Effect of Marginal Distributions on the Errors due to Ignoring Dependence

Since copula is independent to marginal distributions, error depends on copulas. For example, dependence of two correlated random variable pairs are defined with same copula and marginal PFs are the same, the type of marginal distributions are independent to error.

Figure 4-10A and Figure 4-10B show joint PDF contours of two failure modes. Figure 4-10A shows a joint PDF contour with different marginal distributions of limit state, the extreme distribution for G1 and the normal distribution for G2. Figure 4-10B shows a joint PDF contour with the same marginal distributions, the normal distribution for G1 and G2. They have the same marginal PFs (Pf1 = Pf2 = 0.1265) and dependence model (the Gaussian copula with ρ=0.7). The shaded region is the region of intersection PF. The Two joint PDFs of the limit states have different contour shapes. However, their errors are the same 19.8% since their marginal PFs and copula models modeling dependence are the same.

The Effect of Ignoring Dependence for Different Copulas

In the previous section, the error due to ignoring dependence for BVN, which is defined with a Gaussian copula, is shown as a function of the magnitude of system PF and the correlation coefficient. In this section, the errors with different dependence models are defined with Clayton, Gumbel and Frank copulas. Since the type of marginal distributions is immaterial to the error, the normal distributions are used as marginal CDFs. Then, the errors are calculated in terms of system PF and reliability index. The system PF shown in Eq. (4-5) is rewritten using copula as

$$\begin{aligned} P_{f,sys} &= F\left(0;z,1\right)+F\left(0;z,1\right)-C\left(F\left(0;z,1\right),F\left(0;z,1\right),\theta\right) \\ \beta_{sys} &= -\Phi^{-1}\left(P_{f\,sys}\right) \end{aligned} \tag{4-16}$$

The magnitude of PF and the strength of dependence are controlled by changing z and θ. PF ignoring dependence is expressed as

$$P_{f,sys} = F\left(0;z,1\right)+F\left(0;z,1\right)-F\left(0;z,1\right)F\left(0;z,1\right) \tag{4-17}$$

The errors in Eqs. (4-9) and (4-10) are shown in Fig. 4-11 for a range of correlation coefficients. It is observed that the error in reliability index decreases as system reliability increases even for strong tail dependence. In the case of system PF, however, the error does not decrease for the Clayton copula, but the error decreases for the other two copulas.

Although the Kendall's tau is used to define the level of dependence, the corresponding linear correlation coefficient is shown for the purpose of consistency. Since there is no universal way to convert Kendall's tau to the linear correlation coefficient, we generate 10,000 samples with a given level of Kendall's tau, from which the corresponding linear correlation coefficient is calculated. This process is repeated for different Kendall's tau to find the specific value of linear coefficient. It is noted that different copulas yield different values of linear correlation coefficients for the same value of Kendall's tau. For example, Kendall's tau of 0.63 with the Clayton copula and standard normal marginal distributions has the strength of dependence 0.8 in terms of the correlation coefficient. Kendall's tau of 0.599 with the Gumbel copula and standard normal marginal distributions has the same dependence in terms of the correlation coefficient.

Table 4-4 presents the magnitudes of minimum system reliability indices for 5% and 1% target errors. From Fig. 4-11 and Table 4-4, we see that, as expected, for the Frank and Gumbel copulas, which have weak tail dependence, the errors in the reliability index decay fast for high reliability index. However, even for the Clayton copula with a strong tail dependence, the error reduces relatively fast. Error in the reliability index converges to zero as the reliability index increases. In Table 4-5, the

magnitudes of maximum system PFs for 10% and 5% errors are shown. The errors in PF with Gumbel and Frank copulas decrease as reliability indices increase since they have a weak tail dependence. For Frank copula, the error becomes less than 5% at the level of 10^{-3} even at the very large correlation coefficient of ρ = 0.9. For the Clayton copula model, on the other hand, the error in PF increases as reliability increases due to its strong tail dependence.

In Table 4-5, magnitudes of system PFs for 10% and 5% errors are shown. Error in the reliability index converges to zero as the reliability index increases. For the error in PF with Gumbel and Frank copula, it decreases as reliability index increases since they don't have strong tail dependence. Frank copula with weak tail dependence, the error becomes less than 1% at the level of 10^{-4} even at the very large correlation coefficient of ρ = 0.9. For the Clayton copula model, on the other hand, error in PF increases as reliability increases due to its strong tail dependence.

The Effect of the Ratio between Marginal Probabilities of Failure

The effect of the ratio between marginal PFs also turns out to have a significant effect on the error. The Gaussian and Clayton copulas are considered since the other copulas have a small error because of their weak tail dependence.

The ratio between P_{f2} and P_{f1} is denoted as α as

$$P_{f2} = \alpha P_{f1} \tag{4-18}$$

Figure 4-12 shows the error with respect to the magnitude of reliability index and logarithmic PF while the strength of dependence is kept as ρ = 0.8. From the graphs, it is clear that the error is maximal when the ratio is 1 and decreases substantially with

increasing ratio. For a strong tail dependence copula, Clayton, the effect is most dramatic so that by the time the ratio is 8, even the errors in PF are near 10%.

As the ratio increases, the error in reliability index and the error in PF decrease. Table 4-6 shows minimum reliability index for 5% and 1% error with respect to the ratio of marginal PFs. The error monotonically decreases as reliability index increases. Table 4-7 shows maximum system PF for 10% and 5% error with respect to the ratio. For Gaussian as a dependence model, the PF for 10% error is 1.4×10^{-4} for the ratio of 1 and the PF for 10% error is 1.7×10^{-4} for the ratio of 4. For the ratio of 8, the error is less than 10% for all PF variation. For Clayton, the error is always larger than 10% but the ratio of marginal PFs affects the error a lot as shown in Fig. 4-11D.

Reliability-based Design with Multiple Failure Modes

Reliability-based design optimization (RBDO) is performed to demonstrate further the effect of ignoring dependence for a structure which is required to be highly reliable. The previous truss structure in Fig. 4-1 is used for RBDO. The optimization formulation is given as

$$\begin{aligned} &Minimize: Mass = A_1 + A_2 \left(\alpha = 45°\right) \\ &subject\ to: \ \beta_{allow} \le -\Phi^{-1}\left(P_{f\,sys}\right) \\ &\qquad P_{f\,sys} = \Pr\left(\{G_1 < 0\} \cup \{G_2 < 0\}\right) \end{aligned} \tag{4-19}$$

where A_1 and A_2 are design variables. FORM is used to evaluate marginal PFs during design optimization iterations and the system PF is calculated by assuming independence. Since the limit states are linear functions of random variables, FORM provides exact marginal PFs of two failure modes, the failure modes are statistically dependent. Table 4-8 shows input variables.

Figure 4-13A shows the weight and system reliability index in terms of design variables. The solid lines with label (equivalent reliability index) are exact contour lines for system reliability index and the dashed lines are corresponding contour lines with independence assumption. The discrepancy between the solid line and the dashed lines represents the error, and the difference in weight due to the error is defined as a weight penalty. For the same allowed system reliability index, some part does not have discrepancy between two constraint lines since one failure mode is dominant so that there is no error in calculating the system reliability index. The filled 2D contour is weight, where light gray represents heavy weight and dark gray represents light weight. Optimum solution provides minimum weight while the system reliability index constraint is not violated. The star marker is the exact optimum solution and the circle marker is the optimum solution ignoring dependence for the target system reliability of $\beta_{allow} = 3$.

As shown in Figs. 4-11 and 4-12, the magnitude of error is inversely proportional to the system reliability index. For the target system reliability of $\beta_{allow} = 3$, the error is very small, while the errors for $\beta_{allow} = 1.5$ ($PF_{allow}=0.067$) and $\beta_{allow} = 2$ ($PF_{allow}=0.023$) are clearly visible.

Figure 4-13B shows minimum weight for given allowed system reliability indices. The star and circle markers are the exact optimum solution and the optimum solution with independence assumption, respectively. There is 3.1% weight penalty for $\beta_{allow} = 1.5$ and the weight penalty is reduced to 0.5% for $\beta_{allow} = 3.5$.

For the allowable reliability index of 3.5, at the optimal design point, the correlation coefficient between the two failure modes is 0.8 and the ratio between marginal probabilities of failure is 1.12 ($P_1=0.00014$ and $P_2=0.00012$).

It is noteworthy that the strong correlation is due to the fact that randomness in the loads and strength affects the two failure modes in a similar way. That dependence does not mean that design improvement in one failure will affect the other failure. For this optimization problem, A_1 will affect only the reliability of element 1 and A_2 will affect only the reliability of element 2.

Summary

In this chapter, the effect of ignoring dependence between failure modes was studied. The effects of tail dependence and the ratio between marginal PFs were found to be significant. For low probabilities of failure, we can conclude that: 1) for errors in system reliability index, we can neglect dependence even for strong tail dependence; and 2) for errors in system PF, we can neglect dependence when the ratio of marginal PFs is high or tail dependence is not very strong.

To demonstrate the effect of ignoring dependence, we started with two failure modes obeying the bivariate normal (BVN) distribution. For the BVN with strong dependence with a correlation coefficient of $\rho = 0.8$, there is 1% error in the system reliability index at 3.28, and there is 10% error in system PF at 10^{-4}.

For other distributions, the decay of errors with increasing reliability index depends on a parameter called tail dependence. To illustrate the effect of tail dependence, we studied four commonly used copulas, Gaussian, Clayton, Gumbel and Frank copulas.

For strong tail dependence between failure modes, such as the Clayton copula, the errors in system PF do not decay even for a low system PF. However, the errors in system reliability index still decay fast for high reliability index. Possibly, small errors in large values of reliability index are acceptable even if the relative errors in PF are high.

This is because similar large errors in PF are inevitable due to small errors in input distributions.

It is also found that the ratio between marginal PFs is influential to the error, especially for strong tail dependence. It is observed that the errors in PF are small when the ratio of marginal PFs is larger than 8 even for a strong tail dependence.

Table 4-1. The number of samples in Fig. 4-3 (numbers in parenthesis are the numbers expected from the exact probabilities).

# of samples	Considering dependence	Ignoring dependence
$G_1 < 0$	1182 (1151)	1126 (1151)
$G_2 < 0$	1153 (1151)	1198 (1151)
$G_1 < 0$ and $G_2 < 0$	679 (665)	138 (132)
$G_1 < 0$ or $G_2 < 0$	1656 (1637)	2186 (2170)

Table 4-2. Effect of linear correlation coefficient on minimum reliability index and maximum PF for the target errors due to ignoring dependence with two failure modes defined with BVN.

Reliability measure	Target error	ρ =0.7	ρ =0.75	ρ =0.8	ρ =0.85	ρ =0.9
Reliability index	5%	1.68	1.79	1.93	2.10	2.31
	1%	2.82	3.03	3.28	3.60	4.04
Probability of failure	10%	3.4×10^{-3}	9.4×10^{-4}	1.4×10^{-4}	6.4×10^{-6}	1.6×10^{-8}
	5%	1.7×10^{-4}	2.4×10^{-5}	1.4×10^{-6}	1.1×10^{-8}	1.5×10^{-11}

Table 4-3. Minimum reliability index and maximum PF needed for the target errors with respect to the strength of tail dependence for given magnitudes of error.

Reliability measure	Target error	ρ =0.8 (BVN)	ρ =0.75 (strong tail dependence)	ρ =0.8 (weak tail dependence)
Reliability index	5%	1.93	3.13	1.44
	1%	3.28	6.92	1.98
Probability of failure	10%	1.4×10^{-4}	N/A	5.0×10^{-2}
	5%	1.3×10^{-6}	N/A	2.5×10^{-2}

Table 4-4. Minimum reliability index for 5% and 1% target errors (in reliability index) versus the strength of dependence measured by the linear correlation coefficient.

Copula	Target error \ ρ	ρ =0.7	ρ =0.75	ρ =0.8	ρ =0.85	ρ =0.9
Clayton	5%	2.88	3.01	3.14	3.26	3.38
	1%	6.50	6.72	6.92	7.10	7.27
Gumbel	10%	1.40	1.50	1.63	1.78	1.96
	5%	2.27	2.42	2.60	2.82	3.12
Frank	10%	1.30	1.37	1.44	1.53	1.63
	5%	1.86	1.92	1.98	2.06	2.17

Table 4-5. Maximum system PF for 10% and 5% target errors in PF (not error in logarithm of PF) with respect to the strength of dependence measured by the linear correlation coefficient.

Copula	Target error	ρ =0.7	ρ =0.75	ρ =0.8	ρ =0.85	ρ =0.9
Clayton		N/A				
Gumbel	10%	3.72×10^{-2}	2.07×10^{-2}	9.63×10^{-3}	3.21×10^{-3}	5.64×10^{-4}
	5%	1.54×10^{-4}	4.79×10^{-5}	9.58×10^{-6}	8.52×10^{-7}	7.29×10^{-8}
Frank	10%	7.7×10^{-2}	6.3×10^{-2}	5.0×10^{-2}	3.9×10^{-2}	2.7×10^{-2}
	5%	7.3×10^{-3}	6.0×10^{-3}	4.9×10^{-3}	3.8×10^{-3}	2.7×10^{-3}

Table 4-6. Minimum reliability index for 5% and 1% target errors versus the ratio with ρ = 0.8.

Copula	Target error	ratio =1	ratio =2	ratio =4	ratio =8
Gausian	5%	1.94	1.84	1.56	1.14
	1%	3.28	3.19	2.94	2.54
Clayton	10%	3.14	2.68	1.92	1.25
	5%	6.96	6.14	4.63	3.31

Table 4-7. Maximum system PF for 10% and 5% target errors with respect to the ratio with ρ = 0.8.

Copula	Target error	ratio =1	ratio =2	ratio =4	ratio =8
Gaussian	10%	1.4×10^{-4}	2.7×10^{-4}	1.7×10^{-3}	N/A
	5%	1.3×10^{-6}	2.5×10^{-6}	1.4×10^{-5}	2.9×10^{-4}
Clayton		N/A			

Table 4-8. Input variables.

Uncertainty variables		Deterministic variables	
Vertical force (v)	$N(30000, 4500^2)$ KN	Angle (α)	45 (degree)
Horizontal force (h)	$N(7000, 350^2)$ N	Height (l)	1 m
Ultimate strength (σ_u)	$N(250,12.5^2)$ MPa		

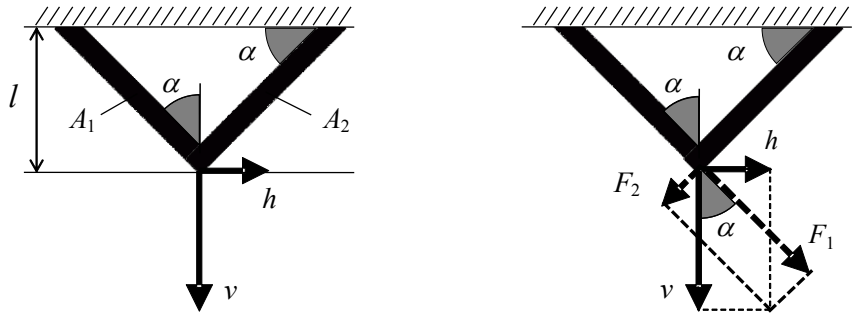

(a) (b)

Figure 4-1. A simple truss example in biaxial loading.

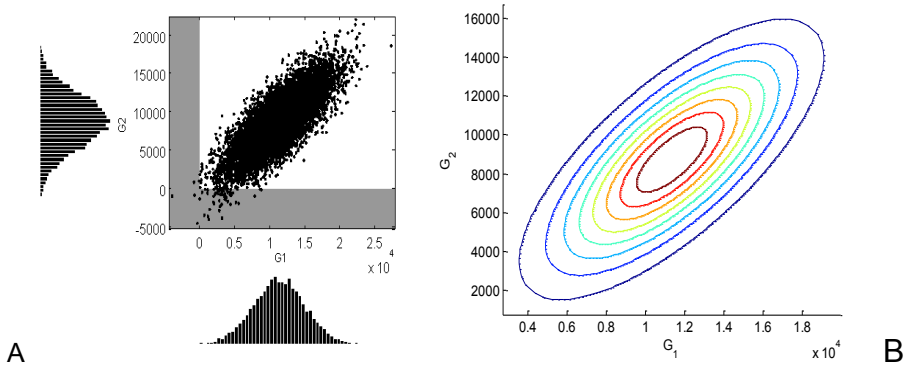

A B

Figure 4-2. Scattered plot of two limit states. A) Scatter plot of random samples (shaded region is the failure region) and B) Contour plot of the joint PDF of G_1 and G_2.

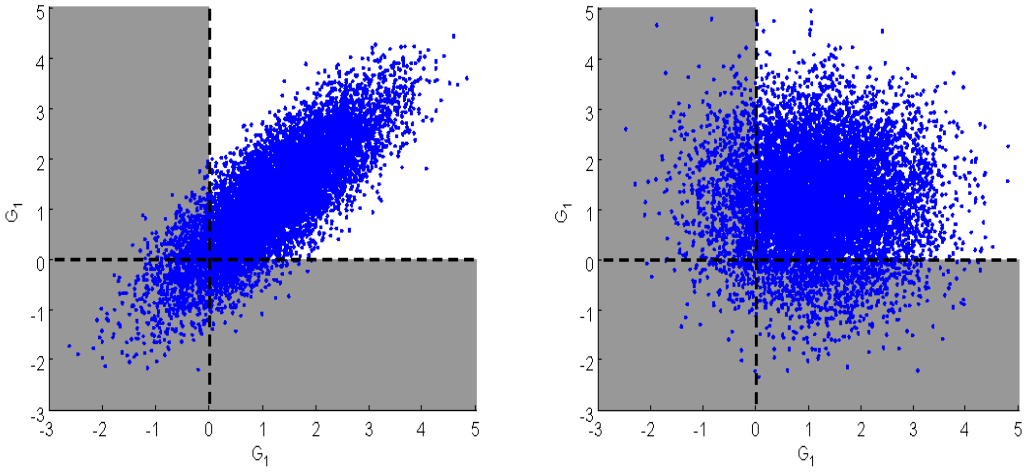

Figure 4-3. Difference between intersection probabilities with and without considering dependence. A) Scatter plot considering dependence and B) Scatter plot ignoring dependence.

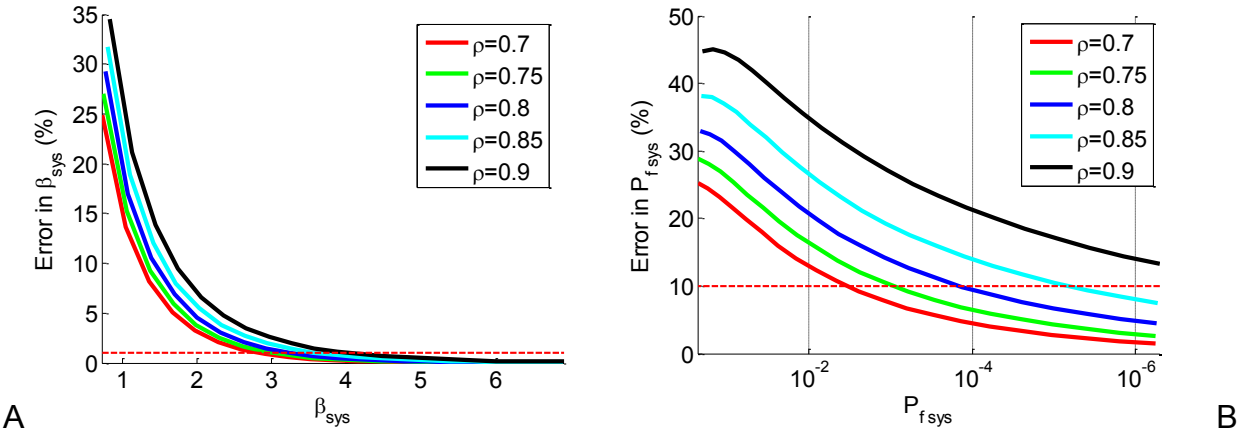

Figure 4-4. The variation of error with the magnitude of system PF for bivariate normal distribution with equal failure probabilities for the two modes. A) Error vs reliability index (BVN) and B) Error vs PF (BVN).

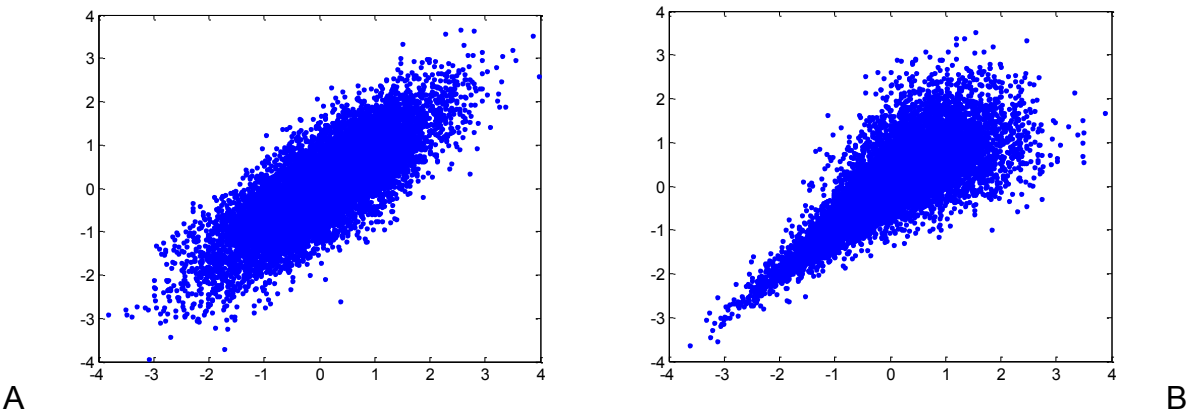

Figure 4-5. Randomly generated 10000 samples having different tail shapes with a linear correlation coefficient of 0.8. A) ρ =0.8 (BVN) and B) ρ=0.8 (strong tail dependence).

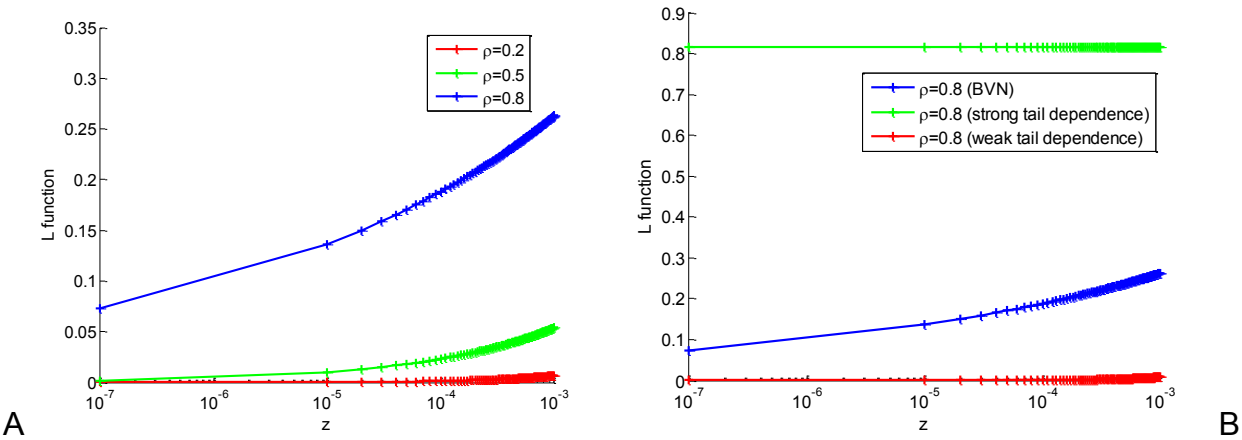

Figure 4-6. Curves of L function with respect to the strength of dependence and tail shape of joint PDF (Asymptotic value of L(z) for z→+0 is 0). A) L function for different values of the strength of dependence (BVN) and B) L function with respect to the shape of joint PDF.

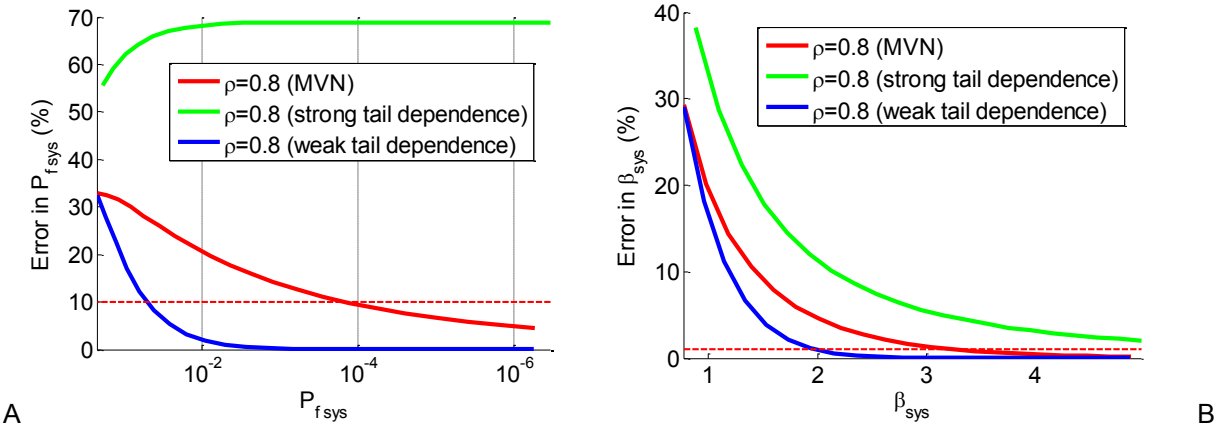

Figure 4-7. The magnitude of error with respect to the strength of tail dependence. A) Error vs PF and B) Error vs reliability index.

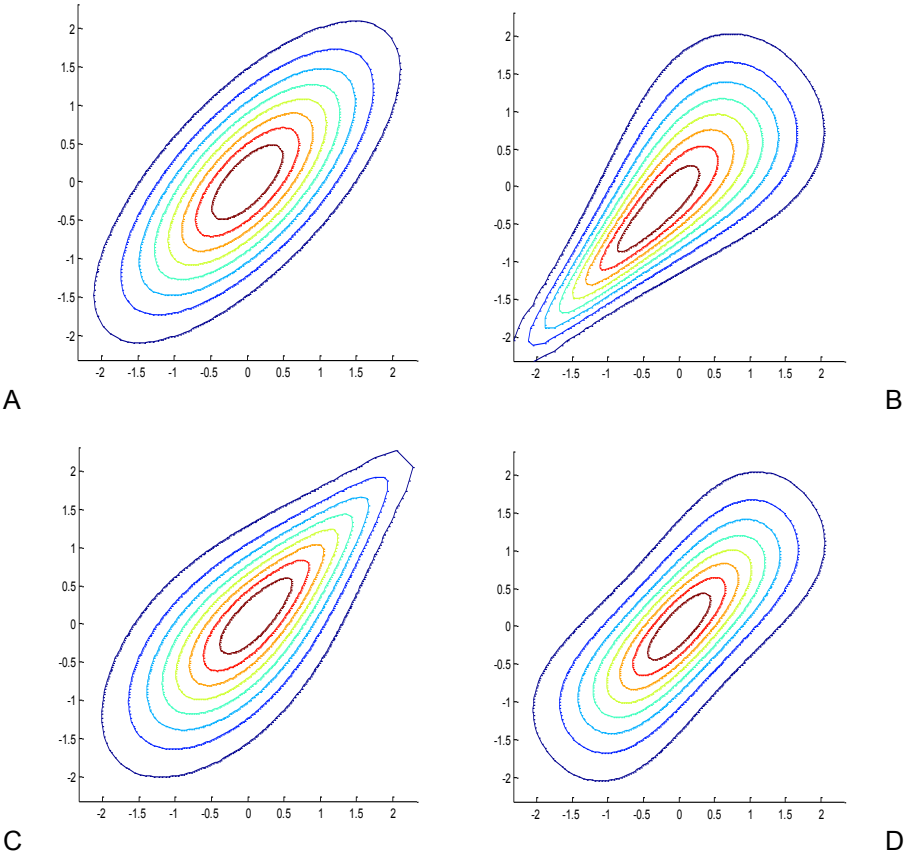

Figure 4-8. Four joint PDF shapes with commonly used copulas with two standard normal marginal distributions with a linear correlation coefficient of 0.7. A) Gaussian copula, B) Clayton copula, C) Gumbel copula and D) Frank copula.

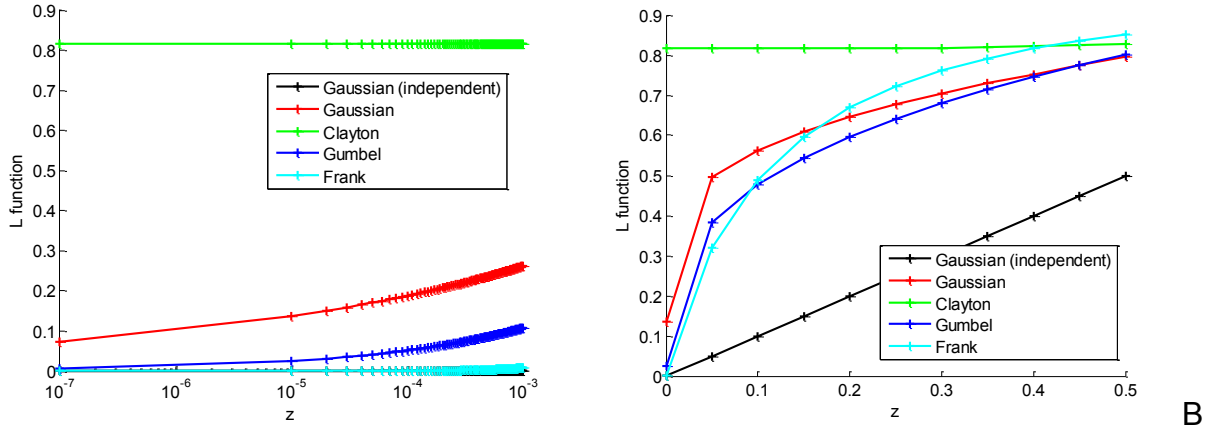

Figure 4-9. L functions for different copulas. A) L function in extreme tail region and B) L function for macroscopic scale.

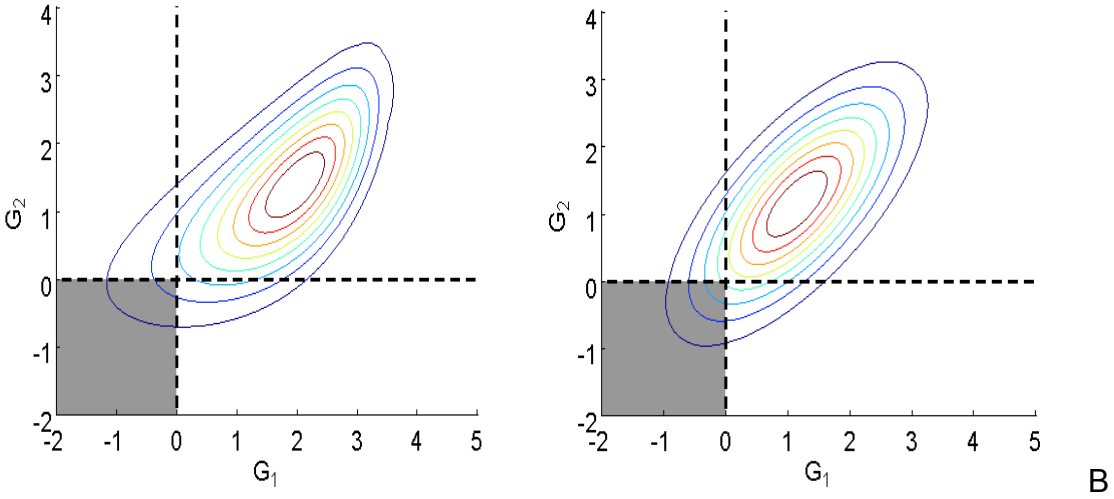

Figure 4-10. Two joint PDFs that have different marginal PDFs for the limit states, but the same individual PFs. A) G_1 follows the extreme distribution with location parameter α=2 and scale parameter β=1, G_2 follows the normal distribution with mean μ=1.143 and standard deviation of σ=1; marginal PFs, G_1 and G_2, are the same $P_{f1} = P_{f2} = 0.1265$ and B) G_1 and G_2 follow the normal distribution with mean μ=1.143 and standard deviation of σ=1; marginal PFs, G_1 and G_2, are the same $P_{f1} = P_{f2} = 0.1265$.

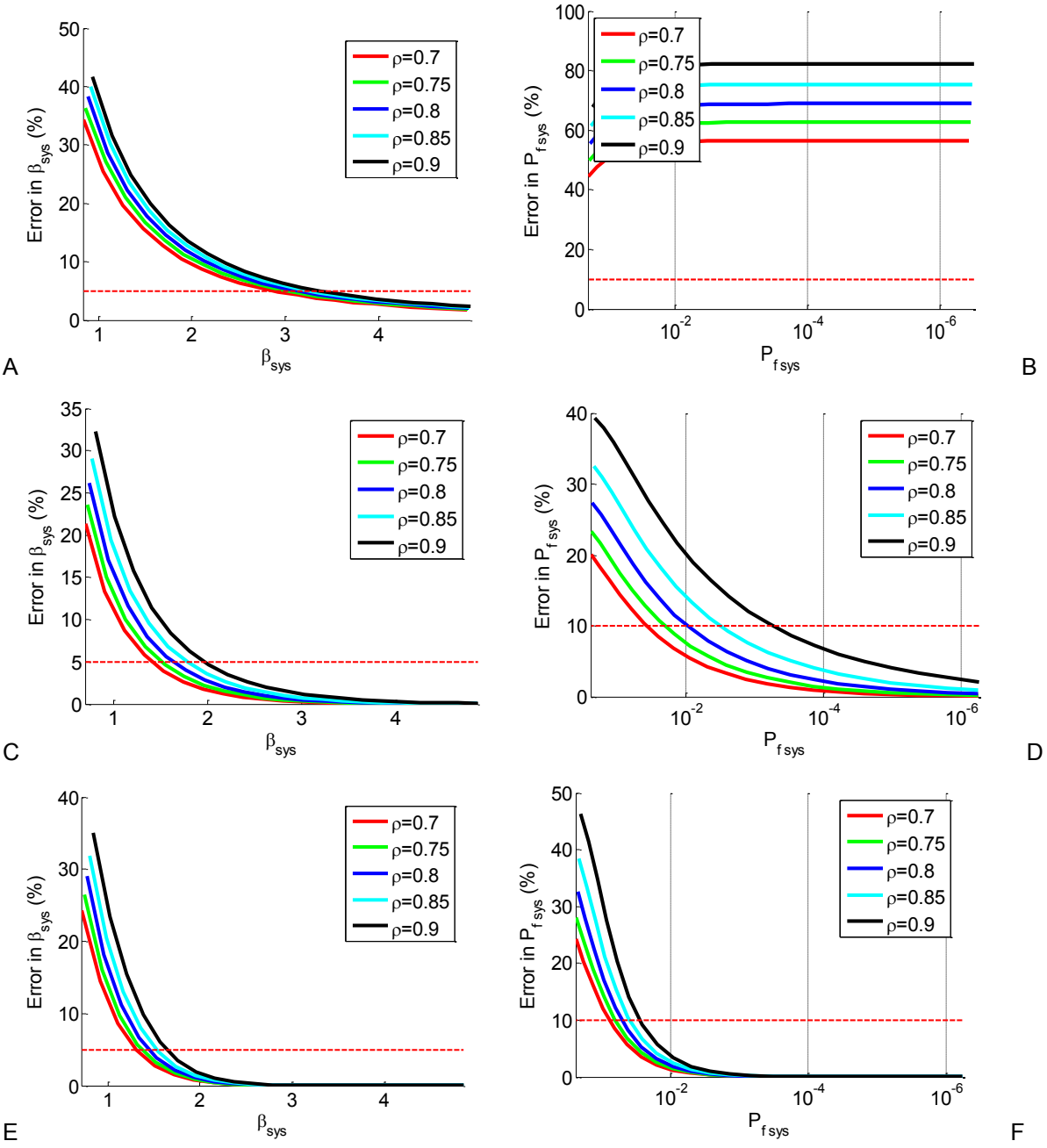

Figure 4-11. The relative error in reliability index and PFs versus system PF. A) Error vs reliability index (Clayton) B) Error vs log PF (Clayton) C) Error vs reliability index (Gumbel) D) Error vs log PF (Gumbel) E) Error vs reliability index (Frank) and F) Error vs log PF (Frank).

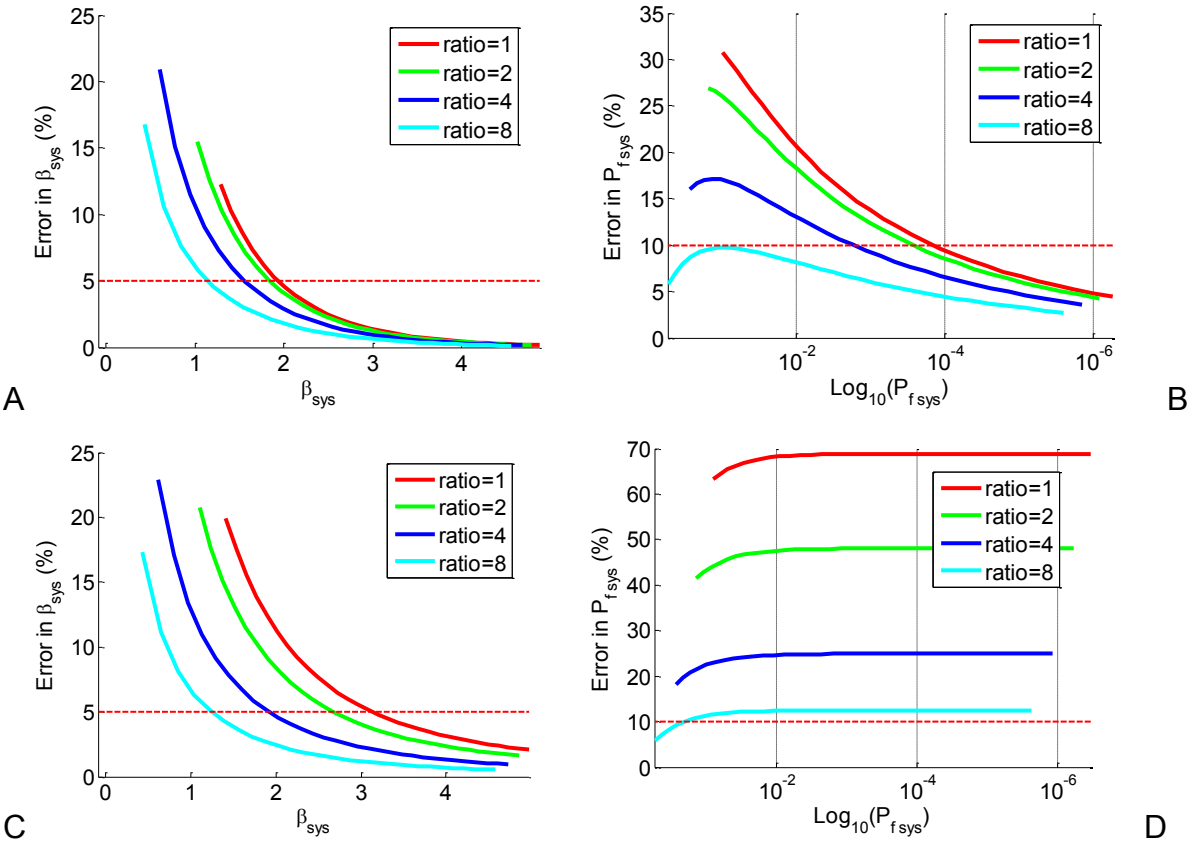

Figure 4-12. The magnitude of error with respect to the ratio between marginal PFs. A) Error versus reliability index for the ratio between marginal PFs (Gaussian) B) Error (in PF) versus log PF for the ratio between two PFs (Gaussian) C) Error versus reliability index for the ratio between marginal PFs (Clayton) and D) Error (in PF) versus log PF for the ratio between two PFs (Clayton).

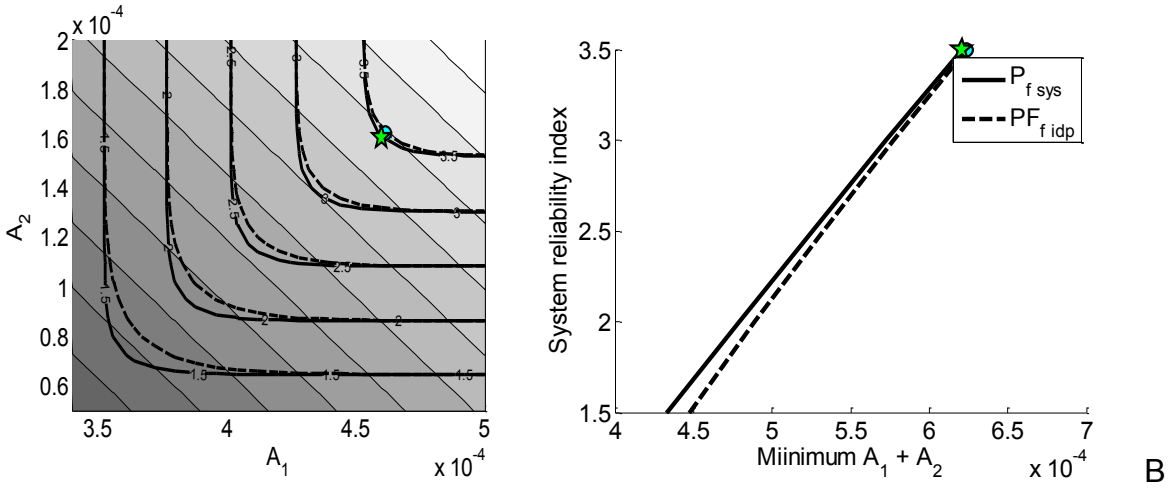

Figure 4-13. Visualization of probabilistic optimization results. A) Weight (bright and dark color represent heavy and light weight, respectively) and constraint lines with respect to the magnitude of allowable reliability index and B) Minimum A1+A2 and corresponding reliability index.

CHAPTER 5
CONCLUDING REMARKS

In this work, we first investigated the effects of coupon and element tests on design weight of a structural element for achieving a certain safety level. The process to estimate element strength based on coupon tests and failure theory and the process to reduce the error in estimated element strength with element tests were modeled. Both epistemic and aleatory uncertainties were considered in the model. For epistemic uncertainty, the sampling uncertainty in coupon, error in failure theory due to imperfect failure theory, and the sampling uncertainty in element tests were considered. For aleatory uncertainty, variabilities in coupon and element tests were considered. A method to estimate 95% conservative element strength was developed based on quantification of remaining uncertainty after tests using Bayesian inference and the convolution integral.

Through numerical examples, typical variability in the coupon tests (7%) and in the element tests (3%) and error in failure theory (±5%) were assumed. It was observed that element test is more influential than coupon test. This is because the error in failure theory is commonly larger than the sampling uncertainties in coupon tests. When failure theory is very accurate (±1%), coupon test is more influential than element test.

We moved to more complex problem to prove the effect of test. A composite panel with a hole model was used for this study and buckling and strength failure modes were considered. Since it turned out that the effect of coupon test is limited, for this study, the effect of element test on reducing reliability was investigated. Unlike common approach to calculate reliability, which calculates reliability based on only aleatory uncertainties, the effect of epistemic uncertainty in reliability calculation is considered separately, from

which a distribution of PF due to the epistemic uncertainty was obtained. The effect of test was quantified by measuring the change of the PF distribution according to test.

Since the composite model has two failure modes, PF is calculated based on predictions of buckling load and strength failure load with the two corresponding errors in predictions contributing to PF. However, typically a single test is performed for structures like the composite panel due to limited resources. An efficient way to include the single test results to reduce both prediction errors was investigated.

To calculate PF considering two failure modes, dependence between two failure modes have to be properly considered. A decomposition method that decomposes two dependent failure modes into two independent failure modes was developed to simplify calculating system reliability without applying any assumptions. With the decomposition method, PF can be calculated by summing two marginal PFs of the decomposed failure modes.

For applying reliability based design on system design, multiple failure modes are often assumed to be independent to avoid complex system reliability calculation with ignoring dependence between failure modes. The error of ignoring dependence between failure modes on evaluating system reliability was investigated by varying the strength of dependence and the ratio between marginal reliabilities. Errors in two frequently used measures, PF and reliability index, were calculated. We found that, the error in reliability index is always negligible when system reliability is very high even for strong dependence between failure modes. The error in PF is also usually negligible when system reliability is very high but the error is not small with high system reliability when tail dependence of two component failures is strong. It has to be kept in mind,

however, that for high reliability, it is very difficult to get accurate probabilities even for one failure mode, because the probability of failure is sensitive to small errors in input distribution. We illustrated the effect of ignoring dependence between failure modes for the design of a 2-bar truss. RBDO ignoring dependence between two bar failures led to only 0.5% heavier design than RBDO using exact system reliability calculation.

APPENDIX A
STATISTICAL FORMULATION OF POSSIBLE TRUE DISTRIBUTIONS

Possible True Distribution of Material Strength

The possible true failure strength of coupons, $\tau_{c,Ptrue}$, is firstly defined as a conditional distribution,

$$\hat{\tau}_{c,Ptrue}\left|\left(\hat{\mu}_{c,Ptrue}=\mu_{c,Ptrue},\hat{\sigma}_{c,Ptrue}=\sigma_{c,Ptrue}\right)\sim N\left(\mu_{c,Ptrue},\sigma_{c,Ptrue}\right)\right. \quad \text{(A-1)}$$

where $\hat{\tau}_{c,Ptrue}\left|(\hat{\mu}_{c,Ptrue}=\mu_{c,Ptrue},\hat{\sigma}_{c,Ptrue}=\sigma_{c,Ptrue})\right.$ is a conditional random variable given $\hat{\mu}_{c,Ptrue}=\mu_{c,Ptrue}$ and $\hat{\sigma}_{c,Ptrue}=\sigma_{c,Ptrue}$. Considering that $\hat{\mu}_{c,Ptrue}$ and $\hat{\sigma}_{c,Ptrue}$ are random, Eq. (A-1) corresponds to an incident of possible true distributions. Normally, a designer has a set of coupons, from which the PTD of parameters need to be estimated. It is obvious that different sets of coupons may yield different estimations of $\hat{\mu}_{c,Ptrue}$ and $\hat{\sigma}_{c,Ptrue}$ due to uncertainty in sampling.

The conditional distribution in Eq. (A-1) is repeatedly generated (inner loop) with randomly generated samples of $\hat{\mu}_{c,Ptrue}$ and $\hat{\sigma}_{c,Ptrue}$ (outer loop). In the outer loop, N samples of mean μ_i (i=1,2,...,N) and standard deviation σ_i are generated from the PTDs of mean and standard deviation, and they are used to make N conditional distributions as in Eq. (A-1). In the inner loop, M samples of possible true failure strengths are generated from individual conditional distributions with a pair of the generated mean and standard deviation $N(\mu_i,\sigma_i)$. Therefore, $N\times M$ samples are used to estimate the PTD of failure strength.

The PTDs of mean and standard deviation are in practices estimated from a single set of coupon tests. Let us assume that n_c coupons are tested, whose mean and standard deviation are $\mu_{c,test}$ and $\sigma_{c,test}$, respectively. Then, these values can first be

used to estimate the PTD of mean, which is nothing but the distribution of sample mean. Since it is assumed that $\hat{\tau}_{c,true}$ is normally distributed, the sample mean also follows a normal distribution [13]. Therefore, the PTD of mean can be estimated by

$$\hat{\mu}_{c,Ptrue} \sim N\left(\mu_{c,test}, \frac{\sigma_{c,test}}{\sqrt{n_c}}\right) \tag{A-2}$$

It is also well known that the standard deviation $\hat{\sigma}_{c,test}$ follows a chi-distribution of order $n_c - 1$. In a way similar to the mean, the PTD of standard deviation can be estimated by

$$\hat{\sigma}_{c,Ptrue} = \frac{\sigma_{c,test}\hat{c}}{\sqrt{n_c - 1}} \text{ and } \hat{c} \sim \chi(n_c - 1) \tag{A-3}$$

Based on Eq. (A-2) and Eq. (A-3), estimated standard deviations of $\hat{\mu}_{c,Ptrue}$ and $\hat{\sigma}_{c,Ptrue}$ can be calculated, respectively, by

$$\text{Estimated standard deviation of } \hat{\mu}_{c,Ptrue} = \frac{\sigma_{c,test}}{\sqrt{n_c}} \tag{A-4}$$

$$\text{Estimated standard deviation of } \hat{\sigma}_{c,Ptrue} = \sqrt{\sigma_{c,test}^2 - 2\frac{\sigma_{c,test}^2}{(n_c - 1)}\frac{\Gamma^2(n_c/2)}{\Gamma^2((n_c - 1)/2)}} \tag{A-5}$$

Note that we can calculate true standard deviations for given number of samples with Eq. (A-4) and Eq. (A-5) when we know true standard deviation of population instead of the test standard deviation from samples.

Finally, from Eq. (A-1) to Eq. (A-3), PTD of material strength is derived as

$$f_{c,Ptrue}(\tau_{c,Ptrue}) = \int_0^\infty \int_{-\infty}^\infty \varphi(\tau_{c,Ptrue} \mid \mu_{c,Ptrue}, \sigma_{c,Ptrue}) f_{\mu c,Ptrue}(\mu_{c,Ptrue}) f_{\sigma c,Ptrue}(\sigma_{c,Ptrue}) d\mu_{c,Ptrue} d\sigma_{c,Ptrue} \tag{A-6}$$

Possible True Distribution of Element Strength

The PTD of element mean failure strength can be expressed as

$$f_{\mu e,Ptrue}\left(\mu_{e,Ptrue}\right)=\int_{-\infty}^{\infty} f_{\mu e,Ptrue}\left(\mu_{e,Ptrue}\mid\mu_{c,Ptrue}\right) f_{\mu c,Ptrue}\left(\mu_{c,Ptrue}\right)\mathrm{d}\mu_{c,Ptrue} \tag{A-7}$$

which is in the form of the convolution integral. The conditional PDF $f_{\mu e,Ptrue}\left(\mu_{e,Ptrue}\mid\mu_{c,Ptrue}\right)$ corresponds to the distribution of $\hat{k}_{3d,Ptrue}$. In the following, the two PDFs in the integrand will be explained.

In this dissertation, $k_{3d,calc}=1$ is used for simplicity, and it is assumed that $e_{k,Ptrue}$ follows a uniform distribution with bounds $\pm b_e$ as

$$f_{k,Ptrue}\left(e_{k,Ptrue}\right)=\begin{cases}\dfrac{1}{2b_e} & \text{if } \left|e_{k,Ptrue}\right|\le b_e\\ 0 & \text{otherwise}\end{cases} \tag{A-8}$$

By using Eq. (A-8), $f_{\mu e,Ptrue}\left(\mu_{e,Ptrue}\right)$ can be obtained from all possible combinations of random variables generated from $f_{k,Ptrue}\left(e_{k,Ptrue}\right)$ and $f_{\mu c,Ptrue}\left(\mu_{c,Ptrue}\right)$. For a given sample of $\mu_{c,Ptrue}$, the PTD of element failure strength can be regarded as a conditional PDF $f_{\mu_{e,Ptrue}}\left(\mu_{e,Ptrue}\mid\mu_{c,Ptrue}\right)$, which is a uniform distribution with a width of $2b_e$ and mean at $\mu_{c,Ptrue}$.

$$f_{\mu e,Ptrue}\left(\mu_{e,Ptrue}\mid\mu_{c,Ptrue}\right)=\begin{cases}\dfrac{1}{2b_e\mu_{c,Ptrue}} & \text{if } \left|\dfrac{\mu_{e,Ptrue}}{\mu_{c,Ptrue}}-1\right|\le b_e\\ 0 & \text{otherwise}\end{cases} \tag{A-9}$$

The PDF in Eq. (A-9) represents the prediction error of a given failure theory. The PTD $f_{\mu e,Ptrue}\left(\mu_{e,Ptrue}\right)$ can be calculated by considering all possible values of $\mu_{c,Ptrue}$ with Eq. (A-9).

By using Eq. (A-9), PDF of the PTD of $\mu_{c,Ptrue}$ is calculated from coupon test results as

$$f_{\mu c,Ptrue}\left(\mu_{c,Ptrue}\right)=\varphi\left(\mu_{c,Ptrue}\mid\mu_{c,test},\frac{\sigma_{c,test}}{\sqrt{n_c}}\right) \tag{A-10}$$

where the notation $\varphi(x\mid a,b)$ denotes the value of normal PDF with mean *a* and standard deviation *b* at *x*. Samples of $\mu_{c,Ptrue}$ are generated from Eq. (A-10), which is then used in Eq. (A-9) to generate samples of $\mu_{e,Ptrue}$. Figure A-1 illustrates the conditional PDF of $\mu_{e,Ptrue}$ for a given sample of $\mu_{c,Ptrue}$, which is drawn from $f_{\mu c,Ptrue}\left(\mu_{c,Ptrue}\right)$ based on $\mu_{c,test}$. Note that $\mu_{e,true}$ is given as a unique value, and is covered by the PTD $f_{\mu e,Ptrue}\left(\mu_{e,Ptrue}\mid\mu_{c,Ptrue}\right)$.

With Eq. (A-9) and Eq. (A-10), the convolution integral in Eq. (A-7) can be directly integrated as

$$f_{\mu e,Ptrue}\left(\mu_{e,Ptrue}\right)=\int_{\frac{\mu_{e,Ptrue}}{(1-b_e)}}^{\frac{\mu_{e,Ptrue}}{(1+b_e)}}\frac{1}{2b_e\mu_{c,Ptrue}}\varphi\left(\mu_{c,Ptrue}\mid\mu_{c,test},\frac{\sigma_{c,test}}{\sqrt{n_c}}\right)d\mu_{c,Ptrue} \tag{A-11}$$

The PDF in Eq. (A-11) is a prior distribution of mean failure strength of elements, which includes the effect of uncertainty from failure theory as well as that of a finite number of samples.

It is reasonable assumption that there is a correlation between variability in manufactured structural elements and variability in coupons, since the structural element is made of the material. As predicting the mean failure strength, we considered the error in failure theory and the effect of a finite number of coupon specimens to estimate variability of the manufactured elements. When a random variable is normally

distributed, the sampling distribution of standard deviation follows a chi-distribution [13]. Standard deviation of element failure strength $\sigma_{e,true}$ can be directly obtained from the $\sigma_{c,true}$ as

$$\sigma_{e,true} = k_{3d,true}\sigma_{c,true} \tag{A-12}$$

where $e_{\sigma,true}$ is the true error in $k_{3d,true}$. Due to the lack of knowledge of the relation between $\tau_{e,true}$ and $\tau_{c,true}$ (epistemic uncertainty), and a finite number of specimens, the PT standard deviation of element failure strength $\hat{\sigma}_{e,Ptrue}$ can be obtained by Eq. (A-12) in terms of two PT variables.

$$\hat{\sigma}_{e,Ptrue} = k_{3d,true}(1-\hat{e}_{k,Ptrue})\hat{\sigma}_{c,Ptrue} \tag{A-13}$$

The $\hat{e}_{k,Ptrue}$ is assumed to be uniformly distributed with zero mean. $\hat{\sigma}_{c,Ptrue}$ follows a chi distribution with order of $n_c - 1$.

The process of obtaining the PT standard deviation of failure strength of structural element $\sigma_{e,true}$ based on Eq. (A-13) is shown in Figure A-2. The PTD of standard deviation of failure strength of structural element $f_{\sigma c,Ptrue}\left(\sigma_{c,Ptrue}\right)$ is the Chi-distribution. Using the two PTDs, the distribution of PT element failure strength of standard deviation $f_{\sigma e,Ptrue}\left(\sigma_{e,Ptrue}\right)$ is obtained.

In the same manner as Eq. (A-7), the combined PTD $f_{\sigma e,Ptrue}\left(\sigma_{e,Pture}\right)$ is obtained using conditional PDF as

$$f_{\sigma e,Ptrue}\left(\sigma_{e,Pture}\right) = \int_{-\infty}^{\infty} f_{\sigma e,Ptrue}\left(\sigma_{e,Ptrue} \mid \sigma_{c,Ptrue}\right) f_{\sigma c,Ptrue}\left(\sigma_{c,Ptrue}\right) \mathrm{d}\sigma_{c,Ptrue} \tag{A-14}$$

For given $\sigma_{c,Ptrue}$, $\hat{\sigma}_{e,Ptrue}$ has a uniform distribution which is centered around $\sigma_{c,Ptrue}$. In this dissertation, $k_{3d,calc}=1$ is used for simplicity, the PTD of $\hat{\sigma}_{e,Ptrue}$ for given $\sigma_{c,Ptrue}$ is defined as a conditional PDF:

$$f_{\sigma e,Ptrue}\left(\sigma_{e,Ptrue}\mid\sigma_{c,Pcalc}\right)=\begin{cases}\dfrac{1}{2b_e\sigma_{c,Ptrue}} & \text{if}\left|\dfrac{\sigma_{e,Ptrue}}{\sigma_{c,Ptrue}}-1\right|\le b_e\\ 0 & \text{otherwise}\end{cases} \tag{A-15}$$

Chi-distribution is used to define PDF of $\hat{\sigma}_{c,Ptrue}$ for the given number of coupon tests n_c and the test standard deviation of coupon test $\sigma_{c,test}$. The PDF of chi-distribution is defined as

$$f_\chi\left(\chi\mid n_c-1\right)=\frac{2^{1-(n_c-1)/2}\,\chi^{n_c-2}e^{-\chi^2/2}}{\Gamma\left((n_c-1)/2\right)} \tag{A-16}$$

where the notation $f_\chi\left(\chi\mid n_c-1\right)$ denotes the value of chi PDF with χ and the number of coupon tests n_c. From Eq. (A-16), the PDF of $\hat{\sigma}_{c,Ptrue}$ for the given number of specimens n_c is obtained as

$$f_{\sigma c,Ptrue}\left(\sigma_{c,Ptrue}\right)=f_\chi\left(\chi\mid n_c-1\right)\frac{\sqrt{n_c-1}}{\sigma_{c,test}}\ \text{ and }\ \chi=\frac{\sqrt{n_c-1}}{\sigma_{c,test}}\sigma_{c,Ptrue} \tag{A-17}$$

In Eq. (A-14), $f_{\sigma e,Ptrue}\left(\sigma_{e,Ptrue}\mid\sigma_{c,Ptrue}\right)$ has finite integrand range so that the equation can be rewritten as

$$f_{\sigma e,Ptrue}\left(\sigma_{e,Ptrue}\right)=\int_{\frac{\sigma_{e,Ptrue}}{(1-b_\sigma)}}^{\frac{\sigma_{e,Ptrue}}{(1+b_\sigma)}}\frac{1}{2b_\sigma\sigma_{c,Ptrue}}f_{\sigma c,Ptrue}\left(\sigma_{c,Ptrue}\right)\mathrm{d}\sigma_{c,Ptrue} \tag{A-18}$$

This PDF is a prior distribution of standard deviation of element failure strength.

Numerical Scheme

For the mean element strength, a range of [0.78, 1.22] was found to be large enough to capture the updated joint probability distribution, because the initial distribution for the mean element strength has very little influence on posterior distribution on both tails. Figure 2-5 shows a typical shape of the initial distribution for the element mean. The standard deviation is bounded in [0, 0.04], as noted in Table 2-4. In order to calculate the updated distribution from Bayesian inference, each range is discretized into 200 equal intervals, and this discretization generates a 200 by 200 grid. The updated joint PDF is calculated at each grid point using Eq. (2-12). Then, the prior is updated using a likelihood function with different numbers of element tests; i.e. n_e= 1, 3, and 5.

The marginal updated distributions are obtained using the updated joint distribution as expressed in Eqs. (15) and (16). For the updated marginal element mean distribution, conditional PDFs for a given 201 mean element strength are integrated over 201 points using Gaussian quadrature with 2 points. Figure A-3 shows an equivalent example that has an 8 by 8 grid. The abscissa and ordinate of the grid are for mean and for standard deviation, respectively. The superscripts *i* and *j* are the horizontal and vertical coordinates of the grid. For example, $\mu_{e,Ptrue}^{3}$ is the value of the mean on the third vertical line. The marginal distribution of the updated mean element strength is formed by calculating PDF values on 9 given mean values. $f_{\mu e,Ptrue}^{upd}\left(\mu_{e,Ptrue}^{3}\right)$ is equal to a value obtained by integrating a conditional PDF of the standard deviation for $\mu_{e,Ptrue}=\mu_{e,Ptrue}^{3}$ over the vertical arrow.

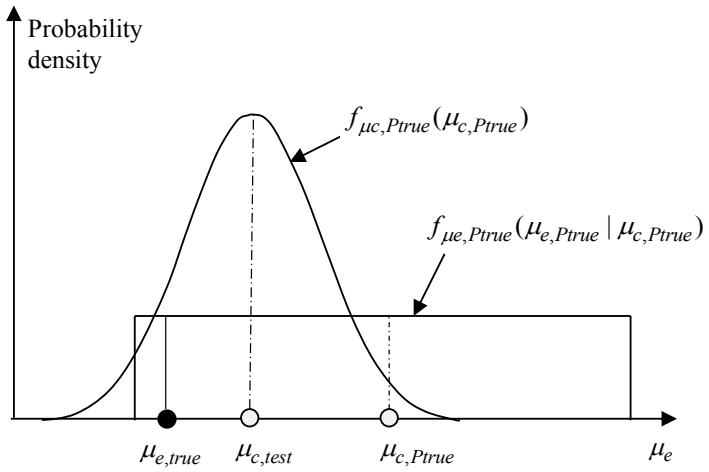

Figure A-1. The possible true distribution of mean failures strength of specimens and the conditional distribution of the element mean failure strength.

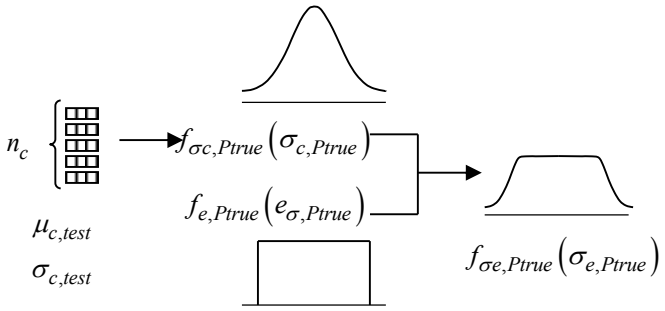

Figure A-2. Process of estimating standard deviation of failure strength.

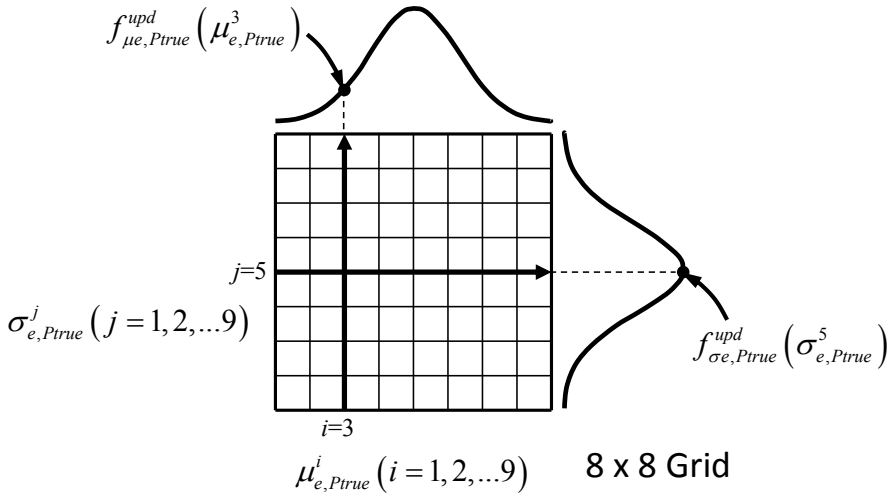

Figure A-3. A 8 by 8 grid for obtaining a joint PDF and its marginal PDFs.

APPENDIX B
COPULAS

An Introduction to Copula

Copulas and their application are important concepts for modeling a joint CDF of correlated random variables. In statistics, definition of copula is stated by Nelson (1999): "Copulas are functions that join or "couple" multivariate distribution functions to their one-dimentional marginal distribution functions. Alternatively, copulas are multivariate distribution functions whose one-dimensional margins are uniform on the interval (0,1)." There are two main reasons why copulas are of interest to students: Firstly, as a way of studying scale-free measures of dependence and secondly, as a starting point for constructing families of bivariate distributions.

The word copula is a Latin noun which means "a link, tie, bond". The word copula was first employed in a mathematical sense by Abe Sklar (1959) in the theorem describing the functions which join together one-dimensional distribution functions to form multivariate distribution functions. In this account of copula is a function to link n-dimensional distributions to their one-dimensional margins.

Definition of Copula

According to Sklar's theorem, if the n-dimensional random variable $\mathbf{X}=[X_1,\ldots X_n]^T$ and each random variable X_i has marginal distributions $F_{Xi}(x_i)$, then there exists an n-dimensional copula C such that

$$F_{X_1,\ldots X_n}(x_1,\ldots,x_n)=C\left(F_{X_1}(x_1),\ldots,F_{X_n}(x_n)\right) \tag{B-1}$$

In this context, a copula is a joint distribution of n-dimensional uniform random variables U_1 to U_n (inverse CDF of a random variable X has always uniform random variable) with

$$C_{\rho}(u_1,...,u_n) = \Pr(U_1 < u_1,...,U_n < u_n) \tag{B-2}$$

where $F_{X_1,...X_n}(x_1,...,x_n)$ is a joint CDF at $\mathbf{x} = (x_1,...,x_n)$. Note that each marginal distribution can has [0 1] range of output. If the marginal distributions are all continuous, then the copula *C* is unique. By the definitions of an n-dimensional copula *C* and marginal CDFs of random variables, the joint probability density distribution of Eq. (B-1) is obtained as

$$f_{X_1,...X_n}(x_1,...,x_n) = c\left(F_{X_1}(x_1),...,F_{X_n}(x_n)\right)\prod_{i=1}^{n} f_{X_i}(x_i) \tag{B-3}$$

where the $f_{X_i}(x_i)$ is a marginal PDF of X_i. The joint pdf of the copula *C* is n[th] derivative of the copula *C*.

$$c(u_1,...,u_n) = \frac{\partial^n C(u_1,...,u_n)}{\partial u_1 ... \partial u_n} \tag{B-4}$$

The joint CDF is expressed as copula in terms of marginal CDFs, it is readily possible to model a joint CDF using marginal CDFs. In other words, thus copula decouples marginal CDFs and the joint CDF, the joint CDF modeled by the copula can be expressed for any type of marginal CDFs. Figure B-1 shows two cases which have the same copula but different marginal CDFs. Two marginal CDFs Gaussian and Weibull distributions with the same mean and standard deviation (parameters μ=0.918, σ=0.044 and a=1, b=5 for Gaussian distribution and Weibull distribution, respectively) are used.

Basic Copulas

Copulas are mainly categorized into two families; Elliptic copulas and Archimedean copulas. Firstly, the elliptic copulas are a class of symmetric copulas, so-called because the horizontal cross-sections of their joint PDFs take the shape of ellipses. Because of their symmetry, a simple linear transformation of variables will

transform the elliptic cross-sections to circular ones. Two common elliptic copulas, Gaussian and *t* copulas are widely used. In this study, only Gaussian copula is used.

Elliptical Copulas

The Gaussian copula is defined as the joint Gaussian CDF of standard Gaussian variables as

$$C_{\boldsymbol{\rho}}(u_1,...,u_n \mid \boldsymbol{\rho}) = \Phi_{\boldsymbol{\rho}}\left(\Phi^{-1}(u_1),...,\Phi^{-1}(u_n) \mid \boldsymbol{\rho}\right), \mathbf{u} \in I^n \tag{B-5}$$

In which Φ and $\Phi_{\boldsymbol{\rho}}$ are the univariate and multivariate standard normal CDFs respectively, and $\boldsymbol{\rho}$ is the correlation matrix between the random variables X_i. By the Eq. (B-5), it is known that the Gaussian copula is wholly defined by the correlation matrix $\boldsymbol{\rho}$. $\Phi_{\boldsymbol{\rho}}$ is the standard normal CDF, which is expressed as a multi-dimensional function.

$$\Phi_{\boldsymbol{\rho}}\left(\Phi^{-1}(u_1),...,\Phi^{-1}(u_n)\right) = \int_{-\infty}^{\Phi^{-1}(u_1)} ... \int_{-\infty}^{\Phi^{-1}(u_n)} \frac{1}{(2\pi)^{n/2}\sqrt{\det \boldsymbol{\rho}}} \exp[-\frac{1}{2}\begin{Bmatrix} z_1 \\ \vdots \\ z_n \end{Bmatrix}^T \boldsymbol{\rho}^{-1} \begin{Bmatrix} z_1 \\ \vdots \\ z_n \end{Bmatrix}] dz_1...dz_n \tag{B-6}$$

PDF of the Gaussian copula, nth derivative of the copula, is expressed as

$$\frac{\partial^n C_{\boldsymbol{\rho}}(u_1,...,u_n)}{\partial u_1...\partial u_n} = \frac{\partial^n \Phi_{\boldsymbol{\rho}}\left(\Phi^{-1}(u_1),...,\Phi^{-1}(u_n)\right)}{\partial z_1...\partial z_n} \frac{\partial z_1...\partial z_n}{\partial u_1...\partial u_n} \tag{B-7}$$

where $\frac{\partial z_i}{\partial u_i} = \frac{\partial z_i}{\partial \Phi}$.

The PDF of the Gaussian copula is finally expressed as

$$c_{\boldsymbol{\rho}}(u_1,...,u_n) = \frac{1}{\sqrt{\det \boldsymbol{\rho}}} \exp[-\frac{1}{2}\begin{Bmatrix} \Phi^{-1}(u_1) \\ \vdots \\ \Phi^{-1}(u_n) \end{Bmatrix}^T \left(\boldsymbol{\rho}^{-1} - 1\right) \begin{Bmatrix} \Phi^{-1}(u_1) \\ \vdots \\ \Phi^{-1}(u_n) \end{Bmatrix}] \tag{B-8}$$

Archimedean Copulas

Archimedean copulas are an associative class of copulas. Whereas the Gaussian copula express implicit formula of *C* with standard normal distributions, most common Archimedean copulas admit an explicit formula for the *C*. Also they allow to model dependence with only one parameter. Nelson (1999) address several reasons why Archimedean copulas find a wide range of applications: (1) The ease with which they

can be constructed, (2) The great variety of families of copulas which belong to this class; and (3) The many nice properties possessed by the members of this class.

The Archimedean copulas belong to the bivariate Archimedean family take the form

$$C(u_1,u_2 \mid \theta) = \Psi_\theta^{-1}\{\Psi_\theta(u_1)+\Psi_\theta(u_2)\} \quad \text{(B-9)}$$

where $\Psi:(0,1)\mapsto(0,\infty)$ is a generator function satisfying three conditions (Nelson 1999): 1) $\Psi_\theta(1)=0$, 2) $\Psi'_\theta(s)<0\ \forall s\in(0,1)$, (i.e. Ψ_θ is strictly decreasing) and 3) $\Psi''_\theta(s)>0\ \forall s\in(0,1)$, (i.e. Ψ_θ is convex)

Copulas provide CDF of multiple random variables. To derive PDF the copulas, Eq. (B-4) is used. Archimedean copula is defined by a single parameter θ. Note that the domain of each Archimedean copula is different, however the θ cannot be a reference of correlation. The Frank copula with $\theta=3$ and the Gumbel copula with $\theta=3$ are not representing the same correlation or dependence between two random variables.

Correlation Measures

Copulas join two random variables with a specified correlation. Many of the properties and correlation measures associated with copulas are scale invariant under monotonically increasing transformation of the marginal distributions because copulas are invariant under monotonically increasing transformation of the marginal distributions. There are several correlation measures and each correlation measure has relation with copula.

Linear Correlation Coefficient (Pearson's Rho)

Linear correlation coefficient measures the degree of linear relationship between two random variables.

$$\rho = \frac{cov(X_1, X_2)}{\sigma_{X_1}\sigma_{X_2}} \quad \text{(B-10)}$$

where $cov(X_1, X_2)$ is covariance between X_1 and X_2 and σ_1 and σ_2 are standard deviations of X_1 and X_2.

Since Pearson's rho only indicates the linear relationship between two random variables, it is not capable of measuring nonlinear relationship. Furthermore, the linear correlation coefficient based on the covariance of two random variables is not preserved by copulas. That is, two pairs of correlated variables with the same copula can have different correlations.

Kendal's Tau

The Kendall's tau, usually denoted by τ, is a constant of the copula and is preserved by copulas. There are different ways of defining τ. Perfectly correlated random variables $U_1=U_2$, τ will be 1. Thus the scaling makes τ look like a correlation coefficient.

In most cases, Kendall's tau and Spearman's rho are very similar, and when discrepancies occur, it is probably safer to interpret the lower value. More importantly, Kendall's Tau and Spearman's Rho imply different interpretations. Spearman's Rho is considered as the regular Pearson's correlation coefficient in terms of the proportion of variability accounted for, whereas Kendall's Tau represents a probability, i.e., the difference between the probability that the observed data are in the same order versus the probability that the observed data are not in the same order.

Kendall's tau is calculated by probability of concordance probability of discordance. When there are two independently generated paired samples of (x_i, y_i) and (x_j, y_j), those have a relation of $x_i < x_j$ and $y_i < y_j$ or $x_i > x_j$ and $y_i > y_j$, the two random

variables are concordant, or else are discordant. Kendall's tau with nearly infinite number of samples is expressed as

$$\tau = P\left[(X_1 - X_2)(Y_1 - Y_2) > 0\right] - P\left[(X_1 - X_2)(Y_1 - Y_2) < 0\right] \quad \text{(B-11)}$$

Practically, two random variables correlation is measured by a limited number of samples. The Kendall's tau based on the samples is defined in terms of estimated probabilities of concordance and discordance.

$$t = \frac{c-d}{c+d} = (c-d)/\binom{n}{2} \quad \text{(B-12)}$$

where the *c* is the number of concordance pairs and *d* is the number of discordance pairs. The c and d are counted by considering all possible pairs of given *n* samples.

For Archimedean copula, Kendall's tau can be obtained in case of generator function $\Psi(s)$ is given and expressed as

$$\tau = 1 + 4\int_0^1 \frac{\Psi_\theta(s)}{\Psi'_\theta(s)} ds \quad \text{(B-13)}$$

Explicit formula of Kendall's tau in terms of the parameter θ is known, Table B-2 provides the formulas.

Bivariate Gaussian copula is defined by linear correlation coefficient *ρ*, but there is no explicit function for Kendall's tau in terms of the *ρ*.

Summaries

Copulas, such as elliptic copulas and Archimedean copulas, are defined by one parameter. As an invariant correlation measure, Kendall's tau provides correlation degree and parameter of copula is expressed as an implicit or explicit function in terms of *τ*. When samples are generated, the Kendall's tau should be estimated with Eq. (B.12) and then parameter of desirable copula is calculated with Table B-2.

Correlation between two random variables is modeled by marginal CDFs and copula. Identification of the marginal CDFs is required, goodness of fit (GOF) test to identify the best fit distribution.

Goodness to Fit Test

The adequacy of hypothesized CDF is checked by comparing it to empirical CDF constructed from data. There are several GOF tests; χ^2, Kolmogorov-Smirnov (K-S) and Cramer-von Mises. The χ^2 test compares the difference between the empirical PDF and the hypothesized PDF and requires sufficient data. The Cramer-von Mises test is known as a better method than the K-S test. However the method is applicable to limited distributions which should feature symmetric and right-skewed CDF. In this study, K-S test is used to identify the best fit distribution. The K-S test is described well by Haldar and Mahadevan (2000).

The empirical CDF is defined as

$$F_n(x) = \frac{1}{n}\sum_{i=1}^{n} I_{X_i<x} \tag{B-14}$$

where $I_{X_i \le x}$ is the indicator function, equal to 1 if $X_i \le x$ and equal to 0 otherwise.

The K-S test measures the difference between the empirical CDF and the hypothesized CDF; finally pick up the maximum difference as

$$D_n = \max |F_n(x) - F(x)| \tag{B-15}$$

where $F_n(x)$ and $F(x)$ are empirical CDF and hypothesized CDF, respectively. With test statistics, D_n is tested to decide its acceptance or denial by specified confidence level $1-\alpha$. The hypothesis test is defined as

$$\begin{cases} \text{Null hypothesis:} & H_1 : F_n = F \\ \text{Alternative hypothesis:} & H_0 : F_n \neq F \end{cases} \tag{B-16}$$

If $\alpha = 0.05$ and the hypothesized CDF is accepted, then it has 95 confidence of its acceptance.

$$\Pr\left(D_n \le D_n^{\alpha}\right) = 1 - \alpha \tag{B-17}$$

where D_n^{α} is critical value (CV) at the confidence level of $1-\alpha$. It is given as a table by Haldar and Mahadevan (2000). If the p-value is larger than α, the null hypothesis is accepted. If more than one hypothesis CDFs are accepted, a hypothesis having largest p-value is chosen because the p-value indicates how the null hypothesis is strongly accepted. Marsaglia and Wang (2003) describes formulas to calculate the p-value.

In this study, 5 distribution candidates, Gaussian (normal), Weibull (extreme type III), Gamma, Lognormal and Gumbel (extreme type II) are used as hypothesis CDFs and it is shown in Table. B-3. Parameters of each hypothesis CDF can be numerically calculated from mean and standard deviation.

Goodness of Fit for Buckling Load and Strain of the Curved Composite Laminate Panel

To identify the best fit copula, identifying the best fit marginal CDFs should be carried out. Correlation measure, the Kendall's tau is invariant covariance measure for copula. To find best fit copula and marginal CDFs, we performed the following procedure:

However buckling load and surface strain are all negative values, normal distribution is the only distribution to fit the data. Also copula has restriction of the Kendall's tau so that the Kendall's tau should be positive (positive correlation). So that two transformation, $X_1' = -X_1$ and $X_2' = 1 + X_2$ are used to identify marginal CDFs.

For buckling load, Gamma distribution is the best fit CDF and K-S test strongly supports the decision. For surface strain, all K-S test results are not so positive. Normal,

Gamma and Lognormal distribution are accepted but those p-values are quite similar so that Normal distribution is selected for convenience sake. Thus we can use normal CDF to fit the surface strain, X_1 transformation is not required.

Transformation for both random variables are $X_1' = -X_1$ and $X_2' = X_2$, Kendall's tau is 0.3363. With this transformed random variables, the best fit copula will be identified.

Table B-1. Formulas of Copulas ($C(u_1,u_2\mid\theta)$), PDF formulas ($c(u_1,u_2\mid\theta)$), generator functions, and domains of correlation parameters. (for Gumbel, $\bar{u}_1=-\ln u_1$ and $\bar{u}_2=-\ln u_2$)

Copula	$C(u_1,u_2\mid\theta)$	$c(u_1,u_2\mid\theta)=\frac{\partial^2 C(u_1,u_2\mid\theta)}{\partial u_1\partial u_2}$	Generator function $\Psi_\theta(s)$	Domain of θ
Clanton	$\left(u_1^{-\theta}+u_2^{-\theta}-1\right)^{-1/\theta}$	$(\theta+1)(u_1u_2)^{-1-\theta}\left(u_1^{-\theta}+u_2^{-\theta}-1\right)^{-2-1/\theta}$	$\frac{1}{\theta}\left(s^{-1}-1\right)$	$\theta\in(0,\infty)$
Gumbel	$\exp\left(-\left(\bar{u}_1^{\theta}+\bar{u}_2^{\theta}\right)^{-1/\theta}\right)$	$C(u_1,u_2)(u_1u_2)^{-1}\left(\bar{u}_1^{\theta}+\bar{u}_2^{\theta}\right)^{-2+1/\theta}$ $(\bar{u}_1\bar{u}_2)^{\theta-1}\left\{\left(\bar{u}_1^{\theta}+\bar{u}_2^{\theta}\right)^{1/\theta}+\theta-1\right\}$	$(-\ln s)^{\theta}$	$\theta\in[1,\infty)$
Frank	$-\frac{1}{\theta}\ln\left(1+\frac{\left(e^{-\theta u_1}-1\right)\left(e^{-\theta u_2}-1\right)}{e^{-\theta}-1}\right)$	$\frac{-\theta\left(e^{-\theta}-1\right)e^{-\theta(u_1+u_2)}}{\left\{\left(e^{-u_1\theta}-1\right)\left(e^{-u_2\theta}-1\right)+\left(e^{-\theta}-1\right)\right\}^2}$	$-\ln\frac{e^{-\theta s}-1}{e^{-\theta}-1}$	$\theta\in(-\infty,\infty)$

Table B-2. Kendall's tau and domain of *τ*.

Copula	$\tau=f(\theta)$	Domain of τ
Clayton	$1-\frac{2}{2+\theta}$	$\tau\in(0,1]$
Gumbel	$1-\theta^{-1}$	$\tau\in[0,1]$
Frank	$1-\frac{4}{\theta}\left(1-\frac{1}{\theta}\int_0^{\theta}\frac{t}{e^t-1}dt\right)$	$\tau\in[-1,1]\setminus\{0\}$

Table B-3. CDF candidates and distribution statistics. (for Gumbel, γ is Euler-Mascheroni constant of 0.57721566…)

Distribution	Distribution statistics	Domain of *μ*	Domain of *σ*
Normal	μ,σ^2	$\mu\in(-\infty,\infty)$	$\sigma\in[0,\infty)$
Weibull	$\mu=\Gamma\left(1+\frac{1}{b}\right),\ \sigma^2=a^2\Gamma\left(1+\frac{2}{b}\right)-\mu^2$	$\mu\in[0,\infty)$	$\sigma\in[0,\infty)$
Gamma	$\mu=ab,\sigma^2=ab^2$	$\mu\in[0,\infty)$	$\sigma\in[0,\infty)$
Lognormal	$\mu=e^{a+\frac{b^2}{2}},\sigma^2=\left(e^{b^2}-1\right)e^{2a+b^2}$	$\mu\in[0,\infty)$	$\sigma\in[0,\infty)$
Gumbel[1]	$\mu=a+b\gamma,\sigma^2=\frac{\pi^2}{6}b^2$	$\mu\in(-\infty,\infty)$	$\sigma\in[0,\infty)$

Table B-4. Fitting random data to CDF.

1. Transform data to make it applicable to CDF candidates (i.e. domain of random variable *X* from lognormal distribution is $X \in [0,\infty)$)
2. Calculate marginal empirical CDFs with the data
3. Perform GOF test to identify the best fit CDFs
4. Calculate multivariate CDF with the data
5. Using the best fit CDFs, perform GOF test to identify the best fit copula

Table B-5. K-S test to identify the best fit CDF for buckling load and surface strain.

	p-value Buckling load	p-value Surface strain
Normal	0.8534	**0.3006**
Weibull (extreme typeIII)	0.0001	0.0058
Gamma	**0.9338**	0.2998
Lognormal	0.8341	0.3001
Gumbel (extreme type I)	0.0000	0.0058

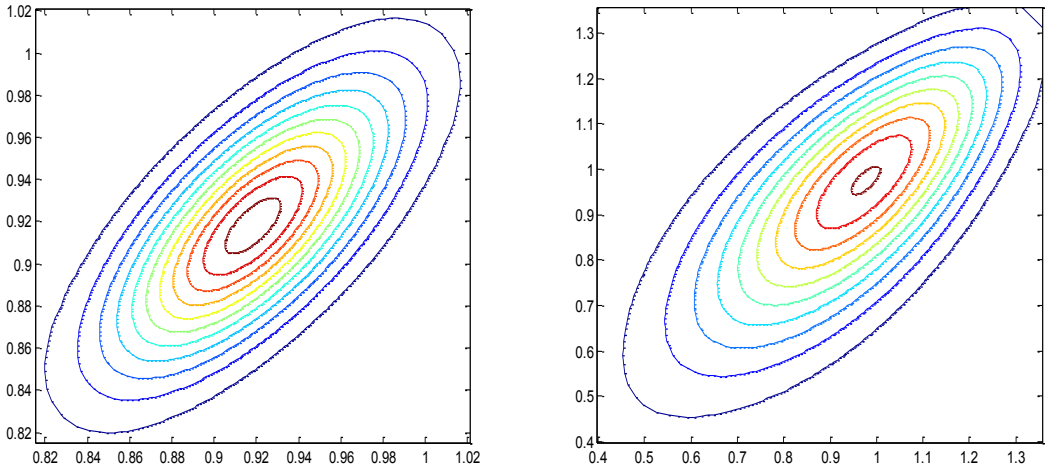

A B

Figure B-1. Joint PDF contours for the same copula (τ=0.5) with different marginal CDFs. A) Gaussian copula + Gaussian marginal CDFs and B) Gaussian copula + Weibull marginal CDFs

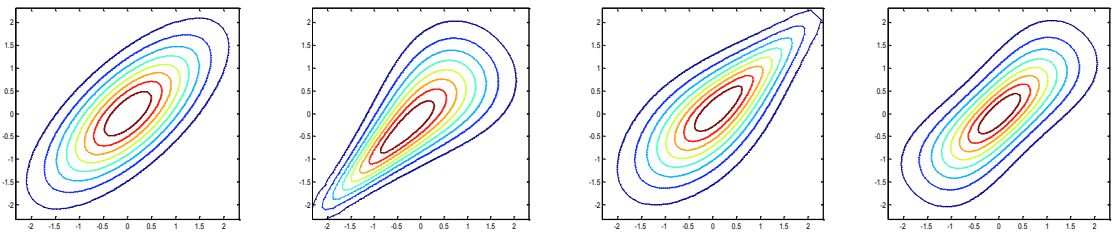

Figure B-2. Gaussian, Clayton, Gumbel and Frank copula with standard normal marginal CDFs (τ=0.5).

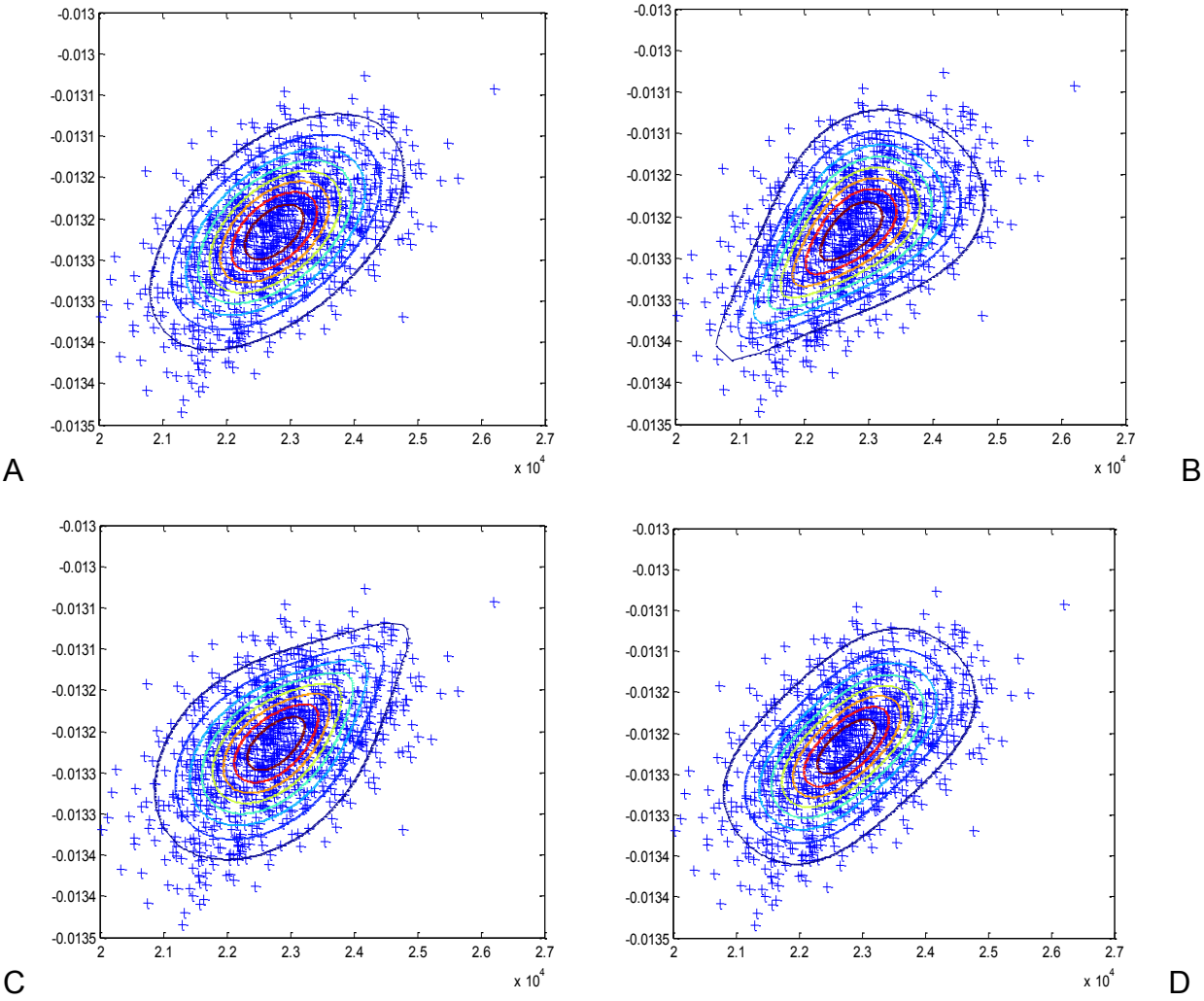

Figure B-3. Gaussian, Copulas and scattered data plots (τ =0.3363). A) Gaussian copula B) Clayton copula C) Gumbel copula and D) Frank copula.

LIST OF REFERENCES

1. Oberkampf, W.L., Deland, S.M., Rutherford, B.M., Diegert, K.V., and Alvin, K.F. (2002), Error and Uncertainty in Modeling and Simulation. Reliability Engineering and System Safety, Vol. 75, pp. 333-357.

2. Composite Materials Handbook, MIL-HDBK-17-1F, Department of Defense, 17 June 2002.

3. ASM Handbook Vol. 21 Composites, ASM International, 2001.

4. An, A., Acar, A., Haftka, R.T., Kim, N.H., Ifju, P.G, and Johnson, T.F., (2008) “Being Conservative with a Limited Number of Test Results,” Journal of Aircraft, 45(6), 1969-1975.

5. Acar, E., Haftka, R.T., Kim, N.H.(2010) “Effects of Structural Tests on Aircraft Safety ” AIAA Journal ,Vol 48(10), 2235–2248.

6. Kumar, S., Villanueva, D., Sankar, B.V., and Haftka, R.T., “Probabilistic Optimization of Integrated Thermal Protection System,” AIAA-2008-5928, 12th AIAA/ISSMO Multidisciplinary Analysis and Optimization Conference, Victoria, British Columbia, Canada, Sept 10-12, 2008.

7. Bharani Ravishankar., "Probabilistic Validation Metrics for Industrial Engineering Analysis Models," AIAA-2012-1443, 53rd IAA/ASME/ASCE/AHS/ASC Structures, Structural Dynamics and Materials Conference, Honolulu, Hawaii, United States, April 23-26, 2012.

8. T. Ishikawa, Reduction of Development Costs of Full Composite Aero-Structure, ICAS Biennial Workshop, 2011 Sept. 5, 2001, Stockholm, Sweden.

9. Gates, D., Boeing 787 wing flaw extends inside plane, The Seattle Times, July 30, 2009.

10. Domke, B., Boeing 787 Lessons Learnt, Airbus, Ref. Pro813399, issue 2, October 20, 2008.

11. Norris, G., Root Cause, Aviation Week & Space Technology, Vol. 172 Issue 7, p24-26, Feb 15, 2010.

12. Ground Test Experience with Large Composite Structures for Commercial Transports, NASA Technical Memorandum TM 84627, March 1983.

13. M. Evans, N. Hastings, and B. Peacock, *Statistical distributions*, Wiley, New York, 1993.

14. Smarslok, B., Speriatu, L., Schulz, W., Haftka, R. T., Ifju, P., Johnson, T. F., “Experimental uncertainty in Temperature Dependent Material Properties of Composite Laminates,” Society for Experimental Mechanics Annual Conference, No. 241, St. Louis, MO, June, 2006.

15. Kight, N. F., and Starnes, J. H., “Postbuckling Behavior of Axially Compressed Graphite-Epoxy Cylindrical Panels With Circular Holes,” Journal of Pressure Vessel Technology 107: 394-402, 1985.

16. Smarslok, B. P., Haftka, R. T., and Ifju, P., “A Correlation Model for Graphite/Epoxy Properties for Propagating Uncertainty to Strain Response,” 23rd Annual Technical Conference of the American Society for Composites, Memphis, Tenn, 2008.

17. M. W. Hilburger and J. H. Starnes Jr., “Effects of imperfections on the buckling response of compression-loaded composite shells,” International Journal of Non-Linear Mechanics 37 (2007) 623-643.

18. C. Park, N. H. Kim, and R. T. Haftka, “Estimating Probability of Failure of Composite Laminated Panel with Multiple Potential Failure Modes“ AIAA-2012-1592, 53rd AIAA/ASME/ASCE/AHS/ASC Structures, Structural Dynamics, and Materials Conference, Honolulu, Hawaii, Apr. 23-26., 2012.

19. Acar, E, Kale, A., and Haftka, R. T., “Comparing Effectiveness of Measures that Improve Aircraft Structural Safety,” *Journal of Aerospace Engineering*, Vol. 20, No. 3, July 2007, pp. 186-199.

20. Jiao, G., and Moan, T., "Methods of reliability model updating through additional events," Structural Safety, Vol. 9, No. 2, 1990, pp. 139-153.

21. A. Urbina, S. Mahadevan and T. L. Paez, (2011) "Quantification of margins and uncertainties of complex systems in the presence of aleatoric and epistemic uncertainty", Reliability Engineering & System Safety, 96 (9): 1114-1125.

22. I. Park, H. K. Amarchinta, R. V. Grandhi, (2010) "A Bayesian approach for quantification of model uncertainty", Reliability Engineering & System Safety, 95: 777-785.

23. J. M. McFarland, B. J. Bichon, Bayesian model averaging for reliability analysis with probability distribution model from uncertainty. 50th AIAA/ASME/ASCE/AHS/ASC structures, structural dynamics and material conference, Palm Springs, CA, 2009.

24. Lincoln, J. W., "USAF Experience in the Qualification of Composite Structures," Composite Structures: Theory and Practice, ASTM STP 1383, P. Grant and C. Q. Rousseau, Eds., American Society for Testing and Materials, West Conshohocken, PA. 2000. pp.3-11.

25. Kale, A.A., Haftka, R.T., and Sankar, B.V., (2008) "Efficient Reliability Based Design and Inspection of Stiffened Panels against Fatigue," *Journal of Aircraft*, **45** (1): 86-97.

26. Park, C., Matsumura, T., Haftka, R. T., Kim, N. H. and Acar.,E., "Modeling the effect of structural tests on uncertainty in estimated failure stress" 13th AIAA/ISSMO Multidisciplinary Analysis and Optimization Conference, Fort Worth, Texas, Sept. 13-15, 2010.

27. Beckman (1980) A New Family of Probability Distributions With Applications to Monte Carlo Studies, Journal of the American Statistical Association, Vol. 75, No. 370. 276- 279.

28. M. McDonald and S. Mahadevan, Uncertainty Quantification and Propagation in Multidisciplinary Analysis and Optimization, AIAA-2008-6038, 12th AIAA/ISSMO Multidisciplinary Analysis and Optimization Conference, 2008.

29. E.J. Dudewicz and Karian, Z.A, The Extended Generalized Lambda Distribution (EGLD) for Fitting Distribution with Moments, (1996) American Journal of Mathematical and Management Science 16: 271-332.

30. E. L. Lehmann and G. Casella, *Theory of point prediction*, Springer-Verlag, New York, 1998.

31. R. E. Neapolitan, *Learning Bayesian Network*, Pearson Education, New Jersey, 2004.

32. Fawcett A, Trostle J, Ward S. "777 empennage certification approach," 11th international conference of composite materials, Gold Coast, Australia, 14–18 July, 1997.

33. FAA Advisory Circular 20-107A, Composite Aircraft Structure, 1984; and companion document by the JAA, ACJ 25.603, Composite Aircraft Structure (Acceptable Means of Compliance), 1986.

34. Pattabhiraman, S., Haftka, R. T., Kim, N. H., "Advantages of condition- based maintenance over scheduled maintenance using structural health monitoring systems", Journal of Reliability and System Safety.

35. Stanley, G. M., Continuum-Based Shell Elements, Ph.D. Dissertation, Department of Mechanical Engineering, Stanford University, 1985.

36. Qu, X., Haftka, R.T., Venkataraman, S., and Johnson, T.F., “Deterministic and Reliability-Based Optimization of Composite Laminates for Cryogenic Environments,” AIAA Journal, 41(10), pp. 2029-2036, 2003.

37. Noh, Y., K. K. Choi, Lee, I., (2010) “Identification of marginal and joint CDFs using Bayesian method for RBDO,“ Journal of Structural Multidisciplinary Optimization ,Vol 40, 35-51.

38. Schmidt, R. (2002). Tail dependence for elliptically contoured distributions. Math. Methods Oper. Res. 55, 301–327.

39. Elishakoff, "Safety Factors and Reliability; Friends or Foes?", Kluwer Academic Publishers, 2004.

40. D.M. Neal, W.T. Matthews, M.G. Vangel and T. Rudalevige; A Sensitivity Analysis on Component Reliability from Fatigue Life Computations; U.S. Army Materials Technology Laboratory, Report No. MTL TR 92-5; February 1992.

41. R. E. Melchers, Important Sampling in Structural Systems, Structural Safety, 1989.

42. Melchers R. E., Structural Reliability Analysis and Prediction, New York: Wiley, pp. 73-83, 1999.

43. A. Dey, and S. Mahadevan, Ductile Structural System Reliability Analysis using Adoptive Importance Sampling, Structural Safety (20), 1998: 137-154.

44. Zheng Y., Das P. K., Improved response surface method and its application to stiffened plate reliability analysis, Engineering Structures, Vol. 22, pp. 544-551, 2000.

45. Ba-abbad, M. A., Nikolaidis, E., and Kapania, R. K., “New Approach for System Reliability-Based Design Optimization" AIAA Journal, Vol. 44, No. 5, 2003, pp 1087-1096.

46. Haldar, A., and Mahadevan, S., Probability, Reliability and Statistical Methods in Engineering. Design, John Wiley & Sons, New York, 2000.

47. M. Hohenbichler and R. Rackwitz First-Order Concepts in System Reliability. Structural Safety, 1983:177-188.

48. Vanmarcke EH. Matrix form formulation of reliability analysis and reliability-based design. Comput Struct 1973:757–70.

49. Ditlevsen O. Narrow reliability bounds for structural systems. J Struct Mech 1979;7:453–72.

50. Y. Noh, Input model uncertainty and reliability-based design optimization with associated confidence level, Ph D. dissertation, Department of Mechanical Engineering, University of Iowa, 2009.

51. C. Park, N. H. Kim, R. T. Haftka, "The Effect of Ignoring Dependence between Failure Modes on Evaluating Structural Reliability", 10th World Congresses of Structural and Multidisciplinary Optimization, Orlando, USA, May, 2013.

52. Sklar, A. (1959), "Fonctions de répartition à n dimensions et leurs marges", Publ. Inst. Statist. Univ. Paris 8: 229–231.

53. Nelson R.B. (1999), An Introduction to Copula, Springer, New York.

54. H. Joe, Multivariate Models and Dependence Concepts (1997).

55. P. Georges, A-G. Lamy, E. Nicholas, G. Quibel, T. Roncalli, Multivariate survival modeling: a unified approach with copulas, 2001.

56. Ang AH-S, Abdelnour J, Chaker AA. Analysis of activity networks under uncertainty. J Eng Mech Div ASCE 1975;101(EM4):373–87.

57. Venter, G.G., 2001. Tails of copulas. In: Proceedings ASTIN Washington, USA, pp. 68–113.

58. G. Frahm , M. Junker, and R. Schmidt (2006). Estimating the tail-dependence coefficient: Properties and pitfalls, Insurance: Mathematics and Economics 37, 80-100.

59. I. Kroo, 2004, “Collectives and complex system design,” “Von Karman Institute (VKI) Lecture Series on Optimization Methods and Tools for Multicriteria/Multidisciplinary Design”, von Karman Institute for Fluid Dynamics, Rhode-Saint-Genèse, Belgium.

60. I. Kroo, 2004, “Innovations in Aeronautics,” 42nd AIAA Aerospace Sciences Meeting, Reno, NV, January 5-8, 2004.

61. C. Park, N. H. Kim, and R. T. Haftka, “Effects of Structural Tests on Aircraft Design Safety” ASME 2011 International Design Engineering Technology Conference & Computer and Information in Engineering Conference, Washington, DC, USA, August. 28-31, 2011.

62. Cairns, Douglas S. Class Lecture. Introduction to Aerospace. Montana State University, Bozeman, MT. Spring 2010.

63. Niu Michael Chun-Yung. Airframe Structural Design: Principles and Practices. AIAA Education Series, 1988.

64. Owen, D. B., "Factors for One sided Tolerance Limits and for Variables Sampling Plans", Sandia Corp. Monograph SCR-607, 1963.

65. Villanueva, D., Haftka, R.T., Sankar, B.V. (2011). Including the Effect of a Future Test and Redesign in Reliability Calculations, AIAA Journal, Vol. 49 (12), pp. 2760-2769.

66. Villanueva, D., Haftka, R.T., Sankar, B.V. (2010). Including Future Tests in the Design and Optimization of an Integrated Thermal Protection System, AIAA 2010-2597, 12th AIAA Non-Deterministic Approaches Conference, Orlando, FL.

67. Matsumura, T. and Haftka, R.T., (2013), "Reliability Based Design Optimization Considering Future Redesign With Different Epistemic Uncertainty Treatments," Journal of Mechanical Design, Vol. 135(9), 091006-091014.

68. Joo ho Choi, Dawn An, Jun ho Won, Bayesian Approach for Structural Reliability Analysis and Optimization Using the Kriging Dimension Reduction Method, ASME Journal of Mechanical Design 132(5),051003,2010.05.

69. Oberkampf, W. L.; Diegert, K. V.; Alvin, K. F.; and Rutherford, B. M. 1998: Variability, Uncertainty, and Error in Computational Simulation. AIAA/ASME Joint Thermophysics and Heat Transfer Conference, ASME-HTD-Vol. 357-2, pp. 259–272.

70. Oberkampf, W. L. 1998: Bibliography for Verification and Validation in Computational Simulation, SAND98-2041, Sandia Natl. Lab.

71. James M. Whitney, Structural Analysis of Laminated Anisotropic Plates, Technomic, Lancaster, Pennsylvania, 1987.

72. Schillinger, D., Stochastic FEM Based Stability Analysis of I-Sections With Random Imperfections, Diploma Thesis, Department of Civil Engineering, University of Stuttgart, 1985.

73. Park, O., Haftka, R.T., Sankar, B.V., Starnes, J.H., and Nagendra, S., “Analytical-Experimental Correlation for a Stiffened Composite Panel Loaded in Axial Compression,” Journal of Aircraft, 38 (2), 379-387, 2001.

74. Nagendra, S., Jestin, D., Gürdal, Z., Haftka, R.T., and Watson, L.T., “Improved genetic Algorithms for the Design of Stiffened Composite Panels,” Computers & Structures, Vol. 58, No. 3, pp. 543-555, 1996.

75. Matsumura, T., Haftka, R.T. and Sankar, B.V. “Reliability Estimation Including Redesign Following Future Test for an Integrated Thermal Protection System” *9th World Congress on Structural and Multidisciplinary Optimization, Shizuoka, Japan, June 14-17, 2011*.

76. Villanueva, D., Haftka, R.T., Sankar, B.V. “Accounting for Future Redesign in the Optimization of an Integrated Thermal Protection System“, *AIAA-2012-1933, 14th AIAA Non-Deterministic Approaches Conference, Honolulu, HI, 2012*.

77. Joseph M. Manter and Donald B. Paul, Airframe Structures Technology for Future Systems, ICAS 2000.

78. X. Jiang, S. Mahadevan, (2007) "Bayesian risk-based decision method for model validation under uncertainty", *Reliability Engineering & System Safety*, 92: pp. 707-718.

79. Simulia, D. C. S. "ABAQUS 6.11 Analysis User's Manual." *Abaqus 6.11 Documentation* (2011): 22-2.

80. J. Li, J. Chen, and W. Fan. The Equivalent Extreme-value Event and Evaluation of the Structural System Reliability, *Structural Safety* 2007;29(2):112-13.

81. Oberkampf, W., J. Helton, C. Joslyn, S. Wojtkiewicz, and S. Ferson. Challenge problems: uncertainty in system response given uncertain parameters. *Reliability Engineering and System Safety*, 85(1-3) (2004).

82. Acar, E. and Haftka, R.T. (2007) “Reliability-Based Aircraft Structural Design Pays, Even with Limited Statistical Data” *Journal of Aircraft* ,Vol 44(3), 812–823.

83. Park, Chanyoung, Nam H. Kim, and Raphael T. Haftka. (2013) "How coupon and element tests reduce conservativeness in element failure prediction." *Reliability Engineering & System Safety*, Vol 123, 123-136.

BIOGRAPHICAL SKETCH

Chan-Young Park graduated from Seoul National University in 2003 with a Bachelor of Science in Naval Architecture and Ocean Engineering. As an undergraduate student he participated in a Human Powered Vessel competition and his team was awarded with the first prize twice. He also worked as an undergraduate research assistant for an structural optimization research. He was working at MIDAS IT as a developer over 3 years. He had experience in developing commercial finite element analysis software. He joined the University of Florida in 2010. His research interests include: design under uncertainty, uncertainty quantification, finite element methods and structural optimization.